DISSERTATIONES
CHIMICAE
UNIVERSITATIS
TARTUENSIS
172

KATRIN KESTAV

Crystal Structure-Guided Development of Bisubstrate-Analogue Inhibitors of Mitotic Protein Kinase Haspin

DISSERTATIONES CHIMICAE UNIVERSITATIS TARTUENSIS
172

DISSERTATIONES CHIMICAE UNIVERSITATIS TARTUENSIS
172

KATRIN KESTAV

Crystal Structure-Guided Development of Bisubstrate-Analogue Inhibitors of Mitotic Protein Kinase Haspin

UNIVERSITY OF TARTU
Press

Institute of Chemistry, Faculty of Science and Technology, University of Tartu

Dissertation is accepted for the commencement of the degree of *Doctor philosophiae* in Chemistry on 10th of May, 2018 by the Council of Institute of Chemistry, Faculty of Science and Technology, University of Tartu

Supervisors: Darja Lavõgina, PhD
Institute of Chemistry, University of Tartu, Estonia

Opponents: Prof Dr Richard Engh
Department of Chemistry, UiT the Arctic University of Norway, 9037-Tromsø, Norway

Harri Härmä, PhD
Department of Chemistry, University of Turku, Finland

Commencement: August 29th, 2018 at 10:15 room 1020, 14A Ravila St., Institute of Chemistry, University of Tartu

This research has been supported by grants from the Estonian Research Council (PUT0007 and IUT20-17); by the SGC, a registered charity (number 1097737) that receives funds from AbbVie, Bayer, Boehringer Ingelheim, the Canada Foundation for Innovation, Genome Canada, GlaxoSmithKline, Janssen, Lilly Canada, the Novartis Research Foundation, the Ontario Ministry of Economic Development and Innovation, Pfizer, Takeda, and the Wellcome Trust [092809/Z/10/Z]; from the Graduate School "Functional materials and technologies", receiving funding from the European Regional Development Fund; by the national scholarship program Kristjan Jaak, which is funded by Archimedes Foundation.

ISSN 1406-0299
ISBN 978-9949-77-759-4 (print)
ISBN 978-9949-77-760-0 (pdf)

University of Tartu Press
www.tyk.ee

CONTENTS

LIST OF ORIGINAL PUBLICATIONS

I **Kestav, K**.; Lavogina, D.; Raidaru, G.; Chaikuad, A.; Knapp, S.; Uri, A. Bisubstrate Inhibitor Approach for Targeting Mitotic Kinase Haspin. *Bioconjugate Chem*. **2015**, *26*(2), 225–234.

II Lavogina, D.; **Kestav, K**.; Chaikuad, A.; Heroven, C.; Knapp, S.; Uri, A. Co-crystal Structures of the Protein Kinase Haspin with Bisubstrate Inhibitors. *Acta Crystallogr. F-Struct. Biol. Cryst. Commun.* **2016**, *72*(5), 339–345.

III **Kestav, K**.; Viht, K.; Konovalov, A.; Enkvist, E.; Uri, A.; Lavogina, D. Slowly on, Slowly off: Bisubstrate-Analogue Conjugates of 5-Iodotubercidin and Histone H3 Peptide Targeting Protein Kinase Haspin. *ChemBioChem.* **2017**, *18*(8), 790–798.

Author´s Contribution

Paper I: The author planned and performed most of the experiments (except the commercial kinase panel) as well as the syntheses (except the synthesis of compounds **15**, **24**, **25**). Additionally, the author participated in writing of the manuscript.

Paper II: The author participated in the synthesis of compounds used in the co-crystallization with kinase Haspin. Additionally, the author participated in writing of the manuscript.

Paper III: The author performed the synthesis of novel compounds (except synthesis of Itc fragment), the equilibrium binding studies, most experiments to determine the association and dissociation kinetics of compounds (except the determination of kinetic properties of non-fluorescent compounds) and thermal shift assay. Additionally, the author was responsible for writing of the manuscript.

ABBREVIATIONS

5-ITu	5-iodotubercidin
AA	amino acid residue
Adc	adenosine-4'-dehydroxymethyl-4'-carboxylic acid moiety
ADK	adenosine kinase
Ahx	6-aminohexanoic acid residue
Akt3/PKBγ	Rac-gamma serine/threonine-protein kinase; protein kinase B
AMSE	5-(2-aminopyrimidin-4-yl)-selenophene-2-carboxylic acid moiety
AMTH	5-(2-aminopyrimidin-4-yl)-thiophene-2-carboxylic acid moiety
ARC	adenosine analogue-oligoarginine conjugate
ATP	adenosine-5'-triphosphate
Boc	*tert*-butoxycarbonyl
cAMP	3′,5′-cyclic adenosine monophosphate
Clk	Cdc2-like protein kinase
CK2	casein kinase 2
CPC	chromosomal passenger complex
DCE	1,2-dichloroethane
DMF	*N*,*N*-dimethylformamide
DMSO	dimethylsulfoxide
DSF	differential scanning fluorimetry
ePK	eukaryotic protein kinase
FA	fluorescence anisotropy
FI	fluorescence intensity
Fmoc	9-fluorenylmethoxycarbonyl
FRET	Förster-type resonant energy transfer
H3	histone H3
H3(1-7)	histone H3 amino acid residues 1-7
H3T3	Thr3 of histone H3
H9	*N*-aminoethyl-5-isoquinolinesulfonamide moiety
Haspin	haploid germ cell–specific nuclear protein kinase
HBTU	2-(1*H*-benzotriazol-1-yl)-1,1,3,3-tetramethyluronium hexafluorophosphate
HOBt	1-hydroxybenzotriazole
IC_{50}	inhibitor concentration that causes 50% reduction of the kinase enzymatic/catalytic activity in the used assay conditions
Itc	5-iodotubercidin-4'-dehydroxymethyl-4'-carboxylic acid moiety
ivDde	1-(4,4-dimethyl-2,6-dioxocyclohex-1-ylidene)isovaleryl
K_D	equilibrium dissociation constant determined from a direct binding assay
K_d	equilibrium dissociation constant determined from a displacement assay
K_i	equilibrium dissociation constant determined from an inhibition assay

MPD	2-methyl-2,4-pentanediol
MSK1	mitogen- and stress-activated protein kinase-1
Mtt	*N*-methyltrityl
Myr	myristic acid moiety
PEG	polyethylene glycol
Pim	proto-oncogene serine/threonine-protein kinase
PIPY	4-(piperazin-1-yl)-7H-pyrrolo[2,3-d]pyrimidine moiety
PK	protein kinase
PKA	cAMP-dependent protein kinase
PKA C	cAMP-dependent protein kinase catalytic subunit, type α
PKI	protein kinase inhibitor peptide
PPI	protein-protein interaction
PYB	3-(pyridin-4-yl)benzoic acid moiety
pH3T3	phospho-Thr3 of histone H3
ROCK2	Rho-associated protein kinase 2
SAC	spindle assembly checkpoint
SPPS	solid phase peptide synthesis
TAMRA	5-carboxytetramethylrhodamine
TFA	trifluoroacetic acid
TIBI	4,5,6,7-tetraiodo-1H-benzimidazole moiety
TIPS	triisopropylsilane
T_m	melting temperature of protein
v	volume percent

ABSTRACT

Both academic institutions and pharmaceutical companies have invested a lot of effort to develop anticancer drugs which would allow regulation of pathways underlying the uncontrollable cell division. In parallel, for the successful treatment of cancer, it is of utmost importance to work out 'easy-to-use' diagnostic tools. Cell division (including mitotic events) is orchestrated by crosstalk of different protein kinases – the enzymes that carry out phosphorylation reaction, through which the processes necessary for the excistence of cell are regulated. Protein kinases are also under study as biomarkers, as the altered activity and/or concentration of kinases may indicate the presence of certain disease. The practical importance of protein kinase research is also demonstrated by the fact that 39 inhibitors targeting protein kinases are approved as drugs by US Food and Drug Administration (FDA).[1,2]

The current thesis describes development of compounds targeting mitotic kinase Haspin. Haspin is an important regulator of mitotic events and had been acknowledged as a 'promising target for the design of inhibitors as potent anticancer drugs'.[3] Novel Haspin-targeting compounds were constructed using principles of design of bisubstrate-analogue inhibitors (adenosine analogue-oligoarginine conjugates or ARCs), where the ATP-site targeting fragment and substrate analogue of protein kinase were interconnected by a flexible linker. The design was guided by the structural information revealed from the results of X-ray analysis of co-crystals of complexes of Haspin and inhibitors. The stability and the kinetics of formation and dissociation of complexes of conjugates with Haspin as well as the selectivity of these fundamental properties for binding with some other protein kinases were established in biochemical studies. As a result of precise targeting of 'binding hotspots' of active site of Haspin the conjugates with high affinity and selectivity were obtained. This reseach also led to the compounds possessing notably long residence time.

LITERATURE OVERVIEW

1. Protein Kinases

1.1. General Properties

Protein kinases (PKs) are the enzymes that catalyse the phosphorylation of substrate proteins, resulting in transfer of the γ-phophoryl group (PO_3^{2-}) from the donor molecule (generally ATP) to Ser, Thr or Tyr residue of the substrate protein (Scheme 1). Thereby, dual negative charge is introduced into the structure of substrate and drastic change in hydrogen bond properties of the sub-site from a donor to acceptor induced, causing the change of conformation of the protein. Hence, the phosphorylation is functioning as a molecular switch by turning the cellular signalling pathways 'ON' or 'OFF'.[4,5]

$$MgATP^{-1} + \text{protein-OH} \xrightarrow{PK} \text{protein-}OPO_3^{2-} + MgADP + H^+$$

Scheme 1. General scheme of phosphorylation of substrate proteins catalysed by PKs.

Phosphorylation level of proteins is highly controlled and balanced by dephosphorylation, which is carried out by phosphoprotein phosphatases.[6] Thus, the reversible character of phosphorylation-dephosphorylation processes is of utmost importance in cellular functioning, *i.e.*, regulation of metabolic pathways, membrane transport, cell division and movement, cell growth and differentiation, and controlled cell death (apoptosis). Consequently, the dysregulation of PKs is associated with many diseases, including cancer, inflammatory diseases, autoimmune diseases, Alzheimer disease, hypertension.[4,6] Thus, over the past decades PKs have become major drug targets as well as targets of intense biotechnological research both in academia and in pharmaceutical companies.[1,4,7]

Human PK gene family includes 538 members (initial human genome sequencing report announced 518 PKs[8]) coded by approximately 2.7% of genes in human genome (ca 19,000–20,000 human protein-coding genes in total).[5,9] Based on the nature of phosphorylatable hydroxyl group in the preferred substrates, *i.e.*, alcoholic (Ser or Thr) or phenolic (Tyr), PKs are classified into serine/threonine PKs and tyrosine PKs, respectively.[4,5] Furthermore, some PKs are able to phosphorylate both types of hydroxyl group and thus are termed as dual specificity PKs (*e.g.*, dual specificity tyrosine-phosphorylation regulated kinases, DYRKs).[5] In addition to the single site phosphorylation, the substrates may also be phosphorylated at multiple sites, whereas it is possible that the subsequent phosphorylation can be facilitated by previous one. This phenomenon is named 'priming phosphorylation', whereas the second phosphorylation may be

ca 100–1000 times more efficient in the presence of the priming phosphoryl than without priming.[10,11]

Generally, most PKs contain K/E/D/D signature sequence in catalytic loop and require divalent cations, such as Mg^{2+} (or Mn^{2+}), for catalysis (see Scheme 1). Still, 50 PKs out of 538 are so-called pseudokinases which lack the catalytically important residues (*e.g.,* absence of αGlu or β3-Lys, changes in the DFG or HRD signatures; see below in sections *1.1.2. General Structural Features of PKs on the Example of PKA C* and *2.2.2. Comparison of Crystal Structures of Catalytical Domains of Haspin and PKA*) and hence do not possess catalytic activity. Still, it has been shown that pseudokinases may act as regulators of catalytically active PKs, function as scaffolding entities (*i.e.*, form complexes with other proteins and recruit those to certain locations in cells), and protect their 'partners' against the phosphorylation by other PKs.[4,5,12,13]

Activation of PKs is achieved by different mechanisms. For instance, many PKs require the phosphorylation (auto-phosphorylation or phosphorylation mediated by other kinases) of one or several Ser, Thr or Tyr residues in their activation loop (also termed as T-loop), which runs between the conserved DFG and APE motifs (see below). Usually, this phosphorylation leads to the conformational changes allowing the right positioning of residues required for the substrate binding and catalysis. Moreover, structural rearrangement causes the loss of steric hindrance and hence allows the access of substrate into the active site. The activity of PKs may also be regulated *via* recruitment of second messengers (molecular cofactors), such as binding of cAMP molecules to R-subunits of PKA (see below in section *1.1.1. PKA C as a Prototype of PKs*), or by additional subunits and regulatory proteins whose expression level is adjustable (*e.g.*, the concentration of cyclins that activate cyclin-dependent PKs, Cdks varies throughout the cell cycle).[6,14]

1.1.1. PKA C as a Prototype of PKs

cAMP-dependent protein kinase or protein kinase A (PKA) is one of the first discovered (Walsh *et al*. in 1968[15]) and well studied PKs due to its clear activation mechanism and structural similarities with other eukaryotic PKs (ePKs).[14,16,17] As PKA is abundant in organisms, it participates in various signalling cascades: it has several important functions including destabilization of cytoskeleton *via* regulation of dynamics of F-actin, relaxation of heart muscles, lipolysis in adipose tissue, antigen induced activation of B- and T-cells, gene expression (by phosphorylating cellular transcription factor nuclear cAMP-response element-binding protein, CREB).[18–20]

The first crystal structure of the active site of a PK was that of the catalytic subunit α of PKA (PKA C) and it was published in 1991[21], paving the road for the X-ray study of 3D-structure of PKs. PKA C is often also used as a prototype of PKs because of its structural similarities with other ePKs: globular bilobal structure, type and localization of catalytically important amino acid residues

(AAs), localization of binding sites for phosphoryl group donor and acceptor, *etc*. Moreover, the concentration of PKA in tissues is relatively high (*e.g*., concentration of 3.1 μM of PKA C in human platelets[22]), its recombinant form can be easily over-expressed and high yields can be achieved during the purification of the kinase.[14,16] Besides, PKA possesses good properties for crystallization, making possible its use as an 'ersatz'-PK for modelling of kinases that are problematic from the aspect of purification or crystallization (*e.g*., Aurora kinases). For this, to obtain the maximum similarity with desired PK, point mutations are introduced into the sequence of DNA of the target PK, resulted in the change in the amino acid composition of PKA.[23]

In its inactive state, PKA is a heterotetrameric holoenzyme containing two catalytic subunits (C) and a dimer of regulatory subunits (R). In humans, there are four types of R-subunits (RIα, RIβ, RIIα, RIIβ) and three types of C-subunits (Cα/β/γ) that differ from each other not only by primary structure, but also by localization and expression level.[4,24] Furthermore, other differences include that RI subunits require the presence of MgATP for the high-affinity binding to C-subunits.[16,18] The activation of PKA is mediated by binding of second messenger 3′,5′-cyclic adenosine monophosphate (cAMP) to the regulatory subunits of PKA. For the activation, two cAMP molecules bind to each regulatory subunit, triggering the change of the structure of R-subunits and thus decreasing the affinity of R-subunits towards C-subunits. Consequently, the complex dissociates into a dimer of R-subunits and two active C-subunits, allowing the free active C-subunits to phosphorylate the Ser and/or Thr residue(s) of downstream substrates of PKA (Scheme 2).[4,25]

$$R_2C_2 + 4\ cAMP \Leftrightarrow R_2(cAMP)_4 + 2\ C \rightarrow \text{phosphorylation of substrates of PKA}$$

Scheme 2. Activation mechanism of PKA: binding of 4 cAMP molecules to the dimer of regulatory subunits leads to dissociation of PKA holenzyme.

Similary to other signal-transduction cascades, cAMP-PKA pathway is under strict spatiotemporal control to maintain the signalling specificity on the cellular level. In cell, signalling nodes are present which combine the enzymes that produce cAMP (adenylate cyclase), decompose cAMP (phosphodiesterases), utilize cAMP (PKA), and enable restoration of the initial phosphorylation levels (phosphoprotein phosphatases). These nodes are held together by so-called A-kinase-anchoring proteins or AKAPs, which are responsible for the appropiate positioning of the aforementioned enzymes to subcellular locations. Thereby, the nodes are essentally able to function independently from each other and thus allow the spatial and temporal compartmentalization at the cellular level.[4,26,27]

1.1.2. General Structural Features of PKs on the Example of PKA C

The structure of catalytic domain of PKs is relatively conserved among the super-family of proteins. PKs have a globular structure and are composed of two major domains – smaller N- and larger C-terminal lobe – which are formed of mainly β-sheets (5 β-strands + 1 α-helix) and α-helixes, respectively (Figure 1). The major domains are, in turn, further divided into 11 subdomains. The lobes are linked by the single polypeptide, known as the hinge or linker region, allowing rotation of the domains during binding of ATP to the cavity formed between the lobes (ATP-binding pocket), which is conserved in the family of PKs.[4,5,14,28–30] The front side of ATP-pocket contains the residues important for the catalysis as well as for binding of ATP; at the same time, the back of hydrophobic pocket is responsible for the regulation of kinase activity (hydrophobic spines, see below).[5] The substrate binds to the site locating on the surface of larger C-lobe, whereas the phosphorylatable Ser or Thr residue is directed to the cleft between the domains. Importantly, the substrate-binding site is less conserved among PKs, hence making more attractive construction of compounds targeting the substrate site.[4,5,14,28–30]

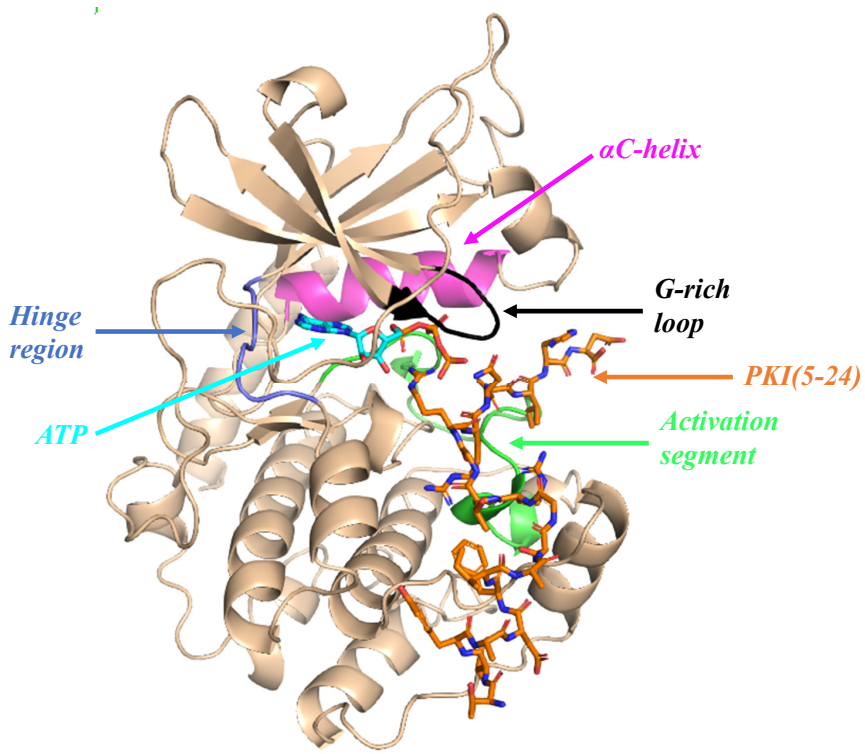

Figure 1. Structural features of PKs as exemplified by the co-crystal structure of PKA C with ATP and PKI(5-24) (PDB 1ATP). The PK is shown as a cartoon; ATP and PKI(5-24) are presented as sticks. G-rich loop is coloured black, activation segment green, hinge region blue, and αC-helix magenta.

As noted above, the highly conserved cleft between N- and C-terminal lobes is functioning as the docking site for ATP, whereas the main contribution to the nucleotide binding comes from the N-lobe. ATP is anchored to the pocket through the hydrogen bonds formed between the adenine moiety and residues in the hinge region, and between the ribose ring and residues in C-terminal domain. In the N-lobe, an extremely flexible and highly conserved glycine-rich loop (G-rich loop) runs over the ATP-binding cleft (Figure 1, Figure 2). It contains the signature sequence GxGxΦG (where x corresponds to any AA and Φ corresponds to hydrophobic residue) and contributes to the nucleotide binding. The G-rich loop of PKA consists of the AA sequence ^{50}GTGSFG^{55}, where ***Phe54*** and ***Gly55*** anchor the β-phosphate of ATP (note: here and in the following text the numbering of AAs of PKA corresponds to PKA C). On the other hand, the amino and hydroxyl groups of ***Ser53*** develop hydrogen bonds with γ-phosphate and ***Gly52*** and ***Gly55*** give the interactions with each other.[4,6,14]

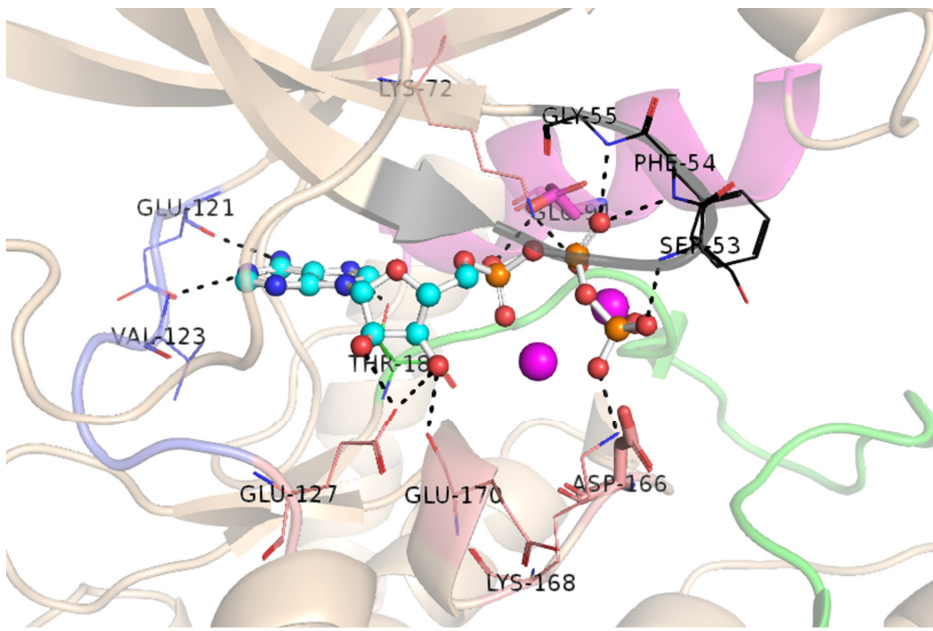

Figure 2. Co-crystal structure of ATP with PKA C (PDB 1ATP). The PK is shown as a cartoon; ATP is presented in ball-and-sticks mode. G-rich loop is coloured black, activation segment green, hinge region blue, and αC-helix magenta. Residues of PK forming interactions with the co-crystallized ATP are shown as lines and are labelled; hydrogen bonds are shows as black dotted lines. Mn^{2+}-ions are shown as magenta spheres.

The β3-strand in N-lobe usually contains the sequence Ala-X-Lys, where the amino group of Lys (***Lys72*** in PKA) forms a salt bridge with the carboxyl group of conserved glutamate (***Glu91*** in PKA) in the centre of αC-helix (Figure 2). The salt bridge is a hallmark of active kinase as this interaction is crucial for the open conformation of the kinase (see below) and hence the catalytic activity of PK (generally, in the inactive state of enzyme, the salt bridge between β3-Lys and αC-Glu is absent). Furthermore, ***Lys72*** of β3-strand in PKA gives the extra stabilizing interactions with α- and β-phosphates of ATP (Figure 2).[4,14]

The adenine base of ATP gives hydrophilic as well as hydrophobic interactions with residues in the ATP-binding site. In particular, the *N6* of adenine base gives interaction with carbonyl oxygen of ***Glu121*** (first AA in the hinge region) in PKA (Figure 2). Moreover, the *N1* and *N7* form H-bonds with amino group of ***Val123*** (hinge region) and hydroxyl group of ***Thr183*** (activation segment, see below). In addition to hydrophilic interactions, the adenine base gives interactions with hydrophobic residues from the N-lobe (***Leu49***, ***Val57***, ***Ala70***, ***Met120***, ***Tyr122***) as well as C-lobe (***Leu173***).[4]

The C-lobe includes a mobile activation segment participating in the transition between the open (active enzyme) and closed conformation (inactive enzyme) of kinase (see below in section *3.2.1. Inhibitors Targeting ATP-Site of PKs*). The beginning of activation segment includes conserved DFG motif, where the first aspartate is directed into the ATP-pocket and coordinates Mg^{2+}, which, in turn, coordinates the β- and γ-phosphates of ATP (Mg^{2+}-binding segment in PKA is ^{184}DFGFA^{188}). The γ-phosphate is additionally coordinated *via* interaction of conserved Lys (***Lys168*** in PKA) of the catalytic loop (Figure 2). Moreover, the residues at the end part of this segment (^{199}CGTP^{202} in PKA) position the phosphorytable Ser/Thr residue of the substrate. Generally, the end sequence of activation segment is conserved APE, where the final glutamate forms catalytically important salt bridge with arginine (***Glu208*** and ***Arg280*** in PKA).[4] Also, all PKs contain a catalytically important aspartate residue (***Asp166*** in PKA) in the catalytic loop, which weakens the bond between the oxygen and hydrogen atoms of the hydroxyl group of the side chain of phophorylatable residue, hence making the oxygen more nucleophilic (Figure 2). In this way, ***Asp166*** enables the nucleophilic attack of the oxygen of side-chain of substrate onto the γ-phosphorus of MgATP. The 2′ and 3′-hydroxyl groups of ribose moiety develop H-bonds with glutamates in the catalytic loop (***Glu127*** and ***Glu170*** in PKA) (Figure 2).[4,6,14,28–30]

Finally, the extra stabilization of PKs is achieved *via* conserved hydrophobic interactions. First, the N-lobe is additionally stabilized by interactions between ***Thr88*** (αC-helix) and ***Leu116*** (β4-strand) in PKA. The kinase domain is further stabilized by interactions of ***Phe102*** (αC-β4 loop in the N-lobe) and ***Gln149*** (αE-helix in the C-lobe). Other hydrophobic interactions involve ***Trp222***, ***Ile250*** and ***Phe238*** in the structure of PKA.[4] In addition to the previously mentioned hydrophobic residues, the catalytic core of PKs is stabilized through hydrophobic residues forming conserved hydrophobic spines.[31–33] First, the regulatory or R-spine is composed of four residues, whereas 2 locate in the C-

lobe and 2 in the N-lobe. In particular, the first residue is generally *His* from HRD motif of the catalytic loop (replaced by ***Tyr164*** in PKA), the second is *Phe* from the DFG motif of activation segment (***Phe185*** in PKA), and the final two are aliphatic residues from αC-helix and β4-strand (***Leu95*** and ***Leu106*** in PKA, respectively).[14,32] Another spine, termed catalytic or C-spine consists of eight residues, wherein 2 come from the N-lobe and 6 from the C-lobe (***Val57***, ***Ala70***, ***Met128***, ***Leu172***, ***Leu173***, ***Ile174***, ***Leu227***, ***Met231*** in PKA). Importantly, the correct assembly of R-spine is a hallmark of active conformation of kinase, whereas the assembly of C-spine after the binding of ATP is essential for the readiness of PK for catalysis.[31,32]

2. Mitosis

2.1. General Overview of the Cell Cycle and Mitosis

The cell cycle is an evolutionally conserved and punctually regulated process that is required for the growth as well for development of organism. The cell cycle starts with the formation of daughter cells from the mother cell and ends with the cell division or death. The cell cycle is divided into four phases: G1 (gap 1), S (synthesis), G2 (gap 2), and M (mitosis) (Figure 3). The first three, *i.e.*, G1, S, and G2, together are known as interphase (Figure 3) that is responsible for the preparation of cell for the next division. Specifically, the cell is growing in phase G1, and the synthesis of mRNA and proteins required for replication of DNA takes place; in S phase, DNA replication and centrosome duplication occurs; in G2, the quality of DNA replication is checked, the cell continues to grow, and protein synthesis is enhanced. A special case of G1 is phase G0 (gap 0), here the cells are in the resting state, but due to external growth factors they can re-enter into phase G1. Alternatively, the cells may also maintain the G0 state for their whole lifespan.[34,35]

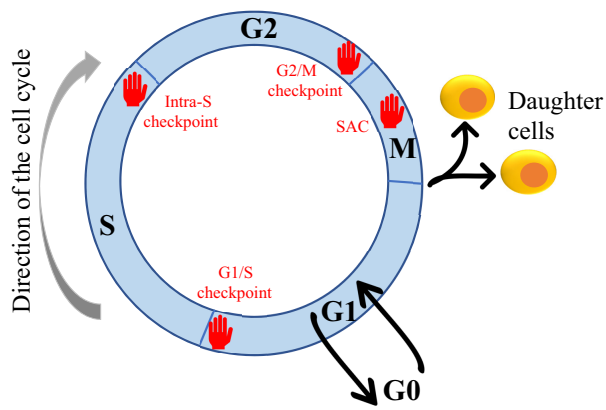

Figure 3. Phases of the cell cycle of eukaryotic cell. 'M' stands for mitosis, red hand images stand for checkpoints.

During the mitosis, the previously synthesized DNA, organelles and cytoplasm are divided between the two daughter cells. Mitosis is further divided into four phases: prophase, metaphase, anaphase, and telophase together with cytokinesis (Figure 4).[34,35] In the first phase, prophase, the chromosomes condence and hence become visible through a transmitted light microscope. Subsequently, the two centrosomes move to the opposite poles of the cell and the mitotic spindle starts to form.[34] Mitotic spindle is a dynamic cell structure that is mainly formed from microtubules and is essential for chromosome segregation.[36] Then, at the beginning of metaphase, the nuclear membrane disappears, and the microtubules of mitotic spindle can associate with sister chromatids. Thereafter, the chromosomes are aligned to the middle plane of the cell by the interplay of forces originating from the mitotic spindle and the chromosomal centromeres. In anaphase, the sister chromatids are allocated to the opposite poles. The last phase of mitosis is telophase together with cytokinesis, during which the cleavage furrow of cell membrane is formed together with the formation of new nuclear envelopes around the separated sister chromatids. Finally, the mitotic cell divides into two daughter cells, whereas each of the latter contains a full set of chromosomes and one centrosome.[34]

As the cell cycle is a crucial process for the cell, it requires a precise control by checkpoints at the certain timepoints of the cycle. The regulation and functioning of checkpoints are carried out *via* the signalling cascades of proteins. This control mechanism detects and, when possible, repairs the defects which are arisen during the cycle, or the cell is sent to the programmed cell death (apoptosis) or cellular senescence (cellular state where the cells cease to divide).[34,35] First, before the cell is ready to enter the S phase, it must pass the G1/S checkpoint which ensures that the cellular 'machinery' is prepared for the DNA replication and DNA is not defective or damaged; otherwise, the entry to the S phase is delayed until the damage is removed, or the cell is sent to apoptosis. Next, the intra-S checkpoint slows down the replication of DNA in order to minimilize the risk of synthesis errors. Before the M phase, the cell must undergo the G2/M checkpoint, which controls the success of DNA replication and checks the readiness for mitosis. The spindle assembly checkpoint (SAC; also known as mitotic checkpoint) in metaphase controls the correct assembly of spindle and ensures that the chromosomes are suitably attached to microtubules of spindle *via* kinetochores, hence ensuring the fidelity of chromosome segregation to generate identical daughter cells.[35–37] The defects in the regulation of checkpoints lead to the genetic damage and uncontrollable cell proliferation, which occurs, for instance, in case of tumor cells (cancer).[34,35,37]

2.2. Mitotic Protein Kinases

The protein signalling cascades that regulate mitotic events transfer the signal mainly through phosphorylation of proteins (*i.e.*, functioning of mitotic PKs) and protein-protein interactions (PPIs). Thus, the mitotic events are regulated by crosstalk of different mitotic PKs.[36,38] The collaboration of mitotic PKs triggers the comprehensive reorganization of cellular structures, covering the chromosome function, spindle assembly, chromosome segregation, and cytokinesis.[38–40] The main PKs that orchestrate mitosis are the following: cyclin-dependent PKs (Cdks), Polo-like PKs (Plks), Aurora PKs, and Never-in-mitosis-A-related PKs (NIMAs) (Figure 4). The relatively new players in control of mitotic events include Haspin (Gsg2) and Greatwall (MAST-L).[36,39,40]

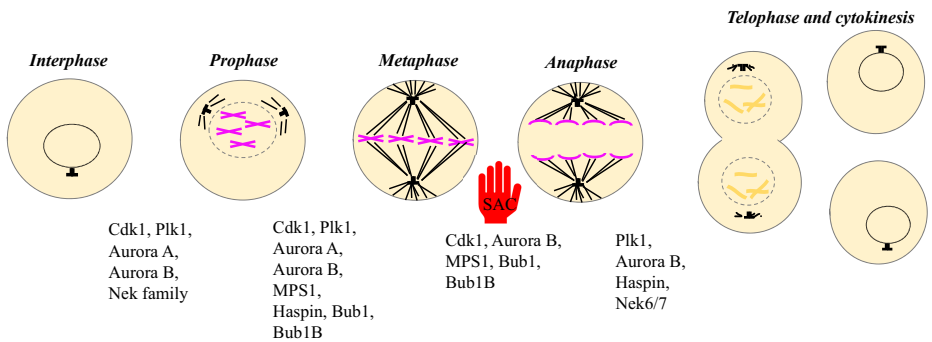

Figure 4. Regulation of mitosis by PKs. Red hand image denotes the spindle assembly checkpoint (SAC).

The activity of PKs is spatiotemporally regulated by post-translational modifications (*i.e.*, autophosphorylation or phosphorylation by upstream PKs, or ubiquitination which leads to the degradation of protein) or PPIs (that alter the activity as well as the cellular location of PKs).[36,38] However, differently from the other ePKs, mitotic PKs often have a divergent highly conserved motif(s) in the activation core (*e.g.*, HRD or DFG motif), which may also point to the unusual mechanisms of regulation of their activity.[36]

Indeed, since the normal regulation of mitosis is crucial for normal functioning of the cell, the elevated level of mitotic PKs can serve as cancer biomarkers, as the cancer cells have a faster life cycle and the cells divide uncontrollably.[35,38] Therefore, the compounds which are able to identify and down-regulate the elevated activity of mitotic PKs are of great interest for diagnosis and treatment of related diseases, especially in cancer.[35,38] In the following paragraphs, the features and functions of Haspin, which is stated to be a key player in mitosis, are discussed in depth.

2.2.1. Haspin

Haploid germ-cell-specific nuclear protein kinase (Haspin; also known as germ cell-specific gene 2 protein or Gsg2; molecular weight of human Haspin is 88,495 Da, it comprises 798 residues[41]) is a basophilic Ser/Thr PK and plays a critical role in the normal progression of mitosis by regulating the behaviour of chromosomes during the cell division.[42] Haspin is encoded by the germ-cell specific gene-2. It was first identified in mice.[43,44] The further genomic analysis has revealed that Haspin is expressed in many eukaryotic organisms, including yeasts, microsporidia, plants, nematodes, flies, fish, amphibians, and mammals. Thereby, the C-teminal lobe where the catalytic domain locates, is more conserved among the species than the N-lobe.[41,42,45–47] In humans, the expression level of the protein is the highest in testis (in particular in round spermatids), but Haspin is abundant in all haploid as well as diploid proliferating somatic cells, including thymus, bone marrow and variety of fetal tissues.[42,45,48]

Haspin belongs to the group of atypical PKs as it has distinctive catalytic core compared to the canonical ePKs. Haspin lacks several highly conserved structural features generally required for catalysis, but also contains some special structural inserts (discussed below). Furthermore, it has low sequence homology to other ePKs; hence, it was initially presumed that Haspin is an inactive pseudokinase. However, the catalytic activity of Haspin was demonstrated in assays with histone H3 (H3), which was phosphorylated by Haspin at *Thr3*, To date, this protein remains the only well-established physiological substrate of Haspin.[48–50] In addition to this site, H3 is phosphorylated at many sites during mitosis, including *Ser10*, *Thr11*, and *Ser28*, whereas the phosphorylation of *Ser10* by mitotic kinase Aurora B is the best known.[48] H3 together with H2B, H2A and H4 form the nucleosomal octamers around which the DNA is orderly packed. The posttranslational modifications of these histones have crucial roles in the regulation of control of chromatin structure, which, in turn, is one of the central processes of cell division. Therefore, not surprisingly, the histones are important targets of PKs that orchestrate mitosis.[49] H3 is phosphorylated by Haspin during prophase and dephosphorylated by PP1γ in anaphase (see below).[41] Notably, the methylation of *Arg2* and trimethylation of *Lys4* of H3 affect the affinity of H3 towards Haspin due to the bulkiness of methylated residues. As a result, the correspondingly modified H3 is not suitable for binding to the narrow substrate site of Haspin and hence the catalytic activity of Haspin is regulated by epigenetic modification of its substrate.[50,51] The distinctive structural features of Haspin as well as its activation and pathways are discussed in the following paragraphs.

2.2.2. Comparison of Crystal Structures of Catalytical Domains of Haspin and PKA

Analogously to other ePKs, Haspin has a bilobal structure consisting of a small N-terminal lobe and a large C-lobe. As mentioned above, the activation segment of ePKs typically consists of ca 35 residues located between the conserved DFG and APE motifs. In particular, it contains ATP/Mg^{2+} binding DFG motif, short β-strand (β9), activation loop, and P+1 loop. Generally, the unphosphorylated activation loop is disordered or fixed to inactive conformation and, when required, the phosphorylation stabilizes the loop appropriately for substrate binding. However, Haspin is featured with variety of unusual structural fragments and inserts that form an atypical catalytic core (Figure 5).

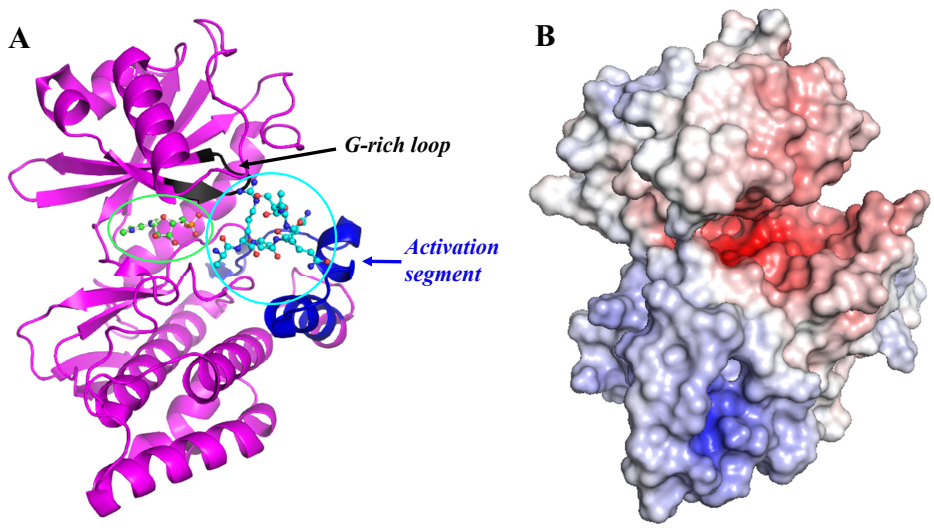

Figure 5. A) Overlay of co-crystal structures of Haspin kinase domain with AMP (PDB 3DLZ) and histone H3(1-7) (PDB 4OUC). PK is shown as a cartoon; AMP and histone H3(1-7) are presented in ball-and-stick mode and surrounded by green and cyan circles, respectively. The G-rich loop is coloured black and activation segment dark blue. B) Electrostatic surface potential of kinase domain of Haspin (PDB 2VUW). Electronegative and electropositive areas are shown with red and blue colour, respectively.

The comparison of catalytically important residues/motifs of Haspin and PKA C discussed in the following text is given in Table 1. First, the highly conserved ATP/Mg^{2+} binding DFG motif (Asp-Phe-Gly) of ePKs is replaced by DYT (Asp-Tyr-Thr). Second, the APE motif (Ala-Pro-Glu; generally locating at the C-terminus of activation segment) and P+1 loop are absent and replaced by a large helical insert (αAS; AAs ***Gln718*** to ***Lys727***) (Figure 6). Third, there is additional β-sheet (β9′) and the activation segment is further stabilized by

aromatic residues. Moreover, the ***Arg648*** in HRD motif (His-Arg-Asp) forms hydrogen bonds with the residues ***Trp733*** and ***Glu735*** locating at the tip of the activation segment, whereas generally the arginine of HRD interacts with phosphates of ATP.[50,52] In the upper lobe of Haspin, there is an additional helical insert (upper lobe helix or α-ulH; AAs ***Tyr569*** to ***Phe593***). While usually the P-loop (G-rich loop (conserved glycines in Haspin ***491***, ***493***, ***496*** and PKA ***50***, ***52***, ***55***) is highly mobile, in Haspin it is stabilized *via* polar interactions of α-ulH, *i.e.*, ***Lys489***, ***Glu492***, ***Asn588***.[50,53] Also, the α-ulH may have the function to regulate the activity of Haspin by binding to the N-terminal tail of Haspin and sterically hinder the binding of substrates and thus regulating the activity of Haspin.[50] Next, the C-lobe contains a β-hairpin insert, which is stabilizing the active conformation of αC-helix, but, at the same time, the C-lobe lacks αG-helix. Overall, the activation segment of Haspin is well-structured and adopts open but stable conformation, which presumably points to the constitutively active conformation of kinase domain of Haspin.[50,52]

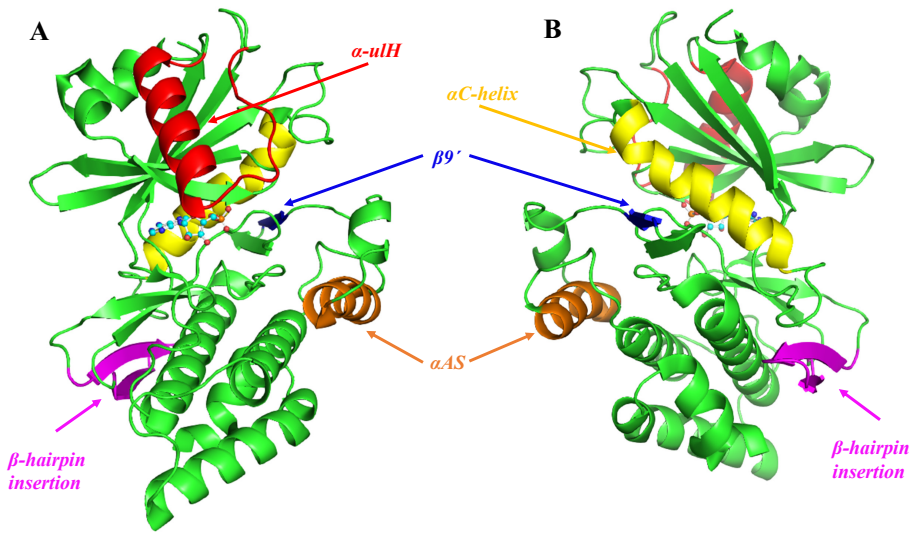

Figure 6. A) Structural features of Haspin on example of co-crystal structure of the kinase domain of Haspin with AMP (PDB 3DLZ). PK is shown as a cartoon; AMP is presented in ball-and-stick mode (C atoms cyan, O atoms red, N atoms blue, P atoms orange). α-ulH is coloured red, β-hairpin insertion magenta, αAS helix orange, β9′ sheet dark blue, and αC-helix yellow. B) Rotated view of A).

As other ePKs, ATP-binding pocket is a narrow groove between the two lobes.[50] The K_M values of ATP towards full-length and trunctated kinase domain of Haspin are given in Table 2. The adenine ring of ATP is bound to the hydrophobic cleft locating between the lobes. The *N1* and *N6* amino groups of adenosine moiety give H-bonds with ***Glu606*** and ***Glu608*** in hinge region (an

analogous interaction with ***Glu121*** and ***Val123*** in PKA co-crystal structure with ATP) (Figure 7). The hydroxyl groups of ribose moiety give interactions with ***Asp611*** (***Glu127*** in PKA), whereas 3′-hydroxyl additionally interacts with ***Gly653*** (***Glu170*** in PKA). Furthermore, the α-phosphate of nucleotide is co-ordinated *via* conserved ***Lys511*** (***Lys72*** in PKA) and, at the same time, ***Lys511*** forms the salt bridge with ***Glu535*** of αC-helix (the latter is a hallmark of active kinase, as discussed above).[50] Next, in Ser/Thr PKs γ-phosphate forms a charge-reinforced hydrogen bond with highly conserved *Lys* (***Lys168*** in PKA, which interacts with γ-phosphate of ATP, aspartate of HRD, activation loop and substrate peptide), and this interaction is required for phosphoryl transfer. However, in Haspin the function of conserved *Lys* is fulfilled by ***His651***.[47,50]

Table 1. Summarizing table of important residues/motifs of Haspin and PKA C discussed in text (PDB 4OUC, 1ATP)

	Haspin	***PKA C***
G-rich loop (GxGxΦG)	^{491}GEGVFG^{496}	^{50}GTGSFG^{55},
DFG	^{687}DYT^{696}	^{184}DYT^{186}
Y/HRD	^{647}HRD^{649}	^{164}YRD^{166}
APE	- (αAS: *Gln718* to *Lys727*)	*206-208*
β3-Lys – αC-Glu pair	*Lys511 – Glu535*	*Lys72 – Glu91*
Activation segment	*687-726*	*184-208*
***N1* and *N6* amino groups of adenosine moiety**	*Glu606* and *Glu608*	*Glu121* and *Val123*
Hydroxyl groups of ribose moiety	*Asp611* *Gly653*	*Glu127* *Glu170*
α-phosphate of nucleotide	*Lys511*	*Lys72*
Intracatalytic loop salt bridge	*Asp649 – His651*	*Asp166 – Lys168*

In addition to the previously mentioned polar contacts, the nucleotide ring system is stabilized by hydrophobic and π-π interactions with aromatic AAs of Haspin (*e.g.*, ***Phe607***, ***Tyr688***, ***Trp652***, ***Val704***, ***Leu710***, ***Phe719***, ***Tyr722***, ***Trp733***).[50,52] Notably, in Haspin structure there is no Mg^{2+} binding site in vicinity of DYT motif; however, a Mg^{2+} ion is coordinated by ***Asp716***, ***Gln718***, ***Trp652***, and ***Tyr747*** in the interface of catalytic loop. Therefore, it is suggested that the divalent metal ion is still essential for the stabilization of active state of Haspin.[50]

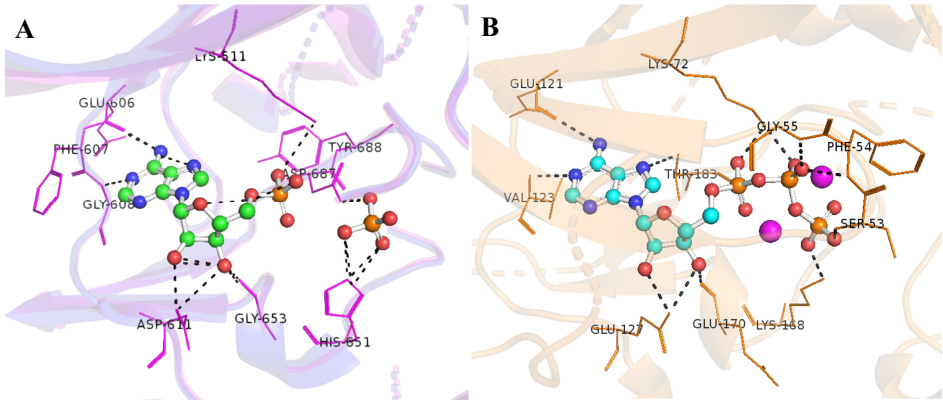

Figure 7. Comparison of interactions of nucleosidic molecule bound to ATP-site of Haspin or PKA C. A) Co-crystal structure of kinase domain of Haspin with AMP (PDB 3IQ7, 3DLZ). PK is shown as magenta (PDB 3DLZ) and blue (PDB 3IQ7) cartoon. B) Co-crystal structure of PKA C with ATP (PDB 1ATP). PK is shown as orange cartoon. Residues of PKs forming interactions with the co-crystallized small molecules are shown as lines and are labelled; hydrogen bonds are shows as black dotted lines. Mn^{2+}-ions are shown as magenta circles (note: no electron density can be observed for Mg^{2+}-ion(s) near ATP-site in co-crystal of Haspin with AMP).

The substrate-binding site of Haspin is located on the surface of the C-lobe. The K_M values of H3 peptide towards full-length and trunctated kinase domain of Haspin are given in Table 2. As the activation segment contains several acidic AAs (***Asp707***, ***Glu708***, ***Asp709***) but lacks P+1 loop and APE motif, it leads to the formation of the highly negatively charged narrow substrate-binding loop. In this way, the substrate pocket of Haspin is ideally suited for binding of basic N-terminal tale of H3 (Figure 5).[48–50] The co-crystal structure of Haspin with N-terminal peptide of histone H3(1-7) [H3(1-7)] revealed a unique U-turn shape binding mode of histone peptide (sharp ca 180° turn at *Lys4*) when positioned to Haspin (Figure 8). Such binding mode is distinct from substrates of other PKs (*e.g.*, PKI(5-24) as an analogue of substrate of PKA C, Figure 8). In particular, *Lys4* is positioned into pocket lined by kinase residues that develop hydrophobic interactions (***Leu690***, ***Val704***, ***Leu710***) as well as charge-reinforced hydrogen bonds (***Asp707***, ***Asp709***) to the alkyl chain and amine group of *Lys4*, respectively. Moreover, *Gln5* forms hydrogen bond with ***Asp714*** and *Thr6* flips back over *Arg2*. Next, *Ala1* (H-bonded with ***Glu613***) and *Thr3* (H-bonded with ***Asp649*** and ***Gln718***) are directed inside the substrate binding cleft. *Arg2* is located in the relatively deep hydrophobic pockets of the N-terminal lobe formed between the two loops of the kinase (***Val494*** from the G-rich loop and ***Ala587*** from the loop preceding α-uIH helix). However, the side-chain of *Arg2* protrudes to the N-lobe, while its guanidine group and the carboxyl oxygen develop H-bonds with ***Asp588*** and ***Gln718***, respectively.[54]

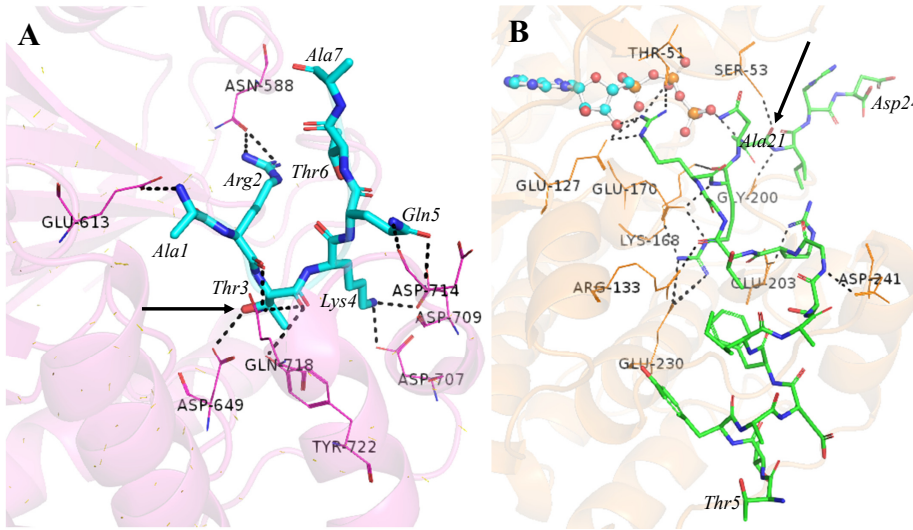

Figure 8. Comparison of substrate-sites of Haspin and PKA C. A) Co-crystal structure of Haspin with H3(1-7) (PDB 4OUC). B) Co-crystal structure of PKA C with ATP and PKI(5-24) (PDB 1ATP). PKs are shown as cartoons; ATP is depicted in ball-and-sticks mode (C atoms cyan, O atoms red, N atoms blue, P atoms orange); H3(1-7) and PKI(5-24) are shown as sticks; residues of peptides are shown in *Italic* [note: in case of PKI(5-24) only *Thr5*, *Asp24* and *Ala21* are marked for clarity]; the locations corresponding to phosphorylatable residues are indicated with black arrows [note: in case of PKI(5-24) the phosphorylatable residue is replaced with Ala (*i.e.*, *Ala21*)]; residues of PKs forming interactions with the co-crystallized peptides are labelled and shown as lines; hydrogen bonds are shown as black dotted lines.

Table 2. K_M^{app} values of ATP towards Haspin and PKA C and K_M^{app} values of histone H3 or Kemptide towards Haspin or PKA C

Construct	***K_M^{app} (ATP) μM***	***K_M^{app} (histone H3 or Keptide) μM***
Haspin(452-798)[52]	180 ± 18	0.7 ± 0.03 histone H3(1-50)-GST
His_6-Haspin(470-798)[50]	55	0.35 histone H3(1-21)
GST-Haspin(452-798)[55]	180 ± 23	ND
MBP-Haspin(full-length)[50]	290	0.058 histone H3(1-21)
MBP-Haspin(full-length)[56]	200	0.098 histone H3(1-21)-biotin
Wild-type PKA C[57]	17 ± 5	20 ± 8 Kemptide (LRRASLG)
His_6-PKA C[57]	14 ± 6	20 Kemptide (LRRASLG)

K_M^{app} – apparent Michaelis-Menten constant; ND – not determined; His_6 – hexahistidine tag; GST – glutathione S-transferase tag; MBP – maltose-binding protein tag.

The reported consensus sequence of Haspin substrates is Ala/Val-Arg-*Ser/Thr*-Lys-(X-noAsp/Glu), where *Ser/Thr* denotes the phosphorylatable residue and X corresponds to any AA except Asp or Glu[54] (for comparison: the consensus sequence of substrates of PKA is Arg–Arg/Lys–X–*Ser/Thr*-Leu/Ile[58]). Based on this, the sequence of N-terminal tail of H3 is in complete agreement with the key consensus sequence of Haspin. Notably, based on the aforementioned consensus sequence, their location in mitotic cells and the supporting mass spectrometric studies, the centromere protein T (CENP-T; AAs *Thr14/27/57* and *Ser72*) and histone H2A (*Thr16*) are also possible substrates of Haspin.[54] Recently, Hada and co-workers have demonstrated that Haspin was responsible for phosphorylation of TH2A (germ cell-specific variant of H2A) at *Thr127 in vivo*.[59]

2.2.3. Regulation of Haspin Activity and The Role of Haspin in Cellular Pathways

In agreement with the aforementioned Haspin-catalyzed phosphorylation of *Thr3* of H3 (H3T3), it has been reported that the application of siRNA of Haspin leads to the decrease of phosphorylation of H3T3. Moreover, the depletion causes delocalization of cohesin and the members of chromosomal passenger complex (CPC; discussed below) from centromeres, increased amount of monoorientated sister chromatid pairs, misalignment of chromosomes in metaphase, the activation of SAC, and mitotic arrest.[48,49,60–62] On the other hand, the overexpression of Haspin causes increased stabilization of chromosome arm cohesion, abnormal dissociation of sister chromosomes, and mitotic delay before anaphase. Besides, in case of overexpression of Haspin, phospho-Thr3 of H3 (pH3T3) is detectable throughout the cell cycle, whereas normally it is only detectable between the late G2 and anaphase.[48,49,63,64] Surprisingly, the experiments with Haspin knock-out mice have shown the normal fenotype as well as fertility of animals; however, the lack of Haspin may be balanced by other, but to date still unknown mechanisms.[65]

As previously discussed, large number of ePKs require (auto)phosphorylation of the activation loop to obtain the catalytic activity. However, in case of Haspin this regulation mechanism is unlikely as in the co-crystal of catalytic domain, the activation segment is structured by the surrounding interactions (*e.g.*, salt bridge, hydrophobic interactions) and hence is in constitutively active conformation.[50,52] Human Haspin is expressed nearly on a constant level throughout the cell cycle, but its activity peaks in mitosis.[48,50] In interphase, Haspin is found in nuclei and during mitosis it is located to condensed chromosomes throughout the process, to the centromeres during nuclear envelope breakdown, to spindle microtubules in metaphase, and to the midbody in telophase.[49] Overall, in early mitosis Haspin becomes associated with condensed chromosomes and is mainly concentrated in central regions, but also locates along the chromosomal arms in smaller amounts.[49] Such ‘traveling’ of Haspin during the cell cycle is associated with the sister chromatid cohesion protein

Pds5, through which Haspin is recruited to centromeric chromatin.[66,67] As previously mentioned, H3T3 is phosphorylated at the beginning of mitosis (during prophase) and dephosphorylated in anaphase.[41] If Haspin is constitutively active, the molecular mechanism that temporarily restricts the appearance of pH3T3 just to mitosis is still unclear. In the following text, a brief overview of the present knowledge is introduced.

Ghenoiu and co-workers proposed that the activity of Haspin is autoinhibited in interphase by a basic inhibitory segment next to the kinase domain. The interruption of autoinhibition of Haspin is initiated by a priming phosphorylation of the N-terminal domain by cyclin-dependent PK type 1 (Cdk1; activated by cyclin B upon entry to mitosis), following the recruitment of Polo-like kinase (Plk1), which, in turn, mediates the further abundant phosphorylation of N-lobe at multiple sites. Consequently, the basic inhibitory segment of the N-lobe is unfolded from the C-lobe and hence the steric blocking of catalytic core is removed. Thereafter, Haspin is able to achieve its full catalytic activity.[68] Nevertheless, this hypothesis does not explain why the overexpressed Haspin phosphorylates H3T3 at each stage of the cell cycle, and why the recombinant full-length Haspin is featured with catalytic activity. However, the latter phenomenon may be, in turn, affected by possible impact of affinity tags on the interactions between the N- and C-termini.

The second theory suggests that the N-terminal domain of Haspin is directly phosphorylated by mitotic kinase Aurora B. At the same time, Aurora B-mediated phosphorylation does not influence the activity of recombinant Haspin *in vitro*, but leads to the increase of level of pH3T3 in cells. It has been proposed that such outcome is achieved 1) by displacing an unknown inhibitory protein, which binds to Haspin in interphase, or 2) by enabling the access of Haspin to nucleosomal H3 in cells.[62] Aurora B is a Ser/Thr PK that is a key player in mitosis and mediates the chromosome attachment to spindle. Also, it has an outstanding role in pathways of Haspin (Figure 9).

In particular, Aurora B is a member of CPC, which also incorporates the Inner Centromere Protein (INCENP), Borealin and Survivin.[69,70] The localization of CPC changes throughout the cell cycle, whereas its correct localization ensures the spatiotemporal control of phosphorylation of substrates involved in the repair of errors of interactions between chromosomes and microtubules, activation of SAC, and regulation of contractile mechanisms that lead to cytokinesis.[69] Haspin starts to phosphorylate H3T3 in late G2/early prophase, whereas in late prophase pH3T3 is spread along the chromosome arms.[63,70,71] The phosphorylation of H3 at *Ser10* (pH3S10) catalysed by Aurora B disrupts interaction of the heterochromatin protein 1 (HP1) with H3 and dispelles HP1 from chromatin (Figure 9). Consequently, H3 is released and H3T3 phosphorylation by Haspin is favoured.[70,72] Next, the pH3T3 binds to Survivin leading to the recruitment of CPC to centromere.[61,70,73] Furthermore, the CPC localization to centromere is facilitated by interaction with Shugoshin *via* Borealine, whereas the latter binds the histone H2A which is phosphorylated at *Thr120* by the PK named budding uninhibited by bemoyl 1 (Bub1).[70,74] At the same time,

the phosphorylation of Haspin by Aurora B acts as a positive feedback loop by facilitating the formation of pH3T3.[62,70]

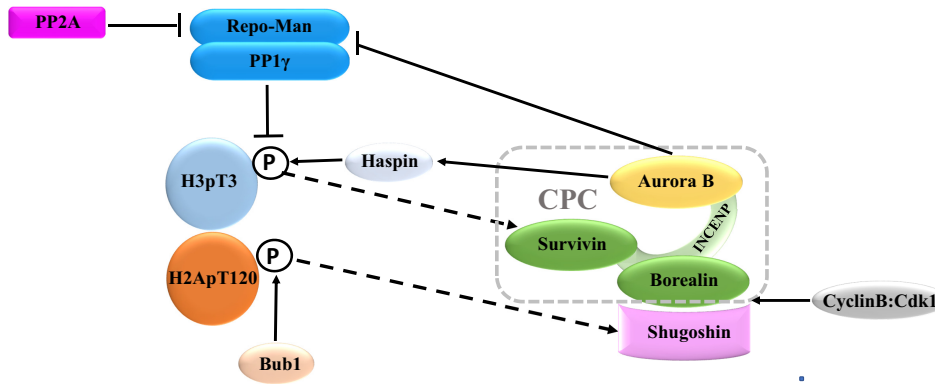

Figure 9. Illustrative scheme of Haspin-involving pathways in prometaphase/metaphase. Normal arrow indicates activation, enhancement, facilitation of interaction; blunt-ended arrow indicates inactivation or depletion; dashed arrow indicates recruitment.

Then, during the transition to prometaphase, the pH3T3 disappears from the chromosome arms and concentrates to the inner centromeres due to the phosphatase activity: dephosphorylation of pH3T3 is regulated by protein phosphatase PP1γ including its regulatory subunit Repo-Man.[66,70,75] Repo-Man is, in turn, phosphorylated by Aurora B; this phosphorylation inactivates Repo-Man in close proximity to Aurora B pool, prevents chromosomal localization of Repo-Man and hence contributes to increase of level of pH3T3.[70,76] Moreover, Repo-Man interacts with phosphatase PP2A and thereby can locally reverse Aurora B action by allowing the removal of pH3T3 from chromosome arms during prometaphase.[70,76] Overall, the intersection of Haspin, Aurora B and phosphatase pathways regulate the level of pH3T3 and allow the enrichment of pH3T3 as well as CPC at the inner centromeres, thus ensuring the fidelity of progression of mitosis (Figure 9).[74]

Finally, when the criteria of SAC are passed, the cell is ready to enter anaphase. Thereby, the cell division control protein 20 (Cdc20) activates the proteases that degradate different proteins, including cyclin B (activates Cdk1, see above), hence changing the ensemble of intracellular proteins – and before the beginning of new mitosis, Haspin has no prominent function.[70]

3. Inhibitors of Protein Kinases

3.1. General Characteristics

An inhibitor of enzyme is a compound which binds to the enzyme, such as PK, and thereby disables the enzymatic catalysis by preventing the binding of (co-)substrates and/or changing the 3D-structure of enzyme. The inhibitors of enzyme are applied *in vitro* as well as *in vivo* assays to reduce the activity of enzymes and look into the function and signalling pathways of biological catalysts. Furthermore, inhibitors are used to quantify the amount of different enzymes in biochemical assays or in natural milieu.[77] Nevertheless, when using inhibitors *in vivo* assays, it must be taken into consideration that the potency (expressed as K_i or IC_{50} value[1]) as well as selectivity of inhibitor may be remarkably affected by different factors, *e.g.*, the cell plasma membrane-penetrative properties or intracellular stability of inhibitor.[78] Inhibitors are divided into different classes based on the origin (natural or synthetic), binding character (reversible or irreversible), mechanism of binding relative to (co-)substrates of enzyme (competitive, uncompetitive or semicompetitive), and positioning of inhibitor in the complex with enzyme (types I–V).[77]

3.2. Classes of Inhibitors of Protein Kinases

In inhibitor development, there are two directions, first, to develop an inhibitor with a relatively wide selectivity profile targeting a specific family of PKs; second, to develop an inhibitor with narrow selectivity profile possessing high affinity against a specific family member. There is no overall consensus about the acceptable level of selectivity, however, Parang and Sun stated that the selective inhibitor should exhibit at least 100-fold selectivity towards desired target over other kinases.[79] Still, even when the inhibitor shows high selectivity towards a panel of PKs in biochemical assays, its is not guaranteed that the inhibitor is maintaining its selectivity properties in cellular environment with high complexity.[79]

As PKs catalyse the phosphorylation reaction, binding of both the phosphoryl group donor ATP as well as the acceptor substrate protein to the enzyme is required for the reaction to occur. There are different strategies in inhibitor design and development to block or reduce the extent of phosphorylation reaction catalysed by PKs. A frequently used classification is based on the site that the inhibitor is targeting: ATP-binding pocket, substrate-binding pocket, or both simultaneously (bisubstrate inhibitors). Also, inhibitors that bind outside the canonical catalytic core of the PK (allosteric inhibitors) have emerged,

[1] IC_{50} value is A) the concentration of inhibitor at which the rate of phosphorylation reaction is half of maximum (in inhibition assays), or B) the concentration of competitor at which the amount of complex of fluorescent probe and kinase is half of maximum (in binding assays).

which change the conformation of PK and thereby counteract the binding of substrates.[4,79,80] Another classification of PK inhibitors that groups them to types I – V is based on positioning of the inhibitor in complex with the enzyme (Table 3).[1,4,78,80–82] As mentioned above, 39 small-molecule inhibitors of PKs targeting one or multible kinases are approved by FDA for clinical use.[1,2] In the following paragraphs, the properties of ATP-site binding inhibitors, substrate-binding site inhibitors, and bisubstrate-analogue inhibitors are discussed.

Table 3. Classification of inhibitors based on the structure of enzyme-inhibitor complex

Type of Inhibitor	*Binding Features*	*Reversibility (+/-)*
Type I	Inhibitor binds to ATP-pocket of active conformation of PK	+
Type I ½	Inhibitor binds to ATP-pocket of inactive conformation of PK (DFG in)	+
Type II	Inhibitor binds to ATP-pocket of inactive conformation of PK (DFG out)	+
Type III	Inhibitor binds to site next to ATP-pocket (allosteric inhibitor)	+
Type IV	Inhibitor binds far away from ATP-pocket (allosteric inhibitor)	+
Type V	Inhibitor occupies 2 sites (bivalent inhibitor)	+

3.2.1. Inhibitors Targeting ATP-Site of PKs

ATP-binding cleft is located between the two catalytic lobes and during the binding of ATP to PK, two nitrogen atoms of adenine moiety of ATP form hydrogen bonds with the hinge backbone residues (Figure 2, Figure 7). The similar binding mode is generally maintained in the structure of ATP-mimetic inhibitors.[4,16,79] The targeting of ATP-pocket of PKs in cellular environment was first successfully demonstrated by ATP-competiting inhibitors, *e.g.*, staurosporine and H89 (Figure 10), and to date the majority of inhibitors of PKs developed are targeting ATP-binding site of PKs.[4,7,83] Still, as the ATP-binding pocket is relatively highly conserved among PKs that share a large portion of common sequence and structural homology, it was initially presumed that design of the selective ATP-mimetic inhibitors is challenging or rather impossible.[6] Additionally, the efficiency of ATP-mimetic inhibitors is decreased *in situ* due to their competion with high intracellular concentration of ATP (2–10 mM).[79] However, the discovery and approval of clinical use of imatinib (Gleevec, STI-571; Figure 10) in 2001 for the treatment of chronic myelogenous leukemia paved the road for the development of selective ATP-site inhibitors.[84] Nevertheless, in oncology the exposure of ATP-site targeting drugs may lead to mutations in ATP-pocket which can either render binding of ATP more effective, or sterically preclude binding of inhibitors. This situation is called ‘acquired drug resistance’, in which case the tumor initially shrinks in response to the exposure of drug, but eventually starts to increase again.[4,55,85,86]

The tumor resistant to one drug might, however, lack resistance to another drug targeting the same oncogenic kinase – therefore, the development of novel inhibitors of PK featuring versatile scaffolds remains in the limelight.

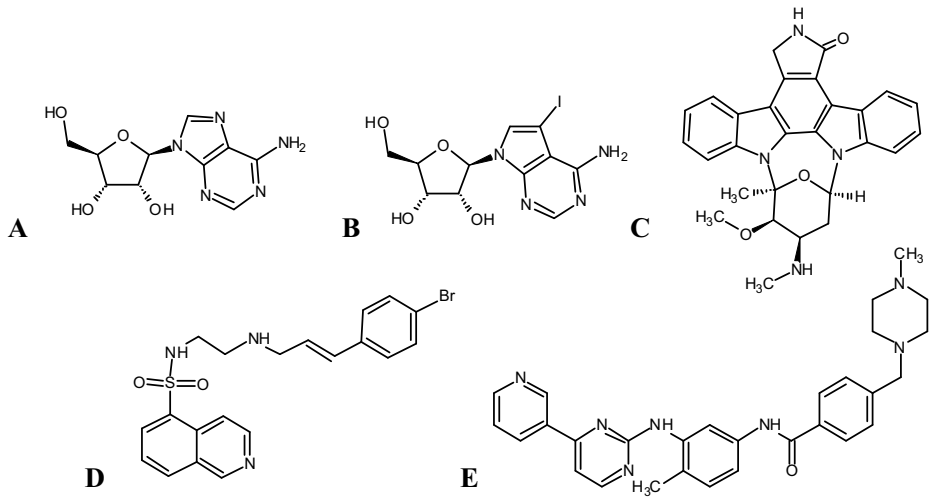

Figure 10. Structures of adenosine (A), 5-iodotubercidin (B), staurosporine (C), H89 (D), and imatinib (E).

The first crystal structure of the active site of a PK (PKA C) was published in 1991.[21] Now, in total, more than half of the kinome is covered by the available crystal structures[87,88] that has revealed the structural diversity of the members of the superfamily of PKs. This knowledge has driven to the structure-guided construction of PK inhibitors. Several regions of PKs, especially the hydrophobic regions adjacent to ATP-binding cleft and the essential gatekeeper residue of ATP-pocket, can be exploited to achieve the selectivity of ATP-mimetic inhibitors.[4,80]

The gatekeeper key residue locates near the hinge connecting the large and small lobes of kinase and closes the access to the hydrophobic 'back pocket' of ATP site. The size of side chain of this AA is crucial: the smaller the residue, the larger the size and higher the accessibility to the hydrophobic pocket behind the ATP-site. Relatively small gatekeeper residue (*e.g.*, Gly, Ala, Ser) results in more spacious ATP-binding site and provides access to the rear part of hydrophobic pocket. On the other hand, when the gatekeeper residue is AA with a large side chain (Phe, Tyr), the accessibility of inhibitors is largely restricted.[4,80]

It is also possible to target the different conformational forms of certain PKs, *i.e.*, the active or inactive forms of PK. One of the important differences between these two states is the rearrangement of highly conserved DFG motif required for the binding of ATP/Mg^{2+}. In particular, the active form is generally

well-characterized and its structure is similar among PKs. As a result of phosphorylation of regulative Ser, Thr or Tyr residues, DFG motif is rotated to its 'in' = 'open' conformation. In active conformation of PK, the side chain of aspartate residue of DFG motif is directed into the ATP-pocket and coordinates Mg^{2+} together with allowing the binding of peptide/protein substrate. Furthermore, the active conformation is usually relatively rigid, which is required to enable the exact positioning of catalytically important residues. This feature is also used to design the compounds which securely fit into the more rigid ATP-pocket (type I inhibitors, see above). In inactive conformation of PK, DFG motif is roted by approximatly 180 degrees (DFG 'out' = 'closed') resulting in closed conformation of the activation loop and formation of additional binding pocket adjacent to ATP-site.[4,79,80]

Initially, it was assumed that the DFG 'out' conformation is unique for certain PKs and the compounds targeting the surrounding binding pocket of ATP-site (type II inhibtors, see above) are endowed with increased selectivity. However, it has been recently concluded that the inactive conformation of PKs can be targeted by different scaffolds, which probably reflects high dynamics of binding pocket; therefore, type II inhibitors may not offer a clear advantage over type I inhibitors in the development of highly selective compounds.[80,89]

Development of inhibitors for Haspin has not been considerably intense, but some successful efforts have been disclosed. Most Haspin targeting inhibitors are directed to the ATP-binding site. The most well-known inhibitor for Haspin is 5-iodotubercidin (5-ITu), which was, however, initially identified both as an inhibitor (IC_{50} = 26 nM) and a substrate for adenosine kinase (ADK) (see below in section *5. PK Selectivity of Itc-Incorporating Conjugate* [Paper III: Kestav *et al*., 2017]). [90–92] Other Haspin-targeting ATP-site inhibitors include β-carboline derivatives, acridine analogues, and imidazopyridazine derivatives (reviewed in [3,93]).

3.2.2. Inhibitors Targeting Substrate-Binding Site of PKs

Indeed, as the ATP-pocket is conserved among proteins of the superfamily of PKs, another strategy of inhibitor development is targeting of the substrate-binding site of PK – as the interactions between the kinase and substrate should vary considerably among different kinases. One strategy is to use peptides or peptidomimetics, which compete with substrate and disrupt protein-protein interactions (PPIs).[94] As PKs phosphorylate the substrates incorporating a certain amino acid sequence (so-called key sequence or consensus sequence, see above), therefore, peptides and their analogues imitating the substrates can serve as substrate-competive inhibitors.[95,96]

The inhibitors targeting substrate binding site of PKs may have an advantage over ATP-mimetics, since the intracellular concentration of protein substrate is remarkably lower compared to the concentration of ATP.[6,79] On the other hand, the substrate binding site of PKs occupies larger area than ATP-site, sometimes

including the grooves on the surface of both, N- and C-teminal lobes of PK. Therefore, to achieve the high affinity, the inhibitor must be sufficiently large as the generated interactions must compensate the energy loss resulting from the removal of structured water layer on the surface of PK. This is a significant shortcoming, as the large molecules often lack the plasma membrane-penetrating properties and the natural substrate imitating peptides are often unstable against the proteolytic degradation in cellular environment.[58,95] However, the stability of peptides can be remarkably improved by using peptidomimetics containing non-proteinogenic AAs or D-amino acids, as well as compounds with altered backbone.[97–99]

One of the first discovered substrate-site binding inhibitors is thermo-stable protein kinase inhibitor peptide or PKI (molecular weight of full length murine PKI is 8 kDa; three isoforms α/β/γ), which is a natural inhibitor of PKA (K_i value of PKIα is 0.2 nM).[100,101] PKI includes the sequence of Arg-Arg-Asp-Ala-Leu, resembling the key sequence of substrates of PKA (Arg–Arg/Lys–X–Ser/Thr-Leu/Ile, where X corresponds to any AA).[58,100] The high affinity of PKI towards PKA is also attributed to the amphiphatic helix that precedes the consensus site, *i.e.*, locates in the N-terminal of consensus sequence.[102]

3.2.3. Bisubstrate Inhibitors

Bisubstrate inhibitors contain two fragments which are covalently linked by a linker, whereas one fragment binds to the ATP-pocket and another to the substrate-binding site. The development of bisubstrate inhibitors is based on the concept that the fragments of inhibitor bind to distinct but still adjacent pockets in the active core of enzyme. As a result of successful design, both fragments maintain their interactions with enzyme.[79,103] The advantage of bisubstrate inhibitors is the synergistic effect compared to the separate components: the free energy of binding of bisubstrate inhibitor is the sum of the binding free energies of separate fragments together with reduced entropic penalty achieved through the interactions of one molecule instead of several fragments with protein.[104] Additionally, the binding of one linked fragment increases the local concentration of another fragment near the corresponding binding site and thus elevates the probability of binding event. When the two fragments are linked by an appropriate linker, the affinity of the obtained conjugate may be around 6 orders of magnitude higher compared to the individual molecules (*i.e.*, when the affinity of individual fragments is at the range of mM, then the suitable linking may endow a conjugate with nM range of affinity).[79,103,105] However, when the length of the linker is not optimal, it precludes simultaneous binding of the fragments of conjugate and thus leads to the loss of achieved improvement in affinity of bisubstrate-type inhibitors. Furthermore, the linker must be sufficiently long and flexible to maintain the conformational mobility of enzyme-inhibitor complex.[106]

The bisubstrate nature of inhibitor towards corresponding PK can be confirmed mainly by three different methods: 1) evaluation of co-crystal structure of inhibitor with PK, 2) kinetic analysis of competiveness of inhibitors *versus* both substrates, and 3) displacement of conjugate from its complex with PK by both an ATP-competive inhibitor and substrate-site targeting inhibitor.[103] From the co-crystal structure of bisubstrate inhibitor with the PK, it is directly possible to show whether the fragments of conjugate occupy the desired substrate-binding sites of kinase or not.[103,107–109] In kinetic analysis, the inhibition mechanism of bisubstrate inhibitor is determined. For this, the phosphorylation level of substrate is monitored, whereas in case of the inhibition pattern of conjugate *versus* ATP is determined, the concentration of ATP is varied, but at the same time the concentration of substrate is kept constant and *vice versa*.[110] Differently, displacement format of an assay requires labeled form of an inhibitor (*e.g.*, using a fluorescent dye) that can then be competitively displaced from its complex with the kinase by increasing concentrations of ATP or substrate peptide/protein.[111,112]

The first bisubstrate inhibitors were developed in 1970s.[113,114] These inhibitors were the analogues of transition-states occurring during the transfer of phosphoryl group from ATP to substrate: the design was based on the assumption that the transition state complex represents the best geometry leading to the decrease of activation energy of catalyzed reaction.[103,115]

The approach where a potent ATP-competing inhibitor was incorporated into the structure of a bisubstrate inhibitor was first used by research group of A. Ricouart in 1991, who linked an isoquinoline sulphonamide-derived ATP-competitive inhibitor H9 (K_i value towards PKA C was 2 μM) with hexa-L-arginine peptidic fragment (the peptide alone possessed mM range of affinity) by using β-alanine and L-serine in the structure of linker. The K_i value of the resulting conjugate towards PKA C was 2 nM.[103,116]

The most well-characterized subtype of bisubstrate inhibitors of PKs are adenosine analogue-oligoarginine conjugates or ARCs developed by Uri and co-workers. The initially developed ARCs were composed of an adenosine analogue (a derivative of adenosine, *e.g.*, Adc, or ATP-competitive inhibitor of target PK), an oligoarginine peptidic fragment, and hydrophobic linker(s) (Figure 11).[103,117] The oligoarginine fragment in the structure of ARCs was necessary for targeting basophilic PKs. Furthermore, it provided the conjugates with properties of arginine-rich cell-penetrating delivery peptides[118], thus enabling the use of compounds in cellular milieu.[119–125] The conjugates incorporating the oligoarginine fragment possessed wide selectivity profile, which could be used, for instance, for development of relatively generic fluorescent probes applicable in biochemical assays.[119–125]

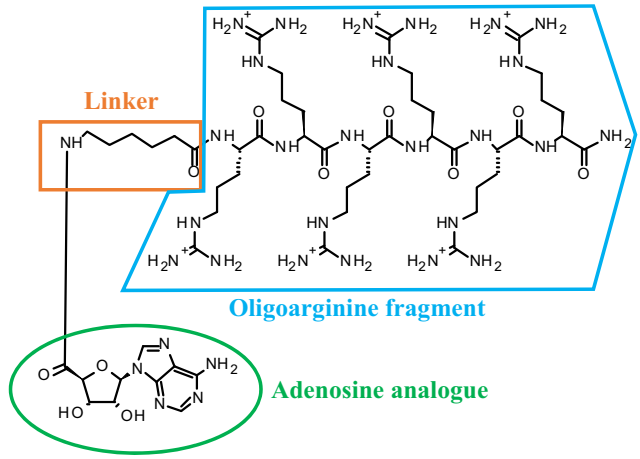

Figure 11. Structure of ARC shown on the example of **ARC-902**.

The subsequent structural modifications and rational design guided by the co-crystal structures of ARCs with target PKs[108,109,126–128] have led to the remarkable increase in stability and affinity of compounds, and, at the same time, allowed tuning of the selectivity of conjugates towards different PKs. To start with, first generation ARCs incorporated L-amino acids in peptidic part, but their replacement with D-counterparts improved significantly the stability of conjugates for proteolytic degradation.[117,121] Next, with the aim to increase the selectivity as well as affinity of conjugates towards specific PKs, the chiral spacer separating two linkers was introduced into the structure of ARCs.[126,127,129] The chiral spacer was obligatory to direct the peptidic fragment of conjugate towards the substrate-site. Finally, the affinity and selectivity of ARCs was successfully tuned by varying the ATP-binding fragment of conjugates with the aim to obtain selective compounds (*e.g.*, Fasudil for Rho-kinase) or, *vice versa*, generic conjugates (*e.g.*, H9).[121,126,128–132] The most recent development in structures ARCs is the replacement of oligoarginine fragment of conjugates with a peptide preferred by the specific target PK (*e.g.*, oligoaspartate or oligoaspartate-imitating peptoid fragment for targeting acidophilic PK CK2).[108,130,132] The latter principle was also applied within this work, taking into account the peptidic preferences of Haspin.

ARCs have been successfully applied as auxiliary reagents in different biophysical and biochemical assays as well as in cellular environment (*e.g.*, live cells, cell lysates).[111,112,122–125,133–138] The methods utilizing ARCs that were applied during this study are discussed in detail in *Methods* under section *2. Biochemical Assays with Detection of Photoluminescence*.

AIMS OF THE STUDY

The aims of the current study were the following:

- biochemical screening of the initial set of ARCs towards Haspin, whereas ARCs represented variable structural scaffolds;
- co-crystallization of Haspin with the most potent conjugates from the initial set;
- rational design of Haspin-selective conjugates and fluorescent probes based on the co-crystal structures of Haspin;
- co-crystallization of novel conjugates with Haspin;
- determination of kinetic properties of association and dissociation of conjugates and fluorescent probes to/from Haspin;
- selectivity studies of novel Haspin-targeting conjugates.

METHODS

1. Synthesis of Compounds

1.1. Solid Phase Peptide Synthesis

The main principles of solid phase peptide synthesis (SPPS) were first published in 1963 by R. B. Merrifield[139], who received the Nobel Prize in Chemistry in 1984. Initially, the method was used to synthesize 'classical' oligopeptides on insoluble support, but to date an increasing number of structural scaffolds representing the peptide analogues (*e.g.*, peptoids)[130,140], oligonucleotides[141,142], *etc* have been assembled by using SPPS.

The synthesis of peptides is carried out on solid polymeric supports (so-called resins; *e.g.*, cross-linked polystyrene-divinylbenzene copolymer), which must be insoluble when immersed in solvents of synthesis but show good swelling properties in these solvents, and, at the same time, be inert to all the reactions performed. Usually, aprotonic solvents with an intermediate or low polarity are used for coupling reactions (*e.g.*, *N,N*-dimethylformamide, DMF or dichloroethane, DCE). Onto the surface and inside the resin beads, a certain amount of reactive groups are introduced onto which the synthesized chain can be assembled. The amount of such centres in moles per mass unit of resin is termed as loading of resin.[143,144] The loading of resin must be as high as possible in order to reduce the cost of synthesis. However, too high loading may cause the steric hindrance to the growing chain (*i.e.*, synthesized peptide) and hence the assessibility of reagents to reaction centres is prevented. This situation is leading to the decrease of yield and should whenever possible be avoided by keeping the loading optimal in relation to length of the synthesized peptide.

The peptide synthesis is carried out in the direction from C- to N-terminus. In order to facilitate the diffusion of reagents to the reaction centres, spacers or peptide linkers are used, elongating the distance between the matrix and the reactive groups and also introducing suitable modifications (*e.g.*, amidation) to the C-terminus of the synthesized sequence (Figure 12).[143] On the other hand, the synthesis of peptide libraries in peptide microarrays by using SPPS can also be performed right on the microchip plate (*i.e.*, without usage of resin), hence allowing the performance of a large amount of parallel syntheses and subsequent high throughput screening on the same microchip plate.[145,146]

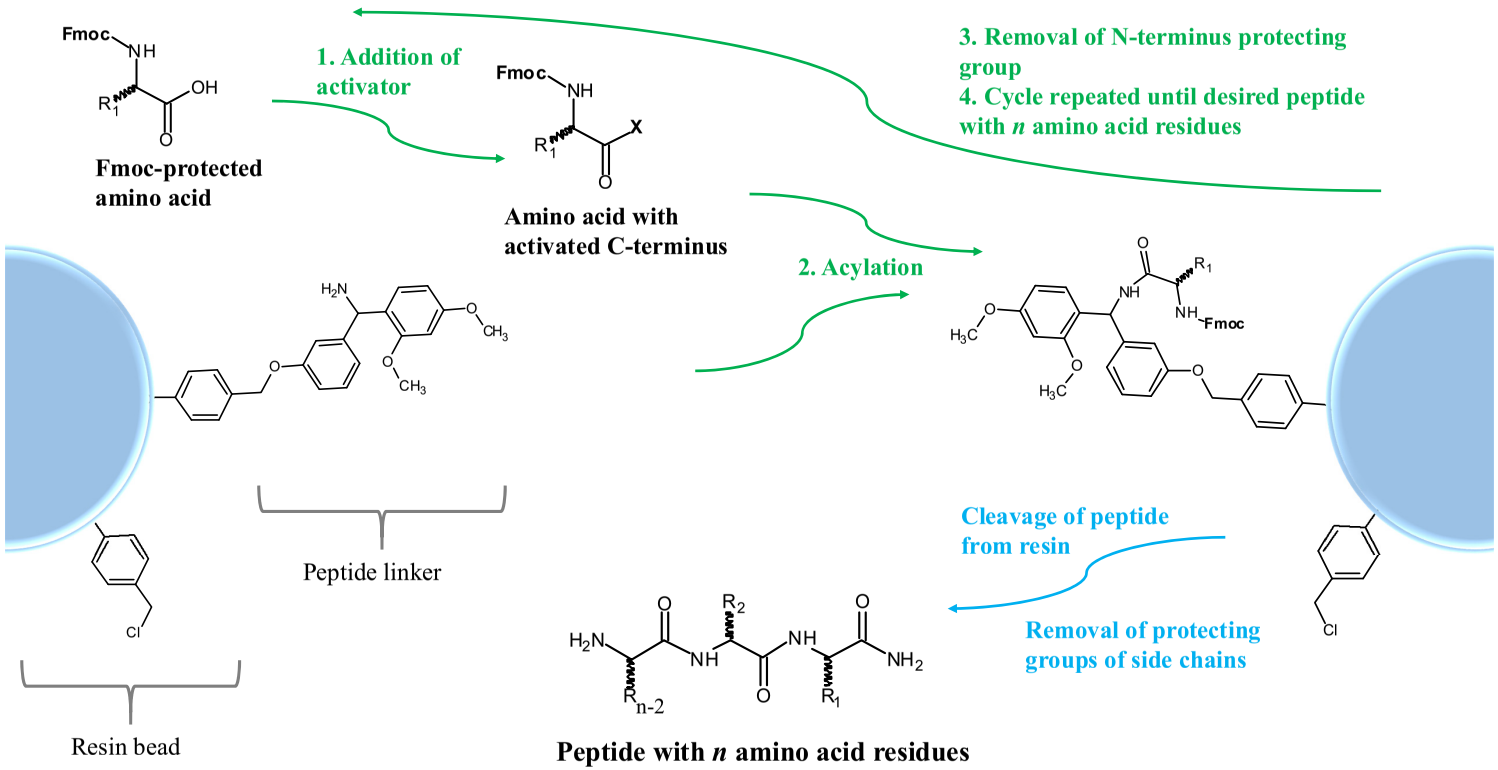

Figure 12. General scheme of SPPS. Markings: X – activated C-terminus; *n* – number of AAs in peptide.

The steps of 'classical' SPPS are as follows. The first amino acid counting from the C-terminus of peptide is activated and attached to the resin *via* its carboxyl group; in this way, this AA becomes the first monomer in the growing peptide chain (Figure 12). The peptide bond formation is a reaction with high activation energy and thus needs the involvement of activators to convert carboxyl group to more reactive species (*e.g.*, active esters). The activators (*e.g.*, 2-(1H-benzotriazol-1-yl)-1,1,3,3-tetramethyluronium hexafluorophosphate or HBTU, 1-hydroxybenzotriazole or HOBt, *N,N'*-diisopropylcarbodiimide or DIC) render the carboxyl group of added amino acid more electrophilic by pulling electrons from it and, consequently, facilitate the nucleophilic attack by the amine group of the resin-bound AA or peptide (Figure 13).[143]

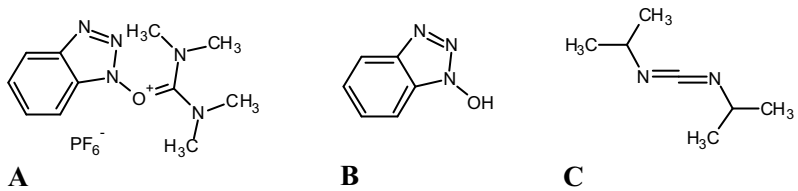

Figure 13. Structures of common activators HBTU (A), HOBt (B) and DIC (C).

Thereafter, the following steps are performed until the peptide with desired length and structure is obtained:

1. removal of group protecting the N-terminus of previous AA,
2. activation of the C-terminus of added AA,
3. coupling of AA (acylation reaction).

Finally, the last step of synthesis is the cleavage of the peptidic chain from the resin, usually accompanied by the simultaneous removal of protecting groups of the side-chains. In Boc-SPPS, the α-amino group protecting (N^{α}-protector) Boc-group is removed by treatment with strong acid, usually with trifluoroacetic acid (TFA); hence, the cleavage of peptide must be performed with even stronger acid, *e.g.*, HF. Differently, the Fmoc-group is removed from N-terminus of amino acid by treatment with a weak organic base, usually with piperidine, whereas the releasing of final peptide from resin can then be achieved using TFA.[143,144]

The successful execution of SPPS requires the usage and removal of protective groups to prevent the undesired side-reactions with a multitude of functional groups that AAs can bear. The main role of N^{α}-protectors is to delocalize the free electron pair of the nucleophilic N-terminal amino group with the aim to avoid the reaction of the added AA with other molecules in solution. The carboxyl group of growing chain is typically attached to the resin and does not require special protection prior to the removal of peptide chain

from carrier (cleavage). In traditional SPPS, two main synthesis strategies are applied based on the N^{α}-protecting groups used throughout the synthesis: *tert*-butoxycarbonyl (Boc) and 9-fluorenylmethoxycarbonyl (Fmoc) (accordingly, the synthetic method is termed as Boc-SPPS or Fmoc-SPPS) (Figure 14). While Boc-group is removed by strong acid (usually TFA), Fmoc-group can be readily removed in milder conditions in a weakly alkaline environment (20% piperine in DMF).[143]

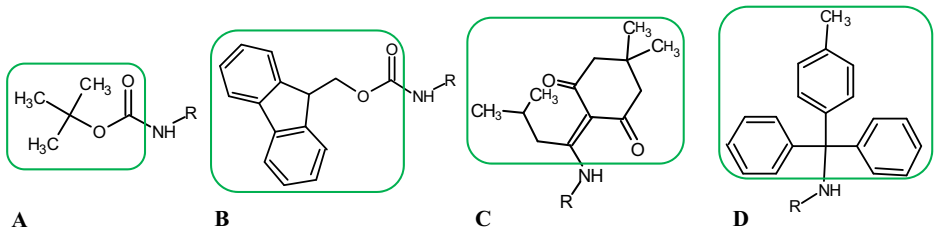

Figure 14. Structures of Boc (A), Fmoc (B), ivDde (C) and Mtt (D) protecting groups.

In case if the side-chains of AAs contain reactive functional groups, the latter must also be protected. In general, the orthogonality rule applies: the groups protecting N-terminus and side-chains must be removable under different conditions.[143] A successful example of application of the orthogonal protecting groups in SPPS was used within given thesis during synthesis of conjugates targeting Haspin.[127,128] Briefly, the H3(1-7)-like peptidic part was synthesized by using traditional Fmoc-SPPS; the side chains of other AAs except LLys which incorporated 1-(4,4-dimethyl-2,6-dioxocyclohex-1-ylidene)isovaleryl group (ivDde-group, Figure 14) contained acid-labile protecting groups. Next, the N-terminus of the assembled peptidic part was protected with the acid-labile Boc-group. Thereafter, the ivDde-group was removed by treatment with 10% hydrazine solution in DMF and *via* the side-chain of Lys, linkers and the nucleosidic fragment were introduced to the structure of the conjugate. Then, 4-methyltrityl (Mtt, Figure 14) group was removed from the side-chain of DLys of C-terminus by treatment with the mixture of TFA/triisopropylsilane/dichloro-methane (1/2/97, *v*/*v*/*v*) and, thereafter, myristic acid moiety (Myr) was linked to the structure of conjugate *via* the side chain of Lys of C-terminal. Finally, the conjugate was cleaved from resin using TFA/H_2O/triisopropylsilane (90/5/5, *v*/*v*/*v*) with simultaneous removal of the protecting groups.[127]

The benefits of SPPS are the simplicity, easy conversion to automated regime, and high speed of execution compared to the synthesis in solution. What is more, the yield of each acylation step is up to 99.8% in case of proper implementation (*e.g.*, suitable reaction time, type and amount of activator, number of equivalents of AAs, complete removal of the reagents by repetitive washing with appropriate solvents). Additionally, easy washing and purification procedures between the intermediate stages (by filtration) also avoid the loss of

material. On the other hand, to force the reaction to completion, large excess of reagents compared to the loading of resin is used (generally 3 to 10-fold excess), which increases the cost of synthesis. Next, analysis of the product at intermediate steps is relatively complicated.[143,144] Still, there are different possibilities to analyse the completion of the coupling on resin bead; *e.g.*, colour tests are frequently used that show the presence or absence of certain functional group(s).[147–149] For instance, the Kaiser test is used to analyse the presence of unreacted amino groups: two molecules of ninhydrin react with free amino group, resulting in Ruhemann´s purple colour in the presence of free primary amino groups (Figure 15).[149] If the acylation reaction has not gone to completion, the coupling reaction should be repeated, or capping should be performed with a small and relatively cheap acylating reagent.[143]

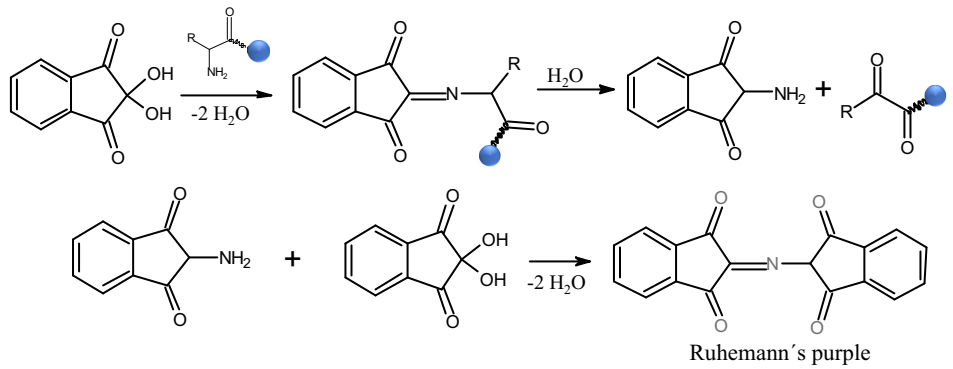

Figure 15. The mechanism of the Kaiser test. In the presence of free primary amino groups, the resin beads turn purple.

2. Biochemical Assays with Detection of Photoluminescence

2.1. Phenomena of Fluorescence and Phosphorescence

Photoluminescence is emission of light from a substance after excitation of electron of outer molecular orbital to the higher excited state by absorption of photon of light. Based on the nature of excited state and intermediate states, photoluminescence can be divided into fluorescence and phosphorescence. The processes occurring during the absorption and emission of a photon of light are illustrated by the Jablonski diagram (Figure 16).[150] Two types of transition may occur for relaxation of the excitated state – radiative and non-radiative. Radiative transition includes the absorption or emission of a photon. One the other hand, non-radiative (thermal) transition involves the vibrational relaxation (*i.e.*, relaxation of the excited state to its lowest vibrational level), internal conversion (*i.e.*, transition from higher electronic excited state to the lower electronic state), and intersystem crossing (see below). In a way, the radiative transition

competes with non-radiative (thermal) transition, where the energy of excited electron is lost without the emission of photon. Thus, the fluorescence and phosphorescence both are more evident at low temperatures due to the slowdown of non-radiative decay.[150,151]

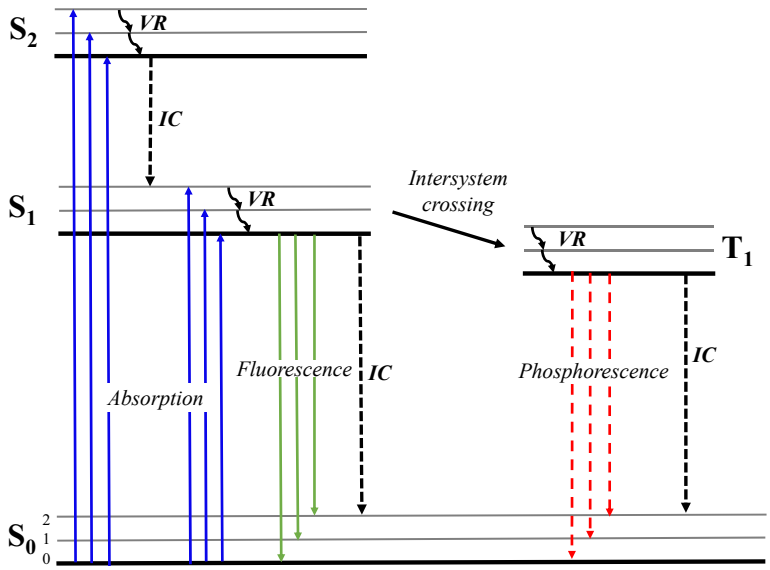

Figure 16. The Jablonski diagram to illustrate the phenomena of fluorescence and phosphorescence. S_0, S_1 and S_2 are the ground singlet state, first and second excited singlet states, respectively; T_1 shows the first excited triplet state; vibrational energy levels are depicted as *0*, *1* and *2*. *IC* refers to internal conversion and is depicted as a dashed line; *VR* refers to vibrational relaxation.

During the absorption of exciting photon, an electron of the fluorophore is excited to a higher excited state (S_1 or S_2), whereas the electron in the excited orbital has an opposite spin to the second electron remained in the ground state orbital. Thereafter, in case if the electron is excited to S_1 (more common), the electron relaxes to the lowest vibrational level of S_1 within picosecond time scale (10^{-12} s or less) during a process called vibrational relaxation, whereas the vibrational energy is given to the solvent; if the electron is excited to S_2, first the electron relaxes to the lowest vibrational level of S_2 (vibrational relaxation), followed by rapid decay to S_1 due to internal conversion (Figure 16). Then, while the electron is returning to the ground state, a photon can be emitted and manifested as fluorescence, which lifetime[2] is usually in 0.1-10 ns range.[150]

[2] Lifetime (τ) is an average time of the excited state of fluorophore (*i.e.*, molecule) in higher vibrational levels prior to returning to the ground state.[150] Note: the term 'lifetime' applies to the set of atoms, as the relaxation time of an individual atom is not predictable in quantum mechanics.

Alternatively, the excited electron can undergo a spin conversion when transferring from the S_1 to the first triplet state T_1 (intersystem crossing; the spin of electron in the T_1 state is at the same orientation as the spin of the electron remaining in the ground state). As the transition from T_1 to ground state is a process 'forbidden' by the quantum mechanical rules, the corresponding emission, *i.e.*, phosphorescence, occurs during significantly longer timescale compared to fluorescence, generally in μs to ms scale. Molecules that incorporate heavy atoms (*e.g.*, iodine, bromine) often hold the property of phosphorescence as the heavy atoms enhance intersystem crossing.[150]

The fluorescent substances or fluorophores are typically aromatic organic molecules but, on the other hand, some elements, lanthanides (*e.g.*, europium, terbium) are also holding excellent properties of photoluminescence.[150] The emission spectrum of a fluorophore depends on structure of the molecule as well as on the surrounding environment (pH, polarity). Generally, the energy of emitted photon is smaller compared to the energy of absorbed photon as there is an energy loss due to thermalization during decay of excited fluorophore to lower vibrational levels; hence, the fluorescence (as well as phosphorescence) appears at higher wavelength (lower energy) than excitation occured. The difference between the wavelength of maxima of absorption and emission spectra is called the Stokes shift. Furthermore, the shape of emission spectrum is usually not related to the excitation wavelength within absorption spectrum. Another important property of a fluorophore is the quantum yield characterizing the number of emitted photons relative to the number of absorbed photons; *i.e.*, the fluorophores with high quantum yield show brighter emission.[150]

The decrease of fluorescence intensity due to the enhanced non-radiative transition (fluorescence quenching) is caused by a variety of factors. Collisional quenching (or dynamic quenching) takes place when the excited fluorophore collides a quencher molecule in solution (*e.g.*, oxygen, halogens, amines, electron deficient molecules); as a result, the quencher may either quench the energy or release a lower energy photon and hence the intensity of fluorescence (or phosphorescence) decreases.[150,152] Additionally, the quenching may result from formation of non-fluorescent complex between the fluorophore and quencher before the excitation of fluorophore (so called static quenching).[150]

2.2. Equilibrium Binding/Displacement Assay with Fluorescence Anisotropy Readout

A phenomenon having importance in biochemical applications is fluorescence anisotropy (or in older literature, term 'fluorescence polarization' is frequently used). In fluorescence anisotropy-based measurements, the sample containing the fluorescent probe is excited by the linearly polarized light and subsequently polarization of emitted light is measured (for this, parallel (||) and perpendicular (⊥) polarizers are used). The fluorescence anisotropy (r) and polarization (P) both are dimensionless quantities and are expressed as:

$$r = \frac{I_{||} - I_{\perp}}{I_{||} + 2I_{\perp}} \qquad \text{(Equation 1)}$$

$$P = \frac{I_{||} - I_{\perp}}{I_{||} + I_{\perp}} \qquad \text{(Equation 2)}$$

where $I_{||}$ and $I_{\perp}$ are the intensities of parallel and perpendicular polarized emission, respectively. Both fluorescence polarization as well as fluorescence anisotropy can be used interchangeably as these both represent the same phenomenon; however, the fluorescence anisotropy is more recommended as the difference ($I_{||} - I_{\perp}$) is normalized by the total intensity ($I_T = I_{||} + 2I_{\perp}$).

The common reason for the decrease of fluorescence anisotropy is rotational diffusion of fluorescent probe in solution within the time in the range of fluorescence lifetime of the probe. As larger particles tend to rotate more slowly, the binding of the probe to a macromolecule leads to increase of fluorescence anisotropy.[150]

The equilibrium binding/displacement assay with fluorescence anisotropy readout (FA assay) used in the current study takes advantage of change of fluorescence anisotropy of solution containing a fluorescent probe. Again, the sample is exited with linearly polarized light and, thereafter, the fluorescence anisotropy of emitted light is measured (Figure 17).[111]

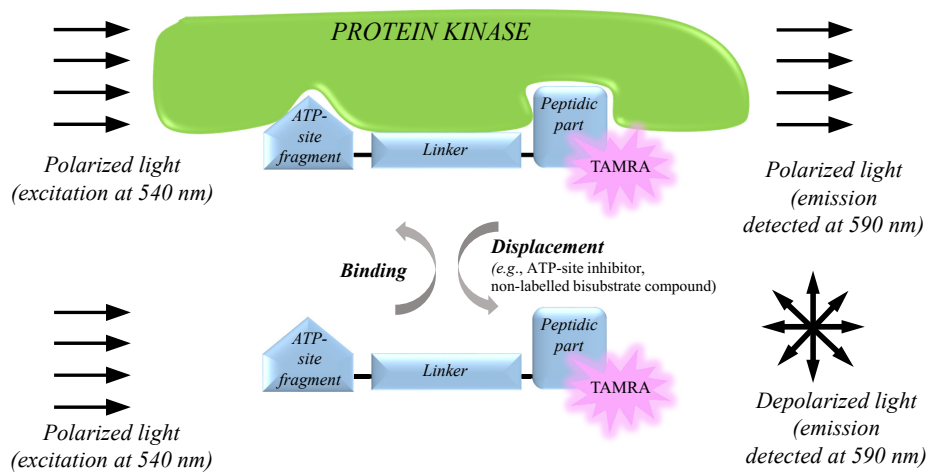

Figure 17. The scheme of equilibrium binding/displacement assay with fluorescence anisotropy readout (FA assay). Protein kinase is shown in green, fluorescent probe in blue, and fluorescent dye in pink.

FA assay can be performed in two formats – binding of the fluorescent probe to the target protein or displacement of the fluorescent probe from its complex

with the protein. In binding assay, a low molecular weight (1.5…2 kDa) fluorescent probe (a binder possessing intrinsic fluorescence properties or a non-fluorescent binder labelled with a fluorescent dye) binds to the active site of the PK (molecular weight over 30 kDa). Therefore, the rotation of PK-bound probe is restricted and hence the light emitted by fluorophore remains polarized (fluorescence anisotropy is high) (Figure 17). On the other hand, when the probe is free in solution (not bound to the PK), it rotates more freely, the emitted light is depolarized and thus the measured fluorescence anisotropy value is low. The data obtained from the binding format of FA assay allows the evaluation of equilibrium dissociation constant of the probe (K_D) or the active concentration of the PK.

The fluorescence anisotropy in FA-binding assay is calculated as follows

$$A = A_f(1 - X_1) + A_b \cdot X_1 \quad \text{(Equation 3)}$$

$$X_1 = Q \cdot X_2/[1 + X_2(Q - 1)] \quad \text{(Equation 4)}$$

$$X_2 = \left\{C + K_D + k \cdot E_0 - [(C + K_D + k \cdot E_0)^2 - 4C \cdot k \cdot E_0]^{\frac{1}{2}}\right\}/2C \quad \text{(Equation 5)}$$

where A correponds to the measured fluorescence anisotropy; A_f and A_b are the values of anisotropy of free probe or the probe-enzyme complex, respectively; C is the total concentration of fluorescent probe, E_0 is the nominal concentration of enzyme, k refers to the fraction of active PK (*i.e.*, ratio of concentration of active PK *versus* nominal concentration of PK), K_D is the dissociation constant of the fluorescent probe; Q value represents the ratio of fluorescence intensities of PK-bound *versus* free probe.[111] In case if the fluorophore is not directly involved in binding of the compound, the value of Q is often close to 1. The Q value remarkably higher than 1 points to the occurrence of non-specific interactions of probe with other components of the assay or binding of assay components to the surfaces (*e.g.*, wall of the plastic tubes, pipette tips, wells of the microplate). On the other hand, the Q value below 1 may point to the fluorescence quenching in the probe-enzyme complex.[153]

In displacement assay, the fluorescent probe is displaced from its complex with PK by an ATP-competitive, substrate-competitive or bisubstrate non-fluorescent inhibitor. Consequently, the fluorescence anisotropy of emitted light decreases (Figure 17). The fluorescence anisotropy of displacement format of FA assay is calculated based on the following equations:

$$A = A_f(1 - X_3) + A_b \cdot X_3 \quad \text{(Equation 6)}$$

$$X_3 = X_4/(3K_D + X_4) \quad \text{(Equation 7)}$$

$$X_4 = 2(X_5^2 \cdot 3X_6)^{\frac{1}{2}} \cdot \cos\left(\frac{\theta}{3}\right) - X_5 \quad \text{(Equation 8)}$$

$$\theta = arccos\{[-2X_5^3 + 9X_5 \cdot X_6 + 27K_D \cdot K_d \cdot E]/[2(X_5^2 - 3X_6)^{3/2}]\}$$ (Equation 9)

$$X_5 = K_D + K_d + 10^{logL} + C - E$$ (Equation 10)

$$X_6 = K_D(10^{logL} - E) + K_d(C - E) + K_D \cdot K_d$$ (Equation 11)

where K_d corresponds to the dissociation constant of the competitive ligand and PK; E and L are the total concentration of active PK and total concentration of competitive ligand, respectively; other components are the same as previously described in case of binding format of FA assay. Based on the obtained data, it is possible to calculate equilibrium displacement constant (K_d) of the non-fluorescent inhibitor.[111]

The benefits of FA assay are its simplicity, speed, homogeneity, and readiness for automation. Unfortunately, low affinity of the fluorescent probe (K_D value higher than 10 nM) leads to the necessity to use the enzyme at high concentration and hence increasing price of the analysis.[111] However, the developed probes with high affinity (K_D value below 1 nM) allow the application of the enzyme at low nanomolar concentration.[108,127,129] Also, FA assay is rarely applicable in biologically complex systems (*e.g.*, live cells, cell lysates), where it is challenging to achieve sufficient homogeneity to excite the probe equally in the entire volume of the sample.[150] Still, recently several examples of successful applications of FA-based assays for cellular measurements have been reported.[154]

2.3. Determination of Association/Dissociation Kinetics by FA Assay

In addition to equilibrium measurements, kinetic measurements (*i.e.*, assessment of association (k_{on}) and dissociation rate (k_{off}) constants) can be carried out with a FA assay. It is assumed that a bimolecular reaction (*e.g.*, binding of enzyme and probe leading to formation of bimolecular complex) proceeds according to the law of mass action and the rate of reaction can be expressed as follows:

$$E + L \underset{k_{off}}{\overset{k_{on}}{\rightleftarrows}} EL$$ (Equation 12)

$$v = -\frac{dL}{dt} = -\frac{dE}{dt} = \frac{dEL}{dt}$$ (Equation 13)

where t is time, E represents the enzyme, L is a small molecular probe and EL is the binary complex; k_{on} and k_{off} are association and dissociation rate constants,

respectively. At equilibrium, the rate of forward and reverse reaction[3] is equal and the equilibrium dissociation constant K_D is defined as: [155,156]

$$K_D = \frac{k_{off}}{k_{on}} = \frac{[E]\cdot[L]}{[EL]} \quad \text{(Equation 14)}$$

In association experiment, the probe is added to the enzyme solution and, thereafter, the anisotropy increase corresponding to the binding of probe occurs until the system reaches the equilibrium (plateau phase), which position in addition to the affinity of the probe depends on the concentration of the probe and enzyme. The association is a bimolecular second-order reaction and follows the second order-association kinetics equation:

$$v = k[L][E] \quad \text{(Equation 15)}$$

$$[L] = [L_0] - [EL],\ [E] = [E_0] - [EL] \quad \text{(Equation 16)}$$

where k is the second-order rate constant; $[E_0]$ and $[L_0]$ are the initial concentrations of enzyme and probe, respectively; $[E]$ and $[L]$ are the concentrations at time point t; $[EL]$ is the concentration enzyme-probe complex at time point t. The association rate constant or on-rate constant (k_{on}) shows the rate of formation of enzyme-probe complex; the unit of k_{on} value is $M^{-1}\ s^{-1}$.

In dissociation experiment, the enzyme and probe are incubated together until the equilibrium is reached. Thereafter, dissociation of the probe from the enzyme is measured. For this, to the solution of enzyme-probe complex a large excess of the displacer is added that occupies the site of probe. Dissociation of the probe from enzyme-probe complex is a unimolecular reaction that follows the kinetics of the first order process, where the concentration of enzyme- probe complex decreases following the one-phase exponential decay equation:

$$\frac{d[EL]}{dt} = -k\,[EL] \quad \text{(Equation 17)}$$

$$[EL] = [EL_0] \cdot e^{-kt} \quad \text{(Equation 18)}$$

where $[EL]$ is the concentration at time point t, t is time and k is the first-order rate constant. The dissociation rate constant (k_{off}) expresses the fraction of complex which decays per time unit; the unit of k_{off} value is s^{-1} or min^{-1}.

A widely used characteristic of dissociation kinetics is the half-time of the process ($t_{1/2}$), which is the period of time during which the number of complexes of enzyme-probe has decreased to half of its initial value. The half-life ($t_{1/2}$) is expressed according to the following equation:

[3] Rate of reaction is a measure, which shows how fast the concentration of reactants and/or products changes in time.[155]

$$t_{1/2} = \frac{ln(2)}{k_{off}} \quad \text{(Equation 19)}$$

Alternatively, a characteristic termed residence time (τ) is used, calculated as reciprocal of the off-rate constant: [156]

$$\tau = \frac{1}{k_{off}} \quad \text{(Equation 20)}$$

In this work, we assumed that the dissociation of ligand from PK follows the classical model with the first order kinetics, which is not affected by the presence of competitive ligand. Recently, facilitation of dissociation of the complex between bifunctional ligand and PK in the presence of high concentrations of competive ligand (over 1 μM) had been reported.[157] This is due to the dynamic nature of the bifunctional ligand: it is possible that at a given instance of time, only one fragment of inhibitor is bound to PK, whereas the other one is not. However, because the bound fragment holds the unbound fragment close to its site in PK, and hence facilitates rebinding. While a fragment of the bisubstrate inhibitor stays unbound, a competitive ligand in high concentration can bind to the corresponding site in PK, and the formed triple complex causes facilitated dissociation of the bifunctional ligand. Importantly, the concentration of the competitive ligand must exceed a certain concentration to ensure its high population in proximity of PK; it was shown that less than 1 μM competitive ligand did not facilitate the dissociation of bifunctional ligand.[157] However, the effect may be divergent in case of different PKs, bifunctional ligands as well as competitors.

2.4. ARC-Lum(Fluo) Probes

ARC-Lum(Fluo) photoluminescent probes are bisubstrate-analogue ARC-type inhibitors which incorporate thiophene- or selenophene-comprising heteroaromatic systems as ATP-analogues and are labelled with a fluorescent dye. The principle of operation of these tandem photoluminescent probes use both phosphorescence as well as a non-radiative Förster-type resonant energy transfer (FRET) phenomenon (Figure 18).[133]

Upon binding of ARC-Lum(Fluo) probe to PK and excitation of complex by flash of light in near-UV ($\lambda < 380$ nm), the FRET occurs from the excited triplet state of a thiophene- or selenophene-incorporating heteroaromatic system (with long lifetime and low quantum yield) to the singlet state of acceptor fluorophore (with short lifetime and high quantum yield) (Figure 18). Thereby, the energy is step-by-step released from the triplet state of the donor to the singlet state of the acceptor fluorophore *via* FRET mechanism. As a result, the process is leading to the long-lifetime luminescence emission at a wavelength corresponding to emission of fluorophore.[133,152] However, in case of FRET phenomenon, certain conditions must be fulfilled. First, the absorption spectrum of acceptor must

partially overlap with the emission spectrum of donor [note: in the composition of ARC-Lum(Fluo) probes, the most efficiently are used fluorescent dyes absorbing light either in the orange (*e.g.*, TAMRA, Cy3B, PromoFluor555) or red region of the spectrum (*e.g.*, Alexa647), or in the intermediate zone (*e.g.*, TexasRed)]. Furthermore, FRET requires the sufficient spatial proximity of donor and acceptor (typically the required distance is in the range of 1–10 nm).[133,150]

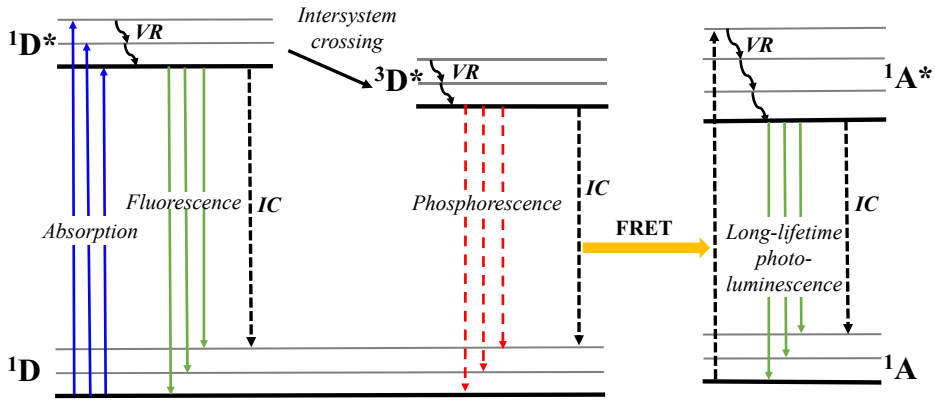

Figure 18. The complemented Jablonski diagram to illustrate the principle of operation of ARC-Lum(Fluo) probes. ^1D, ^1D* and ^3D* denote the ground singlet state, excited single state and excited triplet state of donor, respectively. ^1A and ^1A* denote the ground and excited singlet state of acceptor fluorophore, respectively. *IC* refers to internal conversion and is depicted as a dashed line; *VR* refers to vibrational relaxation.

The free ARC-Lum(Fluo) probe does not emit the long-lifetime luminescence in water environment, as the presence of dissolved molecular oxygen acts as a quencher dispelling the energy of triplet state donor into non-radiative processes.[150,152] Moreover, the long-lifetime luminescence signal of free ARC-Lum(Fluo) probe is negligible even in deoxygenated conditions in water environment.[152] On the other hand, when the photoluminescent probe is bound to the active site of PK, the probe is endowed by the long-lifetime luminescence emission, as the access of oxygen to the probe is hindered by PK.[150,152] Hence, ARC-Lum(Fluo) probes are also named 'PK binding-responsive photoluminescent bisubstrate probes'. Different kinases are able to 'protect' the photoluminescent probe from oxygen to a varying extent, even in case of affinity of ARC-Lum(Fluo) towards these PKs is similar.[152]

Differently from the steady state measurement of fluorescence, measurement of long-lifetime luminescence intensity is performed in cycles: the sample is excited with a flash of light, followed by time delay to achieve decay of background fluorescence and thereafter the measurement of luminescence intensity

is carried out in a certain time window.[133] ARC-Lum(Fluo) probes hold relatively long-lifetime (in the two-digit μs range), which provides an advantage for use of the probes in complicated biological systems (*e.g.*, in cell lysate, blood serum, tissue extract). In this case, the measurable signal does not include the nanosecond range of fluorescence of organic compounds or autofluorescence of cells, leading to the increased sensitivity of the assay.[125,133,134] The additional advantages of ARC-Lum(Fluo) probes include their high brightness and long emission wavelength.[129,133]

2.5. Assays with Time-Gated Measurement of Luminescence Intensity

ARC-Lum(Fluo) probes can be used in biochemical equilibrium binding/displacement assay with time-gated measurement of luminescence intensity (TGL assay). Similarly to FA assay, TGL assay can be performed in binding format, which allows determination of the concentration of active kinase or the affinity of photoluminescent probe, as well as in displacement format, where the affinity of displacing compounds (including fluorescent probes that do not possess long-lifetime emission) can be established (Figure 19).

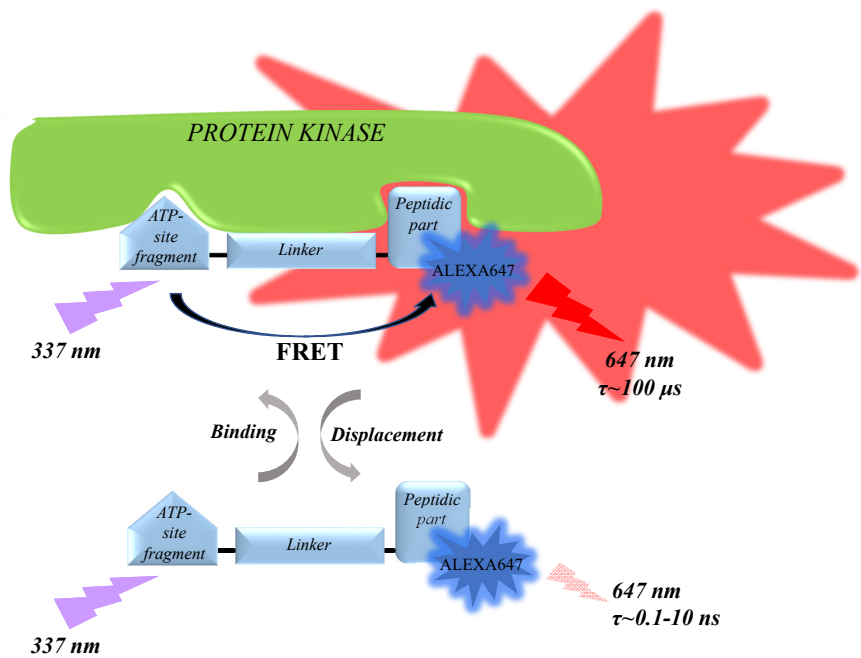

Figure 19. The scheme of the TGL assay. PK is shown in green, photoluminescent probe in light blue, and fluorescent dye in dark blue. The photoluminescence signal produced as a result of binding of photoluminescent probe to kinase is depicted in red.

The benefit of the TGL assay compared to FA assay is that the negligible signal of free ARC-Lum(Fluo) probe enables the use of the photoluminescent probe in high concentrations (up to 1 mM) compared to the use of fluorescent probes in the FA assay (the maximal concentration of probe around 30 nM). Thus, the method allows the determination of affinity of compounds devoid of long-lifetime photoluminescence (non-Lum) by shifting the IC_{50} value away from tight-binding conditions. Tight-binding conditions occur in displacement assay if the IC_{50} value of non-Lum compound stays near the half of the concentration of enzyme used. This understanding follows conclusions drawn according to the Cheng-Prusoff equation:

$$K_d = \frac{IC_{50}}{1+\frac{c[ARC-Lum(Fluo)]}{K_D[ARC-Lum(Fluo)]}} \qquad \text{(Equation 21)}$$

where K_d is equilibrium dissociation constant of the compound under evaluation and IC_{50} corresponds to the concentration of non-Lum compound at which the amount of complex of probe and kinase is half of maximum; c[*ARC-Lum(Fluo)*] and K_D[*ARC-Lum(Fluo)*] correspond to the concentration and equilibrium dissociation constant of photoluminescent probe used, respectively.[129,133] Next, differently from the frequently used surface plasmon resonance (SPR) method, ARC-Lum(Fluo)-based assays are homogenous, automatable and well suitable for the high throughput screening of small-molecule ligands. Furthermore, ARC-Lum(Fluo) probes can be utilized not only in thermodynamic measurements, but also in kinetic measurements – where under suitable conditions, association and dissociation rate constants of the displacing compounds can be established (discussed in *Results and Discussion*).[133]

2.6. Thermal Shift Assay

Thermal shift assay (also known as differential scanning fluorimetry, DSF) is a fast and relatively inexpensive method for the characterization of stability of native protein *versus* low molecular weight ligand-bound protein.[158,159] Thermal shift assay measures the thermal unfolding (denaturation) of the protein in the presence of a fluorescent dye and this method is used for screening of ligands against the protein(s) under investigation.[127,160–164]

The stability of protein is related to its Gibbs free energy of unfolding, ΔG_u. Along with the increase of temperature, the stability of protein decreases.[158] During this process, hydrophobic regions of the protein are revealed, where a suitable fluorescent dye can bind (Figure 20). The fluorescent dye must be highly fluorescent in non-polar environment (*e.g.*, when bound to the hydrophobic regions of unfolded protein) and, on the other hand, in aqueous environment the fluorescence of free dye must be strongly quenched.[158] One of the most used dyes is SYPRO orange due to its high signal-to-noise ratio and high

excitation wavelength (near 500 nm), which decreases the risk of excitation of other molecules in solution.[158,160,163]

Consequently, the fluorescence quantum yield and hence fluorescence intensity of the dye increases with rising temperature, reaching its maximum at the temperature where the protein is in a completely unfolded state. After the maximum signal is achieved, the fluorescence intensity starts to decline due to the aggregation or precipitation of protein at even higher temperatures. The temperature at which the amount of native and unfolded protein is equal or the fluorescence intensity of the protein-dye complex is half of the maximum, is called the melting temperature, T_m.[158,159]

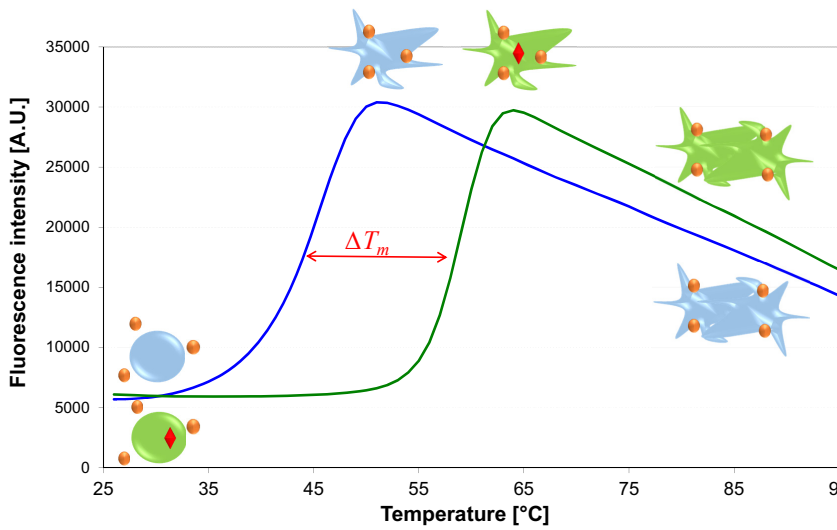

Figure 20. The melting curves of a protein obtained by thermal shift assay. The blue curve corresponds to a native protein and the green curve to a ligand-bound protein. The native and the unfolded protein is marked as a circle and an irregular shape, respectively; the protein-bound ligand is marked as a red rhombus and the molecules of fluorescent dye SYPRO orange shown as orange ovals. The difference between the melting temperature of ligand-bound *versus* native protein (ΔT_m) is highlighted in red.

In most cases, the binding of ligand can increase the stability of the protein due to the contribution of the Gibbs free energy of ligand binding (ΔG_l) to the ΔG_u.[158,160] Reflecting the increase of ΔG_u of protein, the binding of the ligand to protein generally leads to the positive shift of T_m compared to the native protein. The difference between the melting temperature of ligand-bound *versus* native protein is called the thermal shift value, ΔT_m.[158] The studies have shown that the ΔT_m values obtained by thermal shift assay are proportional to the affinity of ligand determined with other methods (*e.g.*, equilibrium binding/displacement assay).[160,163,164] Thus, the linear correlation of -log(K_d) or -log(IC_{50}) *versus* ΔT_m

implies that ΔT_m values around 4 °C usually correspond to K_d values of below 1 μM, whereas ΔT_m values over 8 °C generally correspond to the K_d values below 100 nM.[161–163]

Fluorescence intensity measured by thermal shift assay can be plotted as a function of temperature resulting in sigmoidal curve (Figure 20). The inflection point of transition, *i.e.*, T_m value, is calculated by using Boltzmann equation:

$$y(T) = Min + \frac{(Max - Min)}{(1 + exp(\frac{Tm - T}{a})} \quad \text{(Equation 22)}$$

where the *Max* and *Min* are the values of maximum and minimum fluorescence intensities, respectively, T is the temperature, y is the measured fluorescence intensity, and a corresponds to the slope of the curve within T_m.[158,160]

The advantages of thermal shift assay include the possibility to use the native protein and non-labelled ligands, which eliminates the risk that the label of protein and/or ligand may influence the behaviour of the parties in assay. Other benefits include relatively quick implementation as many samples can be analysed simultaneously, easy set-up of the experiment, and relative cheapness of the assay.[158] On the other hand, the ΔT_m values may sometimes not reflect the relative affinities of ligands towards certain protein targets, hence it is somewhat risky to rank the binding affinities of ligands only according to ΔT_m values.[160,165]

3. Protein Crystallography

3.1. Principles of Protein Crystallography

Crystallography is a technique in where a single crystal is irradiated by focused X-ray beam and a two-dimensional diffraction pattern is recorded. X-ray radiation has a wavelength of 0.1 to 1000 Å (or 10^{-11} to 10^{-7} nm), but in crystallography, 0.4 to 25 Å X-ray radiation is used as it corresponds to the length of chemical bond.[166] Thereafter, the re-calculation of diffraction data by using Fourier method provides the three-dimensional electron density map representing the crystal lattice components. Finally, into the electron density map the atomic model of the structure is built in.[166]

X-ray crystallography allows the determination of highly detailed and precise spatial arrangement of atoms of macromolecules (such as proteins) in the crystal. As the 3D-structure of the molecule usually reflects its function or/and mechanism of action, crystal structures have been used to study PPIs, establish the enzymatic mechanisms of proteins, and provide essential insight for the structure-guided drug design.[166] More than 127,000 structures of proteins, including co-crystal structures of proteins with small-molecular ligands or co-factors, were deposited in Protein Data Bank (PDB) for January 17th 2018. There, around 90% of deposited crystal structures are obtained by X-ray crystallography.[167–169]

A crystal is a three-dimensional substance, where the molecules are regularly arranged into crystal lattice.[170] Protein crystals are different from inorganic crystals in several aspects. To start with, the protein crystals contain a large amount of solvent (water content 40–60% of crystal volume), allowing relatively free diffusion of small compounds through the crystal. Moreover, high water content helps to maintain the native conformation of the protein in crystal. Evaporation of liquid leads to the destabilization of the crystal and, as a result, the loss of crystalline order and diffractive properties; therefore, the crystals must be maintained inside the 'mother liquor' and at a sufficiently low temperature. Another essential difference from inorganic crystals is that in protein crystals, the atoms are not located at the nodes of unit cell. Furthermore, the biomacromolecules are extremely sensitive to the change of environmental conditions (pH, temperature, radiation damage, *etc*; radiation damage discussed more precisely below in section of *Preparation for Diffraction Data Measurement*).[170]

The acquisition of crystal structure of a protein involves four main steps discussed below. Note: only these processes are discussed in detail in which the author has been directly involved and the description is focused on water-soluble proteins with globular structure.

1. Crystallization

Crystallization is a process where a protein gradually precipitates out from the solution and forms a regular crystal lattice.[170] The structure of protein must favour the self-assembly of molecules into periodic crystal lattice by facilitating intermolecular interactions.[166] All molecules of the protein should have the same surface properties, especially the charge distribution to contribute the interactions between the molecules during packing into crystal structure.[170] Thus, a crucial requirement for the protein sample is purity: the higher is the purity (required ≥ 95%) as well as freshness of protein (*i.e.*, reduce the oxidation damage, denaturation), the greater is the chance for formation of crystal.[170,171]

Next, to induce the precipitation of protein and facilitate the formation of protein crystals, an appropriate solvent must be used (usually water-buffer system where an organic solvent is added). On the other hand, the protein of interest must be soluble in this solvent, and the environment should be as similar to the physiological as possible. Furthermore, the salts (*e.g.*, ammonium sulphate), organic compounds (*e.g.*, 2-methyl-2,4-pentanediol, MPD) or polyethylene glycol (PEG) can be added to induce precipitation of protein.[170] Proteins are polyvalent ions, hence its surrounding by other ions influences the interactions of proteins with water molecules and thus the solubility. Most proteins are soluble in water environment in the presence of a low concentration of salts (so-called 'salting in'). Still, simultaneously with the increase of concentration of salt, the solubility of protein decreases (so-called 'salting out') as water molecules are taken away from the surrounding of protein into the hydration layer around the ions of salt. Frequently, ammonium sulphate is

applied due to its high solubility and non-harmfulness for protein at high concentrations. The addition of PEG functions similarly.[170,171] Also, the effect of organic solvents is to clench the ionic layer on the surface of protein and thus allow the protein molecules to approach each other and aggregate, when a suitable orientation is achieved. On the other hand, the organic solvents might denature the proteins and hence the concentrations must be kept at moderate level and the experiments performed at low temperature.[171] What is more, crystallization is also promoted by modification of pH and temperature or addition of protein-stabilizing cofactors, metal ions, *etc*.[170,171] Finally, an important factor is also time, as the equilibrium formation between the soluble and crystallized form of protein is time-consuming.[170]

The process of crystal growth has been well characterized for small molecule crystals, the process has been considered to be similar for proteins. First, the formation of supersaturated solution is required where small protein aggregates can spontaneously form the nucleation centres (or nuclei) required for crystal growth (Figure 21). Thereafter, the supersaturation of solution must be kept at lower level (*e.g*., by changing the temperature or concentration of precipitation agent) to prevent formation of numerous nuclei and thus avoiding the growth of numerous low-grade minute crystals. Instead, the growth of few crystals with sufficient size is favored. Moreover, the slower growth of crystals increases the probability to obtain high quality crystals with smaller number of lattice defects.[170]

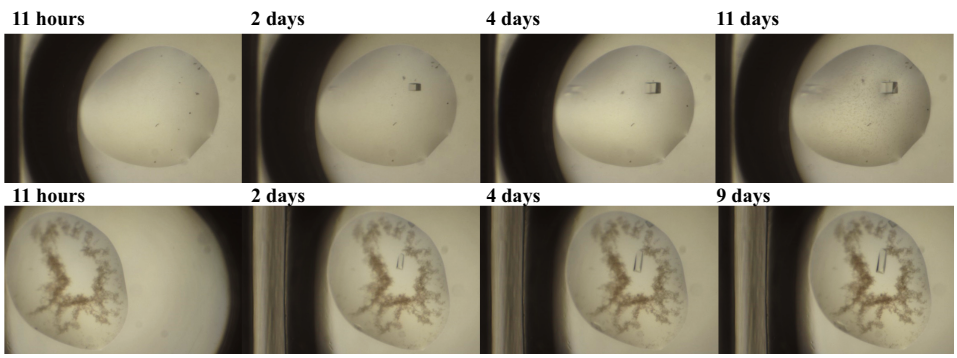

Figure 21. Pictures of growth of Haspin/**ARC-1411** (top row) and Haspin/**ARC-668** (bottom row) co-crystals in time under 3.3x magnification. The crystallization method used was the sitting drop method.

A frequently used crystallization technique method is vapor diffusion, possessing popularity due to the opportunity to use small amount of protein and simple realization. The current technique can be divided into 1) hanging drop and 2) sitting drop methods. In hanging drop vapor diffusion method, the protein and precipitant solutions are mixed on a siliconized glass cover slip and

placed upside down over reservoir which is partially filled with a suitable precipitant. On the other hand, in sitting drop method, the drop of the protein solution locates in microwell adjacent to the reservoir with precipitating solution and the reservoir as well as microwell are covered with a seal. In both methods, the water evaporates from the droplet and condenses to the reservoir solution, causing the increase of concentration of precipitating agent in the protein droplet. Evaporation of water from the drop is caused by the concentration difference of precipitating agent in droplet and reservoir and it occurs until the concentrations are equal, *i.e.*, equilibrium is reached. The vapour equilibrium between the protein droplet and precipitating agent solution in reservoir allows the protein solution to reach supersaturation and then formation of crystallization centres. Additional benefit of vapor diffusion method is the possibility to manipulate with time of arrival of equilibrium by varying the distance between the droplet and reservoir. Furthermore, the concentration of solution in reservoir and the concentration of protein in the microwell can easily be modified by diluting.[170]

Despite the fact that the theoretical background of crystallization of proteins is well known, the parameters necessary for crystal formation within a reasonable period vary significantly. In order to find optimal conditions, large number of variables (concentration of protein, nature and concentration of precipitant, pH, temperature, and/or specific additives in low concentrations) are screened simultaneously. After the initial crystals are obtained, the fine screens are performed near the suitable condition to obtain the crystals with good quality and sufficient size.[171]

2. Preparation for Diffraction Data Measurement

After the protein crystals with sufficient size are formed, the following step is the removal of a suitable crystal from the growth medium (crystal mounting). The mounted crystal is usually kept hydrated in mother liquor to avoid the evaporation of water. Generally, the loop made of fine fibers (nylon loop or cryo-loop) is used, which does not counteract the data collection at different positions of the sample and thus avoids the need for additional manipulation with the crystal before the X-ray experiment. A thin liquid layer spanning the loop keeps the crystal inside the loop due to the surface tension of the liquid.[170,171]

As previously mentioned, the biomolecules are extremely sensitive to radiation damage. The radiation damage of biomolecules is caused by exposure of crystal to high energy X-rays; photons with high energy cause the formation of free radicals (*e.g.*, monooxygen or hydroxyl radicals) inside the macromolecule or solvent, which upon diffusion through the crystal cause the destruction of crystalline order. In order to reduce the effect of radiation damage, sensitive X-ray detectors are used to reduce the exposure time. The radiation damage can also be remarkably reduced by cooling the crystals to cryogenic temperatures (100-120 K) before the measurement of diffraction pattern; at low temperatures, the radicals can still be formed but their diffusion

through the crystal is eliminated. The data collection at cryogenic temperatures (cryocrystallography) allows the prolonged exposure time as well as collection of many datasets from the crystal at different wavelengths.[166,170]

The cryogenic cooling must be performed rapidly (so-called flash-freezing or shock cooling) to facilitate the freezing of water in a vitreous state and prevent the formation of crystalline ice, which may cause formation of cracks in the crystal and hence decrease the quality of diffraction pattern. Cryogenic cooling can be performed by placing the crystals into the stream of cold nitrogen gas or immersing those into liquid nitrogen. Moreover, with the aim to reduce the damage of crystal during flash-cooling, cryoprotectans (*e.g.*, glycerol, PEGs of different molecular weight, MPD) are applied before the shock cooling; alternatively, the crystal can be grown in the medium already containing cryoprotective agent (*e.g.*, methanol).[170,171] Still, flash-cooling of crystals of some protein may be difficult under certain circumstances, and it is impossible to avoid the damage of certain functional groups during the exposure to X-rays (*e.g.*, cleavage of disulphide bond).[170]

3. Data Collection

During the exposure of protein crystal to X-rays, the phenomenon called X-ray diffraction occurs. Diffraction takes place when the wave encounters an obstacle (*e.g.*, atom) on its way; if the dimensions of an obstacle are in the range of light wavelength, bending of the wave around the obstacle occurs (Figure 22). There, the obstacle functions as a new source of the waves, generating new waves with different spreading directions compared to the initial wave. The resulting waves are able to interfere (*i.e.*, the waves combine and give a new wave) by getting stronger or cancelling each other out (constructive and destructive interference, respectively), hence generating a diffraction pattern of minima and maxima of interference.[170]

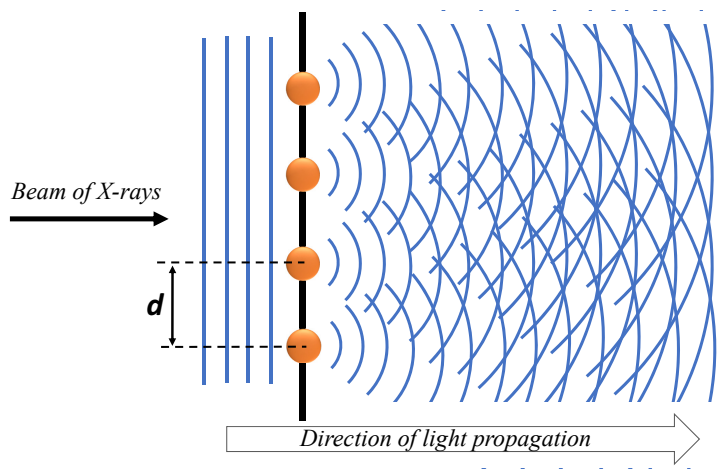

Figure 22. Diffraction from a crystal. *d* corresponds to the distance between the atoms (shown as orange spheres) in the crystal.

The pattern of reflections can be recorded with an area detector, a single-photon counter, or a photographic film.[170] The intensity and position of spots of diffraction pattern provide information about the locations of atoms and the repetitive distance *d* in the crystal, respectively.[166,170] The direction of diffracted beam depends on the X-ray wavelength as well as the unit cell distances in the crystal.[170]

The diffraction of a protein crystal is relatively weak as compared to the crystal of metals or small molecules containing heavy atoms, because proteins mostly consist of atoms with a small number of electrons (*i.e.*, C, N, O). Besides, the diffraction is a cooperative effect of the atoms positioned identically in an elementary cell; as the molecular weight of protein molecule is high, the number of particles in crystal is relatively low which additionally contributes to the weak diffraction intensities. Therefore, in order to obtain the diffraction pattern with reliable quality, it is essential to use high intensity source of X-rays (*e.g.*, synchrotron).[170]

4. Data processing and analysis

The diffraction pattern provides a two-dimensional picture from which it is possible to reconstruct three-dimensional crystal lattice using Fourier transform techniques. However, in order to generate the electron density map, both the amplitude as well as relative angle of phase of each reflection must be known. While the amplitude can be measured directly, as it is proportional to the square root of measured reflection intensities, the detectors do not record the phase of wave. This limitation is known as a phase problem. Different methods can be used to solve the phase problem (*e.g.*, molecular replacement), and when the initial phase is found, it is possible to construct the initial atomic model: the atoms of protein are placed into the obtained electron-density map.[166,170]

The final step during the data processing of diffraction data is refinement. The set of structure factors is computed for the present atomic model and compared to the experimentally obtained data; next, the parameters of the model are modified until there is no remarkable improvement in correlation between the atomic model and the experimental data. The agreement between the calculated and experimental model is expressed as the *R*-value, which is defined as the reliability or residual index. Thus, in case of perfect compliance, *i.e.*, no difference between the calculated and observed values, *R* is equal to zero; along with the increase of differences, the *R*-values increases as well; normally, *R*-value remains below 20%.[166,170] As protein crystals are not rigid structures, difficulties may arise during definition of the electron density for highly flexible and mobile fragments of proteins. Often, the electron density map is absent or poorly defined for N- or C-termini of the protein chain as well as for flexible loops connecting secondary structure elements.[166]

The quality of diffraction pattern is related to the quality of crystal, *i.e.*, regularity of the molecules in crystal lattice, and hence can be interrupted by crystal defects.[170] The reliability and quality of the collected data is characterized by the observed resolution corresponding to lattice spacing.[170,171]

Resolution is defined as the minimal identifiable distance between the structural elements in electron density map.[170] If the resolution remains in same magnitude as the length of chemical bond, then such a bond can be modeled with a high precision. In case of crystal that diffracts to resolution over 4.5 Å, it is possible to obtain only rough information about the shape of protein; the minimal required diffraction remains at the range of 3.5 Å. The resolution of good quality and high quality data is 2.0-2.7 Å (note: 2.7 Å is a minimal resolution to well-define water molecules) and 1.0-2.0 Å (1.5 Å is length of typical C-C covalent bond; 1.2 Å is a full atomic resolution), respectively.[170–172] However, the quality of crystal structure of protein also strongly depends on other structural factors and the claimed resolution may only be apparent.[172]

RESULTS AND DISCUSSION

In the subsequent scheme, the step-by-step workflow used for development of novel Haspin-targeting compounds is presented. The general structure of this workflow is as follows:

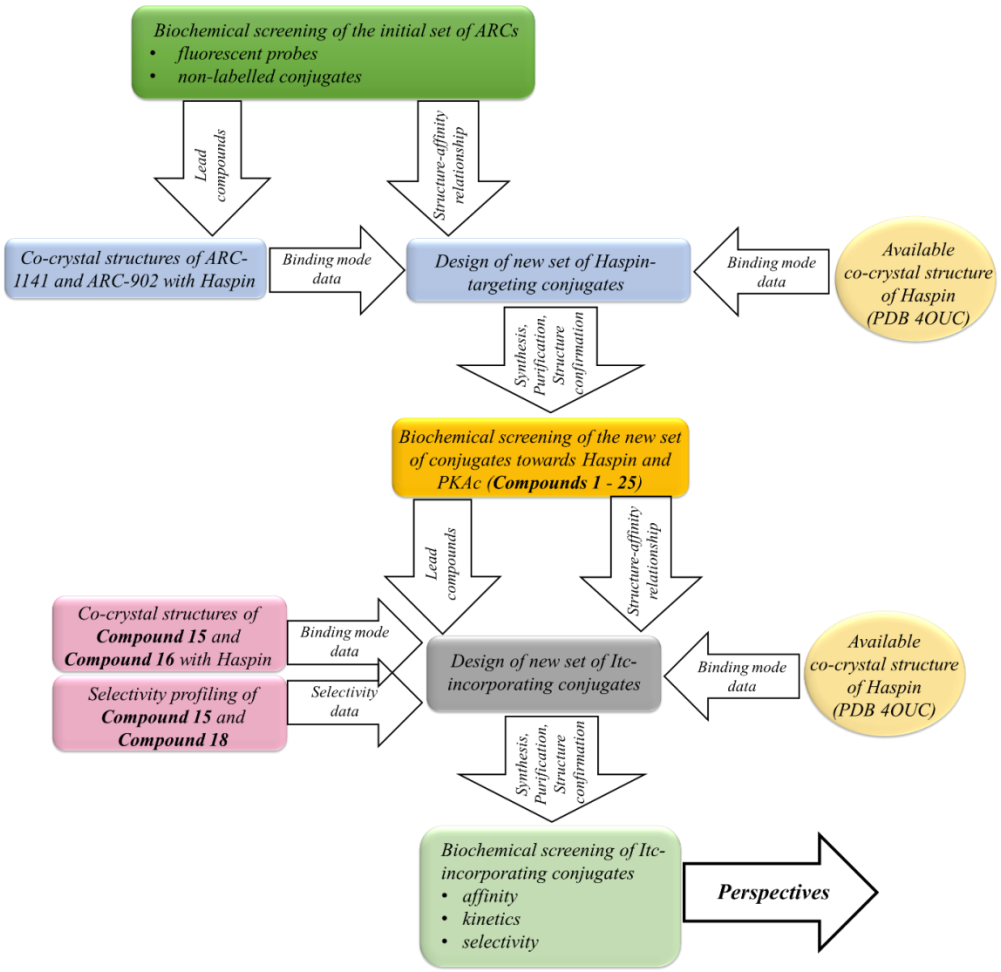

1. Screening of the Inital Set of ARC-Scaffold Towards Haspin [Paper I: Kestav *et al.*, 2015]

The first step in developing Haspin-targeting inhibitors and fluorescent probes involved the screening of ARC-based fluorescent probes towards mitotic kinase Haspin. For this, the equilibrium binding assay with fluorescence anisotropy (FA) readout was used. The aim of this was to choose the suitable high affinity fluorescent probe(s) for the further screening of non-fluorescent ARCs. The probes represented structurally diverse scaffolds; however, all of those incorporated the fluorescent dye with similar optical properties (*i.e.*, TAMRA or Cy3B) as well as an oligoarginine fragment, as it was presumed that Haspin as a basophilic PK[42] should possess high affinity towards compounds comprising the positively charged Arg residues. The probes had previously shown low nanomolar or subnanomolar dissociation constants (K_D values) in studies with different basophilic PKs (*e.g.,* PKA, cGMP-dependent PK, Rho-kinase ROCK2) and a relatively wide selectivity profile in commercial PK panels.[111,126,129,133,173] The codes and schematic structures of ARC-based probes are given in Table 4.

Table 4. Schematic structures, values of equilibrium dissociation constant K_D of fluorescent probes as established in the equlibrium binding assay with Haspin

Compound	*Schematic Structure*	K_D, *nM***
ARC-583	Adc-Ahx-DArg$_6$-DLys*(TAMRA)-NH$_2$	2.0 (0.8)
ARC-669	AMTH-Ahx-DArg-Ahx-DArg$_6$-DLys*(TAMRA)-NH$_2$	9.2 (2.5)
ARC-1042	Adc-Ahx-DArg-Ahx-DArg$_6$-DLys*(TAMRA)-NH$_2$	0.91 (0.28)
ARC-1059	H9-(CH$_2$)$_5$-C(=O)-DArg$_6$-DLys*(TAMRA)-NH$_2$	2.0 (0.3)
ARC-1081	Adc-Ahx-DArg-Ahx-DArg$_6$-DLys*(Cy3B)-NH$_2$	1.0 (0.2)
ARC-1144	AMSE-Ahx-DArg-Ahx-DArg$_6$-DLys*(TAMRA)-NH$_2$	23 (8)

* reveals the attachment of fluorescent dye to the side-chain of DLys; ** standard error values are given in brackets (N ≥ 2).

The assay showed that **ARC-1042** and **ARC-1081** possessed the highest affinity towards Haspin (K_D values of 0.91 nM and 1.0 nM, respectively). Both probes were derived from the same non-labelled precursor compound comprising adenosine-4'-dehydroxymethyl-4'-carboxylic acid moiety (Adc) as the ATP-site targeting fragment, two 6-aminohexanoic linkers (Ahx) separated by DArg residue as the chiral spacer, and the (DArg)$_6$ peptide as the peptidic fragment with amidated C-terminus.

Having sieved out the suitable probes with high affinity, the subsequent step involved the screening of non-fluorescent ARCs towards Haspin by applying

the equilibrium displacement assay with FA readout; **ARC-1081** was used as the fluorescent probe. The screening set included variable structural scaffolds with the aim to identify the conjugates that could serve as lead compounds for development of Haspin-targeting inhibitors (Table 5). All the compounds of screening set were previously reported ARCs or their analogues[121,122,126,173,174], whereas the structural differences were as follows:

- different ATP-site-targeting fragments,
- different chirality and number of arginine residues (0, 2, 6 or 8) in the peptidic fragment,
- different structure and number of linkers (1 or 2),
- incorporation of a chiral spacer between the linker moieties,
- and attachment of a fatty acid moiety.

Schematic structures of compounds of the screening set together with the obtained K_d values are shown in Table 5 (note: here and in the following discussion K_d indicates the equlibrium dissociation constant of non-fluorescent conjugates).

Not suprisingly, the data revealed that the affinity of conjugates towards Haspin was strongly dependent on the number of Arg residues in peptidic fragment, the same tendency had also been reported previously in studies with other basophilic PKs.[121,126,131] Generally, the addition of two Arg residues gave two orders of magnitude gain in affinity (*e.g.*, series: **ARC-1034** → **ARC-582** → **ARC-902**). However, the affinity increase was only observed up to 6 Arg residues in the peptidic part, as 8 residues did not cause significant improvement of affinities (**ARC-902** *versus* **ARC-1090** or **ARC-1197**). Next, DArg residues in peptidic fragment of conjugates were preferred over L-isomers (**ARC-902** *versus* **ARC-341**). The chirality of spacer between the flexible Ahx linkers had no observable effect on the affinity of conjugates for Haspin (**ARC-1012** *versus* **ARC-1038**). The latter effect differed from the previous studies with PKA C, where the D-amino acid as chiral spacer was essential for the high affinity of conjugates.[126] The attachment of fatty acid moiety, *i.e.*, myristoyl moiety (Myr), generally led to drop in affinity of conjugates (**ARC-684** *versus* **ARC-685** or **ARC-1141** *versus* **ARC-1143)**. The latter observation could probably be attributed to the fact that the positive charge of the side-chain of Lys was removed during the introduction of Myr moiety.

Table 5. Schematic structures and values of the dissociation constant K_d of non-fluorescent conjugates of initial set established in the displacement assay with Haspin and fluorescent probe **ARC-1081**

Compound	*Schematic Structure*	K_d, *nM***
ARC-1010	Adc-Ahx	over 15000
ARC-1034	Adc-Ahx-DArg$_2$-NH$_2$	3400 (400)
ARC-582	Adc-Ahx-DArg$_4$-NH$_2$	110 (8)
ARC-902	Adc-Ahx-DArg$_6$-NH$_2$	2.6 (0.3)
ARC-1090	Adc-Ahx-DArg$_8$-NH$_2$	9.0 (1.1)
ARC-341	Adc-Ahx-LArg$_6$-NH$_2$	40 (4)
ARC-342	Adc-Ahx-LArg$_6$-LLys-NH$_2$	33 (2)
ARC-1012	Adc-Ahx-DLys-Ahx-DArg$_2$-NH$_2$	2000 (200)
ARC-1038	Adc-Ahx-LLys-Ahx-DArg$_2$-NH$_2$	2000 (100)
ARC-1041	Adc-Ahx-DArg-Ahx-DArg$_6$-DLys-NH$_2$	0.24 (0.11)
ARC-1176	AMTH-Ahx-DArg-NH$_2$	over 15000
ARC-1102	AMTH-Ahx-DLys-Ahx-DArg$_2$-NH$_2$	over 15000
ARC-668	AMTH-Ahx-DArg-Ahx-DArg$_6$-DLys-NH$_2$	15 (3)
ARC-1141	AMTH-Ahx-DAla-DArg$_6$-DLys-Gly	16 (3)
ARC-1143	AMTH-Ahx-DAla-DArg$_6$-DLys*(Myr)-Gly	66 (5)
ARC-1197	AMTH-Ahx-DArg-Ahx-DArg$_6$-DLys*(-C(=O)-(CH$_2$)$_7$-C(=O)-DArg$_6$-NH$_2$)-NH$_2$	4.7 (0.5)
ARC-3009	H9-C(=O)-CH$_2$-NH-CH$_2$-C(=O)-DArg$_2$-NH$_2$	over 15000
ARC-3010	H9-C(=O)-CH$_2$-NH-CH$_2$-C(=O)-DArg$_6$-NH$_2$	800 (160)
ARC-903	H9-(CH$_2$)$_5$-C(=O)-DArg$_6$-NH$_2$	37 (3)
ARC-1408	PIPY-C(=O)-(CH$_2$)$_7$-C(=O)-DArg-Ahx-DArg-NH$_2$	3700 (600)
ARC-1411	PIPY-C(=O)-(CH$_2$)$_7$-C(=O)-DArg$_6$-DLys-NH$_2$	11 (2)
ARC-684	PYB-Ahx-DArg-Ahx-DArg$_6$-DLys-NH$_2$	17 (3)
ARC-685	PYB-Ahx-DArg-Ahx-DArg$_6$-DLys*(Myr)-NH$_2$	390 (50)
ARC-3125	TIBI-CH$_2$-C(=O)-Ahx-DArg$_6$-DLys-NH$_2$	0.56 (0.09)
-	DArg$_9$-NH$_2$	over 15000

The compounds are listed in alphabetical order according to their ATP-site binding fragments. * reveals the attachment of the fragment indicated in brackets to the side-chain of DLys; ** standard error values are given in brackets (N ≥ 2).

Next, Adc as the nucleosidic fragment possessing similarity to ATP and comprising several chirality centres was preferred over the planar and non-chiral aromatic systems such as AMTH or H9 (**ARC-902** *versus* **ARC-668** or **ARC-903**). The comparison of compounds **ARC-1041** and **ARC-902** both comprising Adc and Arg_6 fragment, revealed that the elongation of linker together with the introduction of chiral spacer increased the affinity. Similar trend had been reported for PKA C.[126] On the other hand, the conjugates incorporating 5-(2-aminopyrimidin-4-yl)-thiophene-2-carboxylic acid moiety (AMTH) did not show the latter effect in case of similar structural modification (**ARC-668** *versus* **ARC-1141**). Moreover, the importance of flexibility and length of linker of conjugates was demonstrated in a series incorporating Hidaka´s inhibitor H9. In particular, **ARC-3010** comprising a relatively short rigid linker possessed over 20-fold lower affinity than its counterpart **ARC-903** incorporating a more flexible linker.

Finally, in addition to ARCs, the affinity of the compound comprising Adc moiety and a linker (**ARC-1010**) and that of nona-arginine peptide alone ($DArg_9$-NH_2) was established. As expected, the results revealed that at the highest used concentration, none of the fragments were able to completely displace the fluorescent probe from the compex with Haspin. Thus, the importance of conjugation of fragments to achieve higher affinity towards Haspin was demonstrated.

Overall, the results indicated that the positively charged Arg residues in peptidic fragment facilitate the binding of conjugates to Haspin. Furthermore, the importance of ATP-site fragment together with the linker structure (flexibility *versus* rigidity) for binding of conjugate was demonstrated, however, the effect was not as significant as number of Arg residues in the peptidic fragment.

The Initial Selectivity Profile Determination of ARC-Based Conjugates of the Initial Set of Compounds

With the aim to determine the selectivity profile of the initial set of ARCs, the thermal shift studies were performed with Haspin as well as CMGC kinase family members Clks (Cdc2-like kinases) and DYRK2 (dual-specificity tyrosine (Y)-phosphorylation regulated kinase 2). These PKs were chosen based on the reported off-targets of Haspin-selective inhibitor 5-ITu.[90]

The results revealed that the data established in displacement assay and in thermal shift assay with Haspin were in good correlation, *i.e.*, the higher ΔT_m values corresponded to lower IC_{50} (or K_d) values, hence reflecting the higher affinity of compounds (Table 6). As discussed above, ΔT_m values around 4 °C usually correspond to K_d values below 1 μM, whereas ΔT_m values over 8 °C generally correspond to K_d values below 100 nM.[161–163] Interestingly, **ARC-685** and **ARC-3010** represented the outliers from the general trend, as those conjugates possessed lower ΔT_m values than expected based on their affinity. Overall, 7 compounds out of 15 showed ΔT_m values over 5 °C, thus indicating submicromolar range of potency. Importantly, all these conjugates incorporated oligoarginine fragment in their structure.

Table 6. Values of thermal shift (ΔT_m) of non-fluorescent conjugates from the inital set in studies with Haspin, Clk1, Clk2, Clk3 and DYRK2

Compound	*Schematic Structure*	ΔT_m, °C** *Haspin*	ΔT_m, °C** *Clk1*	ΔT_m, °C** *Clk2*	ΔT_m, °C** *Clk3*	ΔT_m, °C** *DYRK2*
ARC-1034	Adc-Ahx-DArg$_2$-NH$_2$	4.5 (0.1)	2.5 (0.2)	0.6 (0.1)	0.3 (0.0)	1.2 (0.0)
ARC-902	Adc-Ahx-DArg$_6$-NH$_2$	**8.6 (0.2)**	3.4 (0.1)	1.0 (0.1)	1.8 (0.1)	0.8 (0.0)
ARC-341	Adc-Ahx-LArg$_6$-NH$_2$	**5.7 (0.1)**	2.5 (0.2)	0.8 (0.0)	1.1 (0.1)	0.6 (0.0)
ARC-1012	Adc-Ahx-DLys-Ahx-DArg$_2$-NH$_2$	4.6 (0.1)	1.4 (0.1)	0.7 (0.1)	1.1 (0.1)	1.9 (0.0)
ARC-1038	Adc-Ahx-LLys-Ahx-DArg$_2$-NH$_2$	4.2 (0.1)	0.8 (0.0)	0.3 (0.1)	0.2 (0.1)	0.4 (0.0)
ARC-1102	AMTH-Ahx-DLys-Ahx-DArg$_2$-NH$_2$	2.8 (0.0)	3.2 (0.1)	1.9 (0.0)	1.7 (0.0)	2.8 (0.0)
ARC-668	AMTH-Ahx-DArg-Ahx-DArg$_6$-dLys-NH$_2$	**8.0 (0.1)**	**5.6 (0.0)**	3.9 (0.1)	**6.1 (0.1)**	2.1 (0.0)
ARC-1141	AMTH-Ahx-DAla-DArg$_6$-DLys-Gly	**6.0 (0.1)**	**5.3 (0.1)**	3.1 (0.1)	4.8 (0.2)	2.2 (0.1)
ARC-3009	H9-C(=O)-CH$_2$-NH-CH$_2$-C(=O)-DArg$_2$-NH$_2$	1.1 (0.1)	1.2 (0.1)	0.3 (0.1)	0.2 (0.1)	0.3 (0.1)
ARC-3010	H9-C(=O)-CH$_2$-NH-CH$_2$-C(=O)-DArg$_6$-NH$_2$	2.0 (0.1)	0.7 (0.0)	0.3 (0.1)	0.3 (0.0)	0.2 (0.0)
ARC-1408	PIPY-C(=O)-(CH$_2$)$_7$-C(=O)-DArg-Ahx-DArg-NH$_2$	3.9 (0.0)	4.8 (0.5)	3.2 (0.0)	2.9 (0.1)	2.0 (0.1)
ARC-1411	PIPY-C(=O)-(CH$_2$)$_7$-C(=O)-DArg$_6$-DLys-NH$_2$	**7.8 (0.1)**	**5.8 (0.3)**	3.9 (0.1)	**5.1 (0.2)**	1.1 (0.0)
ARC-684	PYB-Ahx-DArg-Ahx-DArg$_6$-DLys-NH$_2$	**5.7 (0.1)**	-1.8 (0.2)	0.6 (0.0)	2.5 (0.1)	-1.1 (0.0)
ARC-685	PYB-Ahx-DArg-Ahx-DArg$_6$-DLys*(Myr)-NH$_2$	2.8 (0.1)	2.0 (0.2)	-5.2 (0.4)	-1.5 (0.4)	0.4 (0.0)
ARC-3125	TIBI-CH$_2$-C(=O)-Ahx-DArg$_6$-DLys-NH$_2$	**10.1 (0.1)**	**6.5 (0.2)**	4.0 (0.1)	2.9 (0.2)	3.3 (0.0)

The compounds are listed in alphabetical order according to their ATP-site binding fragments. * reveals the attachment of the fragment indicated in brackets to the side-chain of DLys; ** standard error values are given in brackets (N ≥ 2). ΔT_m values over 5 °C are shown in bold.

The ΔT_m values of conjugates in complexes with Clk1, Clk2, Clk3 and DYRK2 were considerably lower than in the corresponding complexes with Haspin. The results indicated that Haspin possessed the higher affinity for conjugates that comprised the oligoarginine fragment, whereas other tested PKs showed the preference based on the nucleosidic fragment, whereas generally AMTH, PIPY and TIBI moieties were preferred. This was not surprising as neither DYRK nor Clk family are considered classically basophilic, although the consensus sequences of their substrates do contain Arg in the certain positions relative to the phosphorylatable residue.[175,176]

Overall, based on the results established in the screening of ARC-based conjugates of initial set, two lead compounds **ARC-1141** and **ARC-902** were chosen for the co-crystallization with Haspin. Both of those conjugates contained oligoarginine fragment in their peptidic part, but incorporated different nucleosidic fragments, *i.e.*, AMTH in case of **ARC-1141** and Adc in case of **ARC-902**.

2. Rational Design and Biochemical Characterization of Haspin-Targeting Bisubstrate-Analogue Inhibitors [Paper I: Kestav *et al.*, 2015; unpublished data]

Co-Crystal Structures of Haspin with ARC-Based Lead Compounds

The crystallization studies resulted in co-crystal structures with high resolution (resolution of 1.87 and 1.70 Å for **ARC-1141** and **ARC-902**, respectively) and both structures showed typical space group $P2_12_12_1$ for the kinase domain of Haspin (Table 7). Expectedly, ARCs were bound to the catalytic cleft of Haspin, whereas the nucleosidic fragment was buried deeper into the cleft between the N- and C-lobe; at the same time, the peptidic fragment was more directed into the solvent (Figure 23 and Figure 24). Also, the electron densities corresponded to the nucleosidic fragment and linker part were unambigously defined. On the other hand, despite the observed high resolution of crystal structures of **ARC-1141** and **ARC-902**, the electron densities of peptidic part were only defined for two (in case of **ARC-1141**) or three (in case of **ARC-902**) arginine residues and, therefore, it was suggested that oligoarginine fragments are relatively mobile and could adopt multiple conformations (Figure 23 and Figure 24). Despite the high resolution, the overall quality of structural factors was low and hence the crystal structures were not deposited into Protein Data Bank.

Table 7. Structural factors of co-crystal structures of **ARC-1141** and **ARC-902** with Haspin

Characteristics	*ARC-1141:Haspin*	*ARC-902:Haspin*
Resolution (Å)	1.87	1.70
R-value	0.160	0.153
Space group	$P2_12_12_1$	$P2_12_12_1$

In co-crystal structure of **ARC-1141** with Haspin (Figure 23), the exocyclic nitrogen of AMTH moiety functioned as a donor of H-bond for ***Glu606*** of Haspin (the same interaction between the *N1* amino group of AMP and Haspin, see Figure 7). Also, the hydrophobic stacking occured between the aromatic AMTH moiety and ***Phe607***. Interestingly, the hydrophobic linker following AMTH moiety made a sharp turn (ca 90º), whereas such positioning had not been seen previously in co-crystals structures of ARCs with PKs.[126,177] The backbone nitrogen of the first DArg following the linker (DArg#1) formed H-bond with ***Gln718***, wherein no interaction was seen for the side-chain of the same arginine residue. Still, the guanidinium group of DArg#1 of **ARC-1141** was probably involved in π-π stacking with the amide bond between ***Gly715*** and ***Asp716*** of Haspin. Next, DArg#2 protruded up to the G-rich loop and formed two charge-reinforced H-bonds with the backbone carbonyl of ***Glu492***.

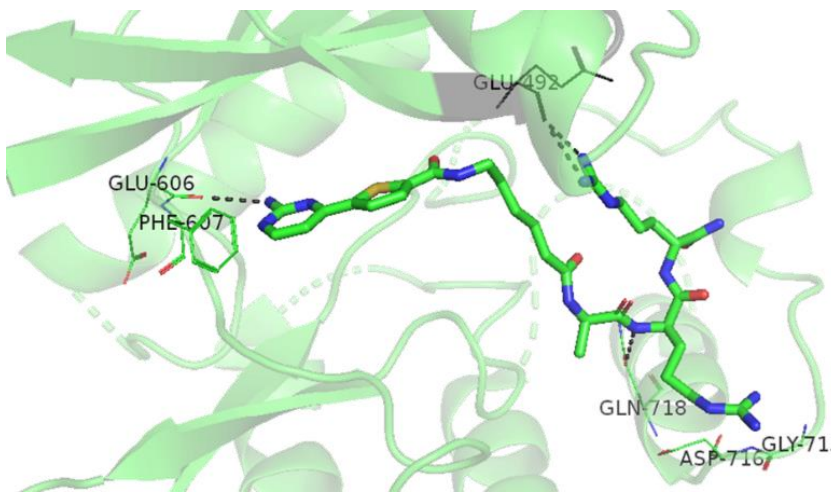

Figure 23. Co-crystal structure of **ARC-1141** with Haspin kinase domain. PK is indicated as green cartoon and ARC as coloured sticks; G-rich loop is shown as black cartoon; residues of PK that form the interactions with the co-crystallized compound are shown as lines and are labelled; hydrogen bonds are shown as black dotted lines.

Differently from **ARC-1141**, **ARC-902** gave remarkably higher number of H-bonds with the kinase domain of Haspin. Similarly, ATP-site targeting Adc moiety formed analogous interactions with Haspin as AMP and **ARC-1141** (Figure 7 and Figure 23, respectively) *i.e.*, a H-bond with ***Glu606*** and a hydrophobic interaction with ***Phe607*** of Haspin. However, the polar interaction with ***Gly608*** was missing. The hydroxyls of ribose moiety of **ARC-902** developed H-bond with ***Asp611*** and ***Gly653*** (Figure 24).

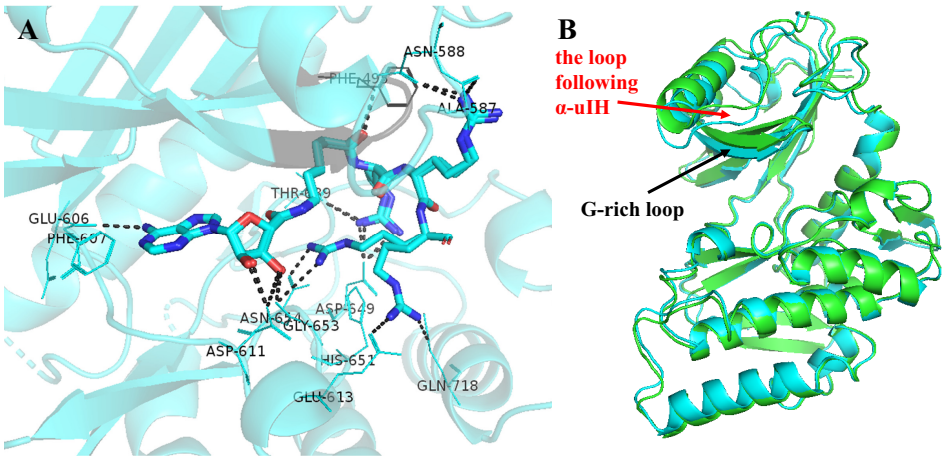

Figure 24. A) Co-crystal structure of **ARC-902** with Haspin kinase domain. PK is indicated as cyan cartoon and ARC as coloured sticks; G-rich loop is shown as black cartoon; residues of PK that form the interactions with the co-crystallized compound are shown as lines and are labelled; hydrogen bonds are shown as black dotted lines. B) Overlay of co-crystal structures of **ARC-1141** (green) and **ARC-902** (cyan). PK is indicated as cartoon. The G-rich loop as well as the loop following the upper lobe helix (α-uIH) are showed by black and red arrows, respectively.

The linker fragment Ahx was positioned under the G-rich loop, which had been previously seen from co-crystal structures of ARCs with PKA C (Figure 24).[126,177] Also, the carbonyl of Ahx gave H-bond with the backbone nitrogen of ***Phe495***. As a result, the co-crystal structure of **ARC-902** with Haspin showed more closed conformation compared to the complex of Haspin with **ARC-1141** (Figure 24, B). Next, DArg#1 of **ARC-902** formed polar contacts with the C-lobe residues ***Asp649*** and ***Thr689***, whereas the latter interactions reflected the typical binding pattern of ARCs revealed within the previous studies with PKA C.[126,177] The next arginine residue (DArg#2) flipped over the G-rich loop and gave H-bonds with the residues of N-lobe of Haspin, *i.e.*, ***Ala587*** and ***Asn588***. The latter interactions were similar to the binding pattern of H3(1-7): *Arg2* of H3 was protruded to the pocket between the G-rich loop as well as the loop

following α-ulH of Haspin and developed H-bond with ***Asn588*** (Figure 32, Figure 24).[54] The last arginine for which the electron density was still defined (DArg#3) was positioned to Haspin in two different conformations, whereas the interactions were developed with ***Glu613*** and ***Gln718*** or ***Gly653*** and ***Asn654***. In case of the latter conformation, a π-π stacking also occurred between the guanidinium group of DArg#3 and the imidazole ring of ***His651*** of Haspin.

Principles of Design of New Set of ARC-Inhibitors

The subsequent step in rational design of Haspin-tageting conjugates involved the comparison of co-crystal structures of Haspin with ARCs (*i.e.*, **ARC-1141** or **ARC-902**) or H3(1-7) (PDB 4OUC), which was published by Maiolica and co-workers in 2014.[54]

The ATP-site targeting fragment was chosen based on the results of structure-affinity studies. Thus, AMTH and Adc moiety were chosen as the ATP-site targeting fragments of conjugates. The previous studies have revealed that the oligoarginine fragment contributes to the increase of affinity, but often leads to the loss of selectivity towards basophilic PKs. Previously, Uri and co-workers had demonstrated that substitution of oligoarginine peptidic fragment of conjugates with oligoaspartate or oligoaspartate-imitating peptoid fragment resulted in high affinity as well as selectivity of conjugates for acidophilic PK CK2.[108,130,132] Therefore, with the aim to incease the selectivity of compounds towards Haspin, H3(1-7)-like peptide representing an analogue of the substrate of Haspin was used as the Haspin substrate-site targeting moiety of new conjugates.

Next, it was necessary to identify the suitable positions for linking ATP-site fragment and H3-like peptide. The overlay of co-crystal structure of Haspin with ARC-based lead compounds **ARC-1141** or **ARC-902** with 5-ITu and H3(1-7) (PDB 4OUC) revealed two positions in the structure of H3(1-7), which were used to link the fragments (Figure 25). In particular, the linking in the proximity of the N-terminus of peptide led to the generation of Set A compounds, and the linking in the proximity of the phosphorylatable *Thr3* led to the generation of Set B compounds (Figure 25).

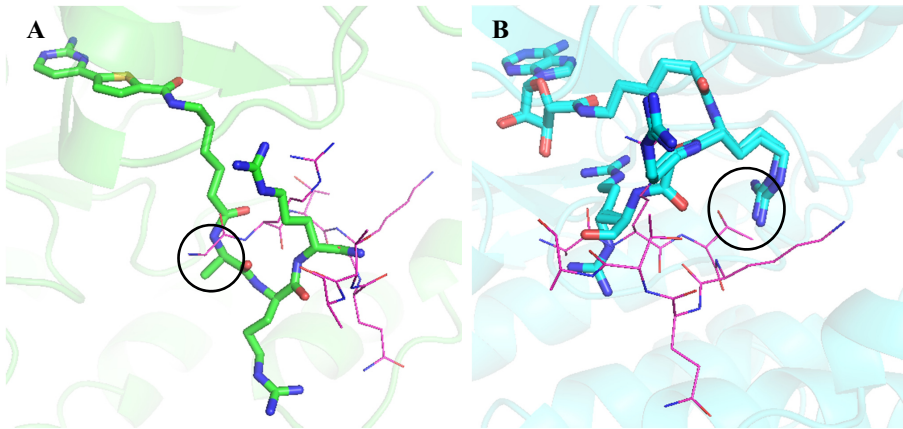

Figure 25. A) Overlay of co-crystals of **ARC-1141** (green) *versus* histone H3 (magenta; residues 1-7, PDB 4OUC) with Haspin. B) Overlay of co-crystals of **ARC-902** (blue) *versus* histone H3 (magenta; residues 1-7, PDB 4OUC) with Haspin. PK is indicated as cartoon; ARCs as sticks and H3 as lines; the black circles show the locations where the linkage between the nucleosidic fragment and peptide was introduced into the structure of novel Haspin-tageting ARCs, leading to the generation of Set A (A) and Set B (B) of novel Haspin-targeting conjugates.

Set A: Linkage via N-Terminal Region of Histone H3(1-7) Analogue Peptide (Compounds 1-13)

ARC-1141 was used as the starting compound for the novel conjugates of Set A. Novel conjugates of Set A incorporated AMTH as ATP-site binding fragment and had amidated C-terminus (schematic structures are given in Table 8). The amidation of C-terminus was required due to the synthetic rationale as well as to mask the negative charge of carboxylate of C-terminus, which was expected to improve the affinity of conjugates for Haspin as a basophilic PK. Other structural variations among the conjugates included acylation of N-terminus of H3(1-7) analogue peptide as well as introduction of linkers with variable length and flexibility. Moreover, in some cases the hexa-(L / D)-arginine fragment was incorporated to the N- or C-terminus of H3(1-7)-like peptide. The purpose of latter structural modification was to improve the cell plasma membrane-penetrative properties[178] of compounds and thus to facilitate the internalization of conjugates into the live cells in the following studies. Furthermore, the addition of number of positive charges of oligoarginine fragment was proposed to lead to the gain in affinity towards Haspin.

The overlay of co-crystals of **ARC-1141** *versus* H3(1-7) revealed that *Ala1* of H3(1-7) located near the DAla moiety of **ARC-1141** (Figure 25). Thus, in **Compounds 1-7**, *Ala1* of H3(1-7) was replaced with DLys (Figure 26). The 3D-structure reavealed that *Ala1* of H3(1-7) pointed away from the ATP-binding site; therefore, it was expected that the change of chirality from L to D should compensate for this difference and 'flip' the side-chain of DLys towards the

ATP-side. Next, the linker as well as AMTH moiety was conjugated with the peptide *via* the side-chain of DLys. Differently from the previous, in **Compounds 8-13**, *Ala1* was substituted with D-diaminopropionic acid moiety (DDap) and *via* its N-terminus, the linker and nucleosidic moiety were connected with the peptide (Figure 26).

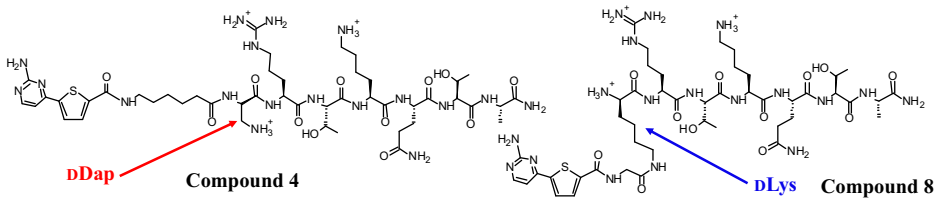

Figure 26. The structures of **Compound 4** and **Compound 8**. D-diaminopropionic acid moiety (DDap) and DLys discussed in text are indicated with red and blue arrows, respectively.

The affinities of novel conjugates (note: Set A as well as Set B) were determined in displacement assay with FA readout by using the fluorescent probe **ARC-1081**. As a reference compound, **ARC-1141** was used. In order to find out whether the new conjugates are potentially selective towards Haspin, the affinities of conjugates for catalytic subunit of cAMP-dependent protein kinase (PKA C) serving as a basophilic reference PK were also established (Table 8).

The displacement data revealed that all the conjugates of Set A showed lower affinity compared to the starting compound **ARC-1141** (Table 8). Nevertheless, the selectivity of novel conjugates (except **Compound 8**) towards Haspin over PKA C was improved by one to three orders of magnitude compared to **ARC-1141**, thus demonstrating the rationale behind replacement of oligoarginine fragment with H3(1-7). The acylation of N-terminus of H3(1-7) fragment of conjugates led to the approximately 2-fold drop in affinity for Haspin; for instance, **Compound 1** with acylated N-terminus possessed K_d value of 15000 nM *versus* **Compound 4** possessed K_d value of 8800 nM. The drop of affinity could be explained by disruption of H-bond between *Ala1* of H3(1-7) and ***Glu613*** of Haspin resulted in acylation of N-terminus. Also, the acylation may mask the positive charge of the free amino group of N-terminus of peptidic fragment, which could be preferred by Haspin (as well as PKA C). The best affinity compound of Set A without Arg_6 peptide towards Haspin was represented by **Compound 8** (K_d value of 5200 nM), as the following optimization (including the introduction of rigid cycles, direct linkage of AMTH moiety with peptide) of linker structure only led to the drop of affinity.

Table 8. Values of the dissociation constant K_d and selectivity index of novel conjugates (Set A) established in the displacement assays with Haspin and PKA C

Nr	*Schematic Structure*	*K_d, nM** Haspin*	*K_d, nM** PKA C*	*Selectivity Index****
ARC-1141	AMTH-Ahx-DAla-DArg$_6$-DLys-Gly	16 (3)	0.06 (0.02)	0.004
1	AMTH-Gly-[Ac-DLys*-LArg-LThr-LLys-LGln-LThr-LAla-NH_2]	over 15000	over 15000	NC
2	AMTH-Gly-[Ac-DArg$_6$-DLys*-LArg-LThr-LLys-LGln-LThr-LAla-NH_2]	130 (20)	89 (6)	0.7
3	AMTH-Gly-[Ac-LArg$_6$-DLys*-LArg-LThr-LLys-LGln-LThr-LAla-NH_2]	82 (10)	39 (3)	0.5
4	AMTH-Gly-[DLys*-LArg-LThr-LLys-LGln-LThr-LAla-NH_2]	8800 (1000)	5800 (600)	0.7
5	AMTH-Abu-[DLys*-LArg-LThr-LLys-LGln-LThr-LAla-NH_2]	13000 (2000)	5000 (500)	0.4
6	AMTH-Abu-[DLys*-LArg-LThr-LLys-LGln-LThr-LAla-DArg$_6$-NH_2]	120 (10)	570 (40)	5
7	AMTH-Abu-[DLys*-LArg-LThr-lLys-LGln-LThr-LAla-LArg$_6$-NH_2]	150 (10)	550 (40)	4
8	AMTH-Ahx-[DDAP-LArg-LThr-LLys-LGln-LThr-LAla-NH_2]	5200 (700)	330 (20)	0.06
9	AMTH-Aoc-[DDAP-LArg-LThr-LLys-LGln-LThr-LAla-NH_2]	over 15000	51 (3)	below 0.004
10	AMTH-DPro-Gly-[DDAP-LArg-LThr-LLys-LGln-LThr-LAla-NH_2]	over 15000	over 15000	NC
11	AMTH-LPro-Gly-[DDAP-LArg-LThr-LLys-LGln-LThr-LAla-NH_2]	over 15000	over 15000	NC
12	AMTH-Inp-Gly-[DDAP-LArg-LThr-LLys-LGln-LThr-LAla-NH_2]	9500 (1300)	3800 (200)	0.4
13	AMTH-Tnx-Gly-[DDAP-LArg-LThr-LLys-LGln-LThr-LAla-NH_2]	over 15000	over 15000	NC

* indicates attachment of the preceding fragment to the side-chain of the amino acid; ** standard error values are given in brackets ($N \geq 2$); *** for each compound, selectivity index was calculated as the ratio of K_d values for PKA C and Haspin. For **Compounds 1-13**, the peptidic fragment corresponding to the modified H3(1-7) sequence is shown in square brackets. NC, not calculated.

As expected, the incorporation of Arg_6 motif led to the remarkable increase in affinity of conjugates (K_d value of 120 nM for **Compound 6** *versus* K_d value of 13000 nM for **Compound 5**). The selectivity profiling towards Haspin and PKA C revealed that the positioning of Arg_6 motif at the N-terminus of H3(1-7) was preferred by PKA C, while the positioning of hexaarginine at the C-terminus of H3(1-7) was preferred by Haspin (**Compounds 2** and **3** *versus* **Compound 6** and **7**, respectively). Notably, the latter supported the previous observations that Haspin preferably phosphorylates the residues near the N-terminus of substrates and the attachment of longer sequences to the N-terminus of phosphorylatable residue disrupts the recognition of substrates by Haspin.[179]

Set B: Linkage *via* Phosphorylatable Region of Histone H3(1-7)-like Peptide (Compounds 14-23)

ARC-902 was used as a starting compound of Set B. The overlay of co-crystals of **ARC-902** *versus* H3(1-7) with Haspin indicated that the side chain of first DArg residue following the linker of conjugate positioned in proximity of the phosphorylatable *Thr3* of H3(1-7) (Figure 25). Similarly to Set A, all the conjugates incorporated amidated C-terminus of H3(1-7) peptide, whereas two strategies were used to link the Adc moiety and histone peptide.

In the first case (**Compound 14**), *Thr3* of H3(1-7) was replaced with LAsp (Figure 27). The side-chain of LAsp was used to link Adc *via* the side-chain of DLys, which, at the same time, functioned as a chiral spacer. Also, on synthetic rationale, *Thr6* of H3(1-7) was substituted by LAla and the N-terminus of H3(1-7) was acylated. In the second case (**Compounds 15-23**), *Thr3* of H3(1-7) was substituted by LLys, to which side-chain Adc was connected *via* a set of linkers (Figure 27). The other structural variations included the introduction of different linkers with variable length and flexibility between the peptide and Adc moiety, and, in one case, Adc moiety was replaced with AMTH (**Compound 21**). Analogously to Set A, in some cases the hexa-(L / D)-arginine fragment was incorporated to the N- or C-terminus of H3(1-7)-like peptide.

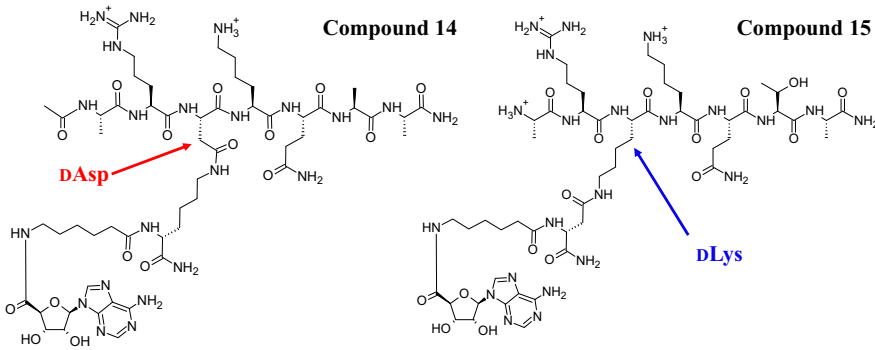

Figure 27. The structures of **Compound 14** and **Compound 15**. The chiral spacer represented by DAsp or DLys discussed in text are shown with red and blue arrows, respectively.

Again, with the aim to establish the initial selectivity properties, the affinity of conjugates for basophilic PKA C was also determined. The K_d values of conjugates towards Haspin as well as for PKA C together with the selectivity indices are shown in Table 9.

The compounds from the Set B possessed generally higher affinity as well as selectivity towards Haspin compared to Set A. Still, the affinity data for novel conjugates of Set B confirmed the previously observed trends of structure-affinity relationship. In particular, the acylation of N-terminus of modified H3(1-7) peptide led to dramatic, *i.e.*, 20-fold drop in affinity (K_d value of 5200 for **Compound 14** *versus* K_d value of 170 nM for **Compound 15**). On the contrary, the introduction of Arg_6 fragment led to the significant increase of affinity and resulted in conjugates with subnanomolar K_d value (K_d value of 0.42 nM and 0.88 nM for **Compound 18** and **19**, respectively), thus showing higher affinity than the reference compound 5-ITu (K_d value of 3.9 nM).

Importantly, the chiral spacer (D-amino acid) in the structure of linker was of utmost importance for the suitable binding of conjugates to Haspin. The affinity of compounds where the chiral spacer was replaced with a linear chain of approximately same length dropped significantly (K_d value of over 15000 nM for **Compound 20** *versus* K_d value of 170 nM for **Compound 15**). This confirmed the previous observation that a long flexible linker facilitates the binding of a bisubstrate inhibitor to its target[106]; still, the chiral spacer in the structure of linker fragment may be required to direct the peptidic part of the conjugate towards the substrate-binding site.[126] Again, the location of Arg_6 fragment confirmed the aforementioned notion that its positioning at C-terminus of H3(1-7) peptide is needed to achieve selectivity towards Haspin over PKA C (**Compound 18** and **19** with selectivity indices of 90 and 30, respectively, *versus* **Compound 22** and **23** with selectivity indices of 0.1 and 1, respectively).

The most efficient novel conjugates without Arg_6 fragment possessed K_d value around 100-170 nM (**Compounds 15-17**). In addition to modest affinity, **Compound 16** (K_d of 150 nM) showed 50-fold higher affinity for Haspin than PKA C. The latter effect was probably due to the free carboxylate instead of amide at the C-terminus of chiral spacer, as its counterpart **Compound 15** with amide showed comparable affinity towards Haspin (K_d value of 170 nM), but 5-fold lower selectivity index.

However, introduction of fatty acid Myr moiety into the structure of conjugate improved the affinity towards PKA C 40-fold, while the K_d value for Haspin remained in the same range (**Compound 17** *versus* **Compound 16**). This observation confirmed the trend previously established for ARCs from the initial set (Table 5), and could probably be attributed to the fact that Myr moiety interacts with the hydrophobic (P+1)-pocket of PKA C.[180]

Table 9. Values of the dissociation constant K_d and selectivity index of conjugates (Set B) established in the displacement assays with Haspin and PKA C

Nr	*Schematic Structure*	*K_d, nM** Haspin*	*K_d, nM** PKA C*	*Selectivity Index****
ARC-902	Adc-Ahx-DArg$_6$-NH_2	2.6 (0.3)	2.7 (0.4)	1
-	5-iodotubercidin	3.9 (0.4)	over 15000	over 4000
14	Adc-Ahx-DLys*[Ac-LAla-LArg-LAsp*-LLys-LGln-LAla-LAla-NH_2]-NH_2	5200 (700)	1700 (100)	0.3
15	Adc-Ahx-DAsp*[LAla-LArg-LLys*-LLys-LGln-LThr-LAla-NH_2]-NH_2	170 (40)	1600 (300)	9
16	Adc-Ahx-DAsp*[LAla-LArg-LLys*-LLys-LGln-LThr-LAla-NH_2]-OH	150 (19)	7700 (1400)	50
17	Adc-Ahx-DAsp*[LAla-LArg-LLys*-LLys-LGln-LThr-LAla-DLys(Myr)-NH_2]-OH	100 (4)	190 (27)	2
18	Adc-Ahx-DAsp*[LAla-LArg-LLys*-LLys-LGln-LThr-LAla-LArg$_6$-NH_2]-NH_2	0.42 (0.14)	38 (4)	90
19	Adc-Ahx-DAsp*[LAla-LArg-LLys*-LLys-LGln-LThr-LAla-DArg$_6$-NH_2]-NH_2	0.88 (0.15)	27 (3)	30
20	Adc-Ahx-Abu-[LAla-LArg-LLys*-LLys-LGln-LThr-LAla-NH_2]	over 15000	5300 (1000)	below 0.4
21	AMTH-Ahx-Abu-[LAla-LArg-LLys*-LLys-LGln-LThr-LAla-NH_2]	over 15000	1600 (700)	below 0.1
22	Adc-Ahx-DAsp*[LArg$_6$-LAla-LArg-LLys*-LLys-LGln-LThr-LAla-NH_2]-NH_2	23 (4)	2.9 (0.6)	0.1
23	Adc-Ahx-DAsp*[DArg$_6$-LAla-LArg-LLys*-LLys-LGln-LThr-LAla-NH_2]-NH_2	14 (2)	17 (2)	1
24	Adc-Ahx-DAsp-NH_2	over 15000	over 15000	NC
25	LAla-LArg-LLys-LLys-LGln-LThr-LAla-DArg$_6$-NH_2	5800 (1800)	over 15000	over 3

* indicates attachment of two fragment or the preceding fragment to the side-chain of the amino acid; ** standard error values are given in brackets ($N \geq 2$); *** for each compound, selectivity index was calculated as the ratio of K_d values for PKA C and Haspin. For **Compounds 14-23**, the peptidic fragment corresponding to the modified H3(1-7) sequence is shown in square brackets. NC, not calculated.

Finally, it was established that the separate fragments of conjugates (*i.e.*, ATP site-targeting fragment with linker and chiral spacer or H3(1-7) peptide with Arg_6 fragment) alone possessed low affinity towards Haspin (Table 9). Hence, it demonstrated the importance of conjugation of fragments targeting different sites of Haspin.

Selectivity Profiling of Novel Conjugates in a Panel of PKs

Based on the results established in displacement assay (Table 8 and Table 9), two novel conjugates were chosen for the following selectivity profile determination towards a panel of 43 kinases (commercial inhibition assay carried out by Carna Biosciences). One of the selected conjugates incorporated only H3(1-7)-like sequence in its peptidic part (**Compound 15**; final total concentration in the assay of 5 μM), whereas the other comprised both H3(1-7) sequence as well as Arg_6 fragment (**Compound 18**; final total concentration in the assay of 1 μM). As a reference, the selectivity data of **ARC-902** (final total concentration in the assay of 1 μM) obtained in the previous studies[121] was included for comparison.

The panel of PKs included important players in mitosis (*e.g.*, Aurora PKs, families of Cdk and Nek) as well as several basophilic PKs (*e.g.*, families of Akt, Pim, ROCK). An abbreviated table of the inhibition percentages of novel conjugates and reference compound **ARC-902** are given in Table 10. The complete dataset is presented in the corresponding publication (Paper I: Kestav *et al.*, 2015).[127]

The results revealed that **Compound 18** possessed wide selectivity profile and inhibited a variety of PKs to the extent over 80%, including most of the basophilic PKs (*i.e.*, AGC and CAMK groups, Aurora B, Clk1). Moreover, **Compound 18** inhibited important mitotic players in families of Cdk (except Cdk7 and Cdk9) and Nek (except Nek2 and Nek7). As expected, the acidophilic PKs (*i.e.*, Cdc7, CK2, Plk family) were not inhibited. The negative inhibition percentage values may either be explained by the fact that the compound activated PKs – or, more likely, that the compound reduced the non-specific binding of PKs to the surfaces. Also, the selectivity profile of **Compound 18** was analogous to the reference compound **ARC-902**, wherein Aurora B, Cdk2/CycA, Nek6, Pim2 and PKCα were inhibited to even greater extent. Overall, based on data above, it can be concluded that the positively charged oligoarginine fragment made the conjugates attractive for basophilic PKs, despite the histone fragment in the structure of compound.

On the other hand, **Compound 15** showed significantly less wide selectivity profile even at 5-fold higher concentration (note: 5 μM concentration was chosen due to the lower affinity of **Compound 15** for Haspin compared to **Compound 18**). Remarkably, only 3 PKs out of 43 were inhibited over 80% (*i.e.*, Haspin, PKA C, ROCK2) and 3 PKs were inhibited to the extent of 60-80% (CHK1, p70S6K and Pim1).

Table 10. An abbreviated table of inhibition profiles of **Compounds 15** and **18** together with reference compound **ARC-902** (reported previously[121])

PK	*PK Group*	*Compound 15* *5 μM*	*Compound 18* *1 μM*	*ARC-902* *1 μM*
Akt1 (PKBα)	AGC	46	97	98**
Akt3 (PKBγ)	AGC	28	94	-
AurA	other	-19	48	-
AurB	other	-8	87	-3***
AurC	other	-93	23	-
BRSK2 (SAD-A)	CAMK	24	57	-
Cdc2 (Cdk1)/CycB1	CMGC	7	99	-
Cdc7/ASK	other	-18	-146	-
Cdk2/CycA2	CMGC	15	98	12***
Cdk2/CycE1	CMGC	-2	88	-
Cdk3/CycE1	CMGC	0	74	-
Cdk4/CycD3	CMGC	-7	72	-
Cdk6/CycD3	CMGC	3	67	-
Cdk7/CycH/MAT1	CMGC	-4	-73	-
Cdk9/CycT1	CMGC	-1	23	-
CK2α1/β	other	-5	-19	-4**
Clk1	CMGC	58	102	-
Haspin	**other**	**102**	**99**	**-**
MSK1	AGC	55	101	98***
Nek1	other	8	84	-
Nek2	other	4	-23	18****
Nek6	other	2	61	6****
Nek7	other	-2	37	42***
Nek9	other	15	65	-
Pim1	CAMK	73	102	-
Pim2	CAMK	59	102	62**
PKA C	AGC	98	100	89***
PKCα	AGC	51	100	69***
Plk1	other	-9	-84	19**
Plk2	other	7	-56	-
ROCK2	AGC	96	102	100***

Colour code:

Colour	**% inhibition**	**Colour**	**% inhibition**	**Colour**	**% inhibition**
	below 20		40-60		above 80
	20-40		60-80		no data

Final total concentrations of ATP in the assay: * 1 mM; ** 5 μM; *** 20 μM; **** 50 μM; no asterisk, close to K_m(ATP) value for a given PK.

The focussed selectivity profile of **Compound 15** demonstrated the successful design of Haspin-targeting selective bisubstrate-analogue inhibitor, as the selectivity of substrate of Haspin translated into selectivity of H3-containing conjugates.

3. Co-Crystal Structures of Haspin with Novel Selective Conjugates [Paper II: Lavogina *et al.*, 2016]

Prior to the given work, 9 crystal structures of catalytic domain of Haspin were deposited in RCSB Protein Data Bank (PDB) (Table 11).

Table 11. Crystal structure of Haspin deposited in Protein Data Bank as of January 21st, 2018

PDB Code	*Haspin Residues*	*Ligand(s)*	*Resolution, Å*	*Year of Deposition*	*Reference*
2WB8	452-798	- (apoenzyme)	2.15	2009	[52]
2VUW	465-798	5-ITu	1.8	2008	[181]
3DLZ	465-798	AMP	1.85	2008	[181]
3E7V	471-798	3-(3-aminophenyl)-N-(3-chlorophenyl)pyrazolo[1,5-a]pyrimidin-5-amine	2.0	2008	-
3F2N	471-798	(2S)-2-{[3-(3-aminophenyl)imidazo[1,2-b]pyridazin- 6-yl]amino}-3-methylbutan-1-ol	1.8	2008	-
3FMD	470-789	H89	2.0	2008	-
3IQ7	465-798	5-ITu	2.0	2009	[181]
4OUC	465-798	5-ITu, H3(1-7)	1.9	2014	[54]
4QT7	465-798	SCH772984	1.4	2014	[182]
5HTB	465-798	Compound 15 (ARC-3353)	1.7	2016	[109]
5HTC	465-798	Compound 16 (ARC-3372)	1.5	2016	[109]

Based on the previously established biochemical potency of novel Haspin-targeting conjugates, two conjugates were chosen for the co-crystallization with kinase domain of Haspin, *i.e.*, **Compound 15** (K_d value of 170 nM) and **Compound 16** (K_d value of 150 nM). Both of those incorporated Adc moiety and H3(1-7) analogue sequence, but no oligoarginine fragment (Figure 28). The difference between the conjugates lied in functional group located at the C-terminus of the chiral spacer: in case of **Compound 15**, it was amide, and in case of **Compound 16**, it was carboxylate. Two high resolution crystal structures were obtained, where the binding mode were unambiguously defined for both conjugates. The data collection and refinement statistics are given in the corresponding publication (Paper II: Lavogina *et al.*, 2016).[109] The new co-crystal structures of conjugates with Haspin were compared with the previously published structures of Haspin with AMP (PDB 3DLZ) and 5-ITu:H3(1-7) (PDB 4OUC).

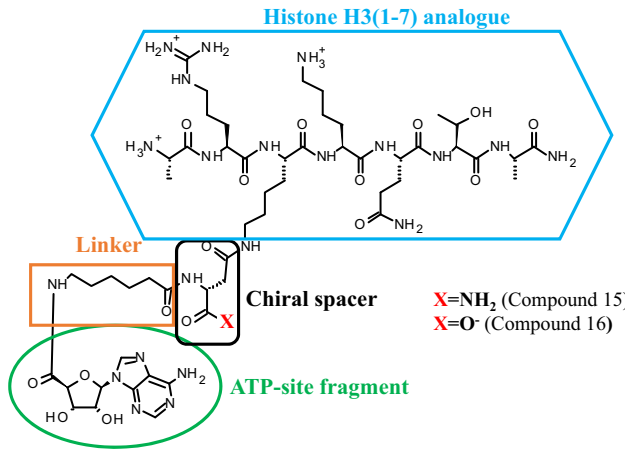

Figure 28. Chemical structures of Haspin-targeting conjugates **Compound 15** and **Compound 16**.

Importantly, the structures confirmed the bisubstrate nature of inhibitors that occupied both ATP- and substrate-site of Haspin (Figure 29). At the same time, **Compound 15** displayed one binding mode in its co-crystal with Haspin, but **Compound 16** showed two binding conformations.

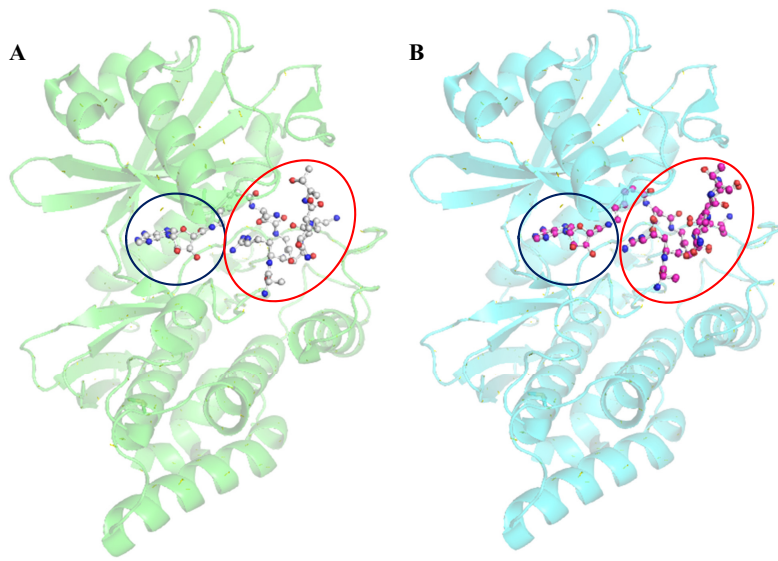

Figure 29. Binding of novel conjugates to Haspin. A) Co-crystal structure of **Compound 15** with catalytic domain of Haspin. PK is shown as green cartoon; conjugate is depicted in ball-and-stick mode (C atoms grey, O atoms red, N atoms blue). B) Co-crystal structure of **Compound 16** with catalytic domain of Haspin. PK is shown as cyan cartoon; conjugate is depicted in ball-and-stick mode (C atoms magenta, O atoms red, N atoms blue). Adc moiety and H3(1-7)-like peptide are surrounded by black and red circles, respectively.

The ATP-site targeting fragment Adc formed characteristic H-bonds between the *N1* and *N6* atoms of purine and backbone of ***Glu606*** and ***Gly608*** in the hinge region (Figure 30). The hydroxyl groups of ribose moiety gave several H-bonds with the side-chain of ***Asp611*** and carbonyl of ***Gly653***.[50] Differently from the previous crystal structures of Haspin, the P-loop together with the α-ulH helix and its connecting loops (AAs 489-532) in N-lobe had shifted upward, causing more open conformation of kinase domain of Haspin. This observation could probably be attributed to positioning of the flexible aliphatic chain of Ahx linker under the G-rich loop of Haspin.

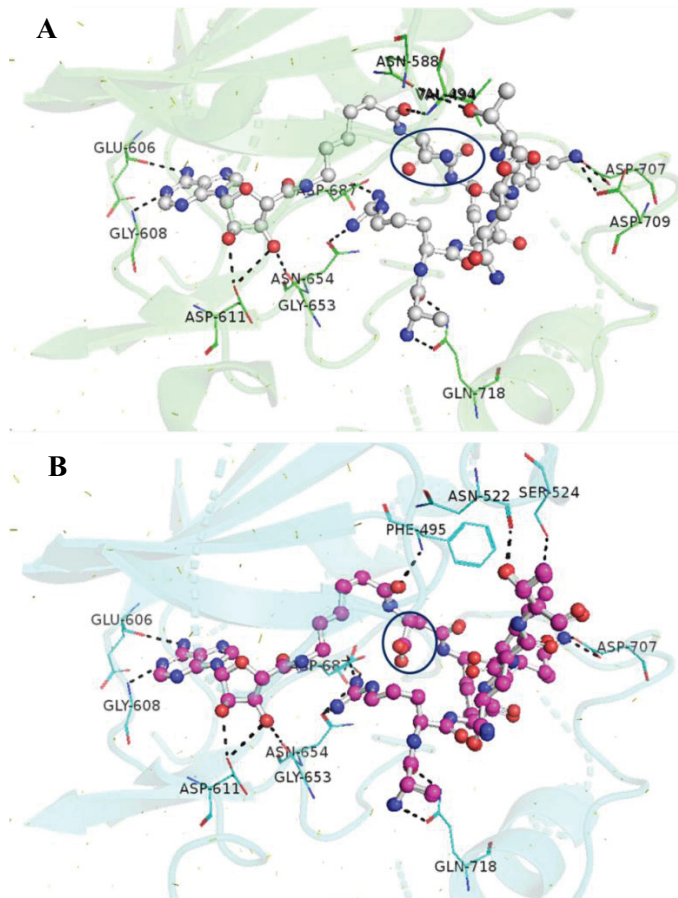

Figure 30. Interactions of conjugates with Haspin. A) Co-crystal structure of **Compound 15** with the catalytic domain of Haspin. PK is shown as green cartoon; conjugate is depicted in ball-and-stick mode (C atoms grey, O atoms red, N atoms blue). B) Co-crystal structure of **Compound 16** with catalytic domain of Haspin. PK is shown as cyan cartoon; conjugate is depicted in ball-and-stick mode (C atoms magenta, O atoms red, N atoms blue). The amino acid residues of Haspin interacting with inhibitor are shown as lines and are numbered; the hydrogen bonds are shown as black dotted lines; a black circle shows the location of the C-terminus of the chiral spacer of the conjugate.

Next, the C-terminus of linker of both conjugates gave the H-bonds with the tip of P-loop, *i.e.*, ***Val494*** and ***Phe495*** in case of **Compound 15** and **16**, respectively (Figure 30). This interaction is not unique for Haspin and an analogous polar contact had been previously seen in the co-crystal structures of ARCs with PKA C.[107,177] Generally, the aromatic side-chain of ***Phe495*** is folded under the P-loop and is required for catalysis as it coordinates the β-phosphate of ATP; in the structure of inactive PKs, this Phe residue is 'pushed out' from under the P-loop as the structure of PK is not prepared for catalysis.[16,17] In case of structure of **Compound 15** with Haspin, ***Phe495*** was positioned perpendiculary to the P-loop, hence favouring the hydrophobic stacking between the amide bond following the linker of the conjugate, the side-chain of ***Phe495*** and the side-chain of ***Lys527*** (Figure 31). In case of **Compound 16**, the side-chain of ***Phe495*** was completely 'pushed out' from under the P-loop. Furthermore, ***Phe495*** contributed to the formation of hydrophobic pocket, which also included side-chains of ***Val494*** and ***Lys527*** as well as Lys residues in the structure of conjugates (corresponding to *Lys4* in H3).

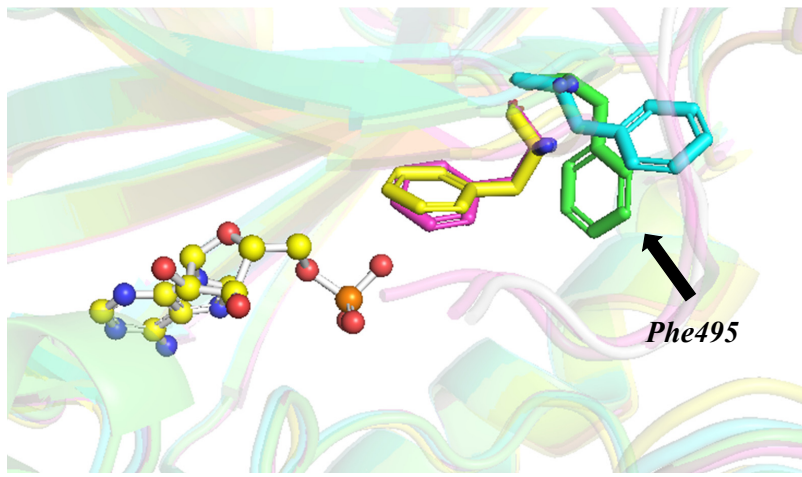

Figure 31. Overlay of the co-crystal structures of **Compound 15** (green) and **Compound 16** (cyan) with PDB entry 4OUC (pink) and 3DLZ (yellow). PK is shown as cartoon; ***Phe495*** from the P-loop is depicted as sticks. AMP is shown as ball-and-stick mode (C atoms yellow, O atoms red, N atoms blue, P atoms orange).

Generally, the H3(1-7)-like peptide in the structure of conjugates showed the characteristic U-turn, whereas the 'bending out' occurred at Lys residue corresponding to *Lys4* in the structure of H3 (Figure 32).[54] On the other hand, the binding mode of rest of the peptide differed considerably from the previously reported binding pattern of H3(1-7) peptide (PDB 4OUC).[54]

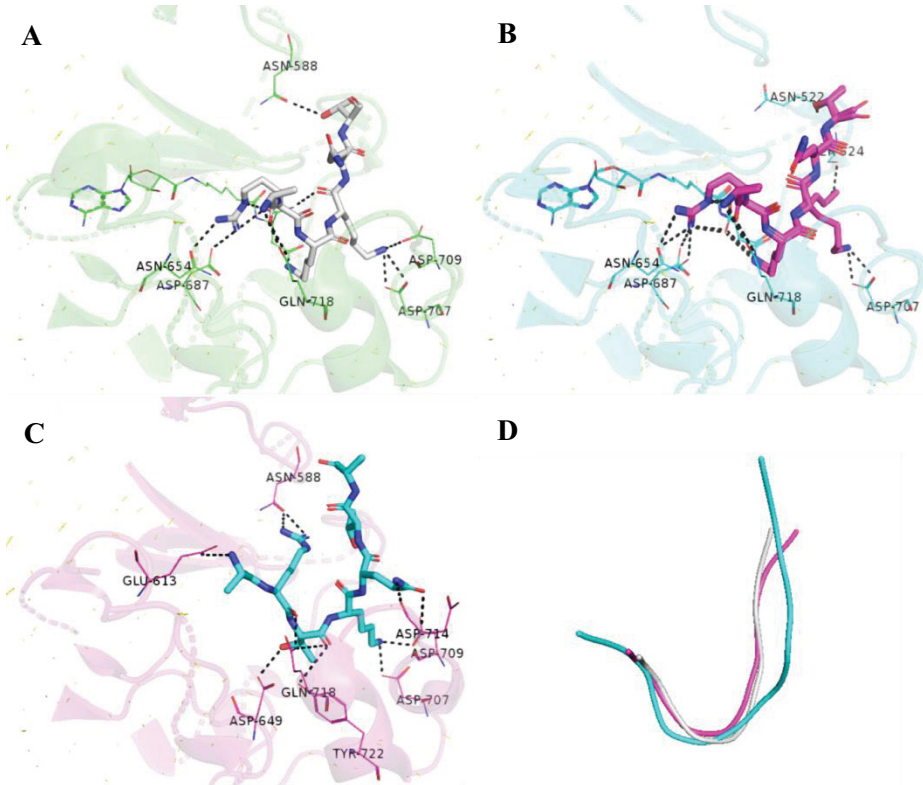

Figure 32. Interactions of H3(-like) peptide with Haspin. A) Co-crystal structure of **Compound 15** with kinase domain of Haspin (PDB 5HTB). PK is shown as green cartoon; peptidic fragment of conjugate is shown as sticks; ATP-site fragment together with the linker part are shown as lines. B) Co-crystal structure of **Compound 16** with kinase domain of Haspin (PDB 5HTC). PK is shown as cyan cartoon; peptidic fragment of conjugate is shown as sticks; ATP-site fragment together with linker part are shown as lines. C) Co-crystal structure of H3(1-7) with kinase domain of Haspin (PDB 4OUC). PK is shown as magenta cartoon; peptide is shown as sticks. D) Overlay of backbone of H3(1-7) peptide (magenta) with peptidic fragment of **Compound 15** (grey) and **Compound 16** (cyan) in co-crystals with Haspin (PK is not shown for clarity).

In PDB 4OUC, *Ala1* of H3 was bound into the small pocket on the surface of Haspin, whereas its N-terminal primary amine gave the H-bond with ***Glu613*** in Haspin.[54] However, in the new structures, the corresponding Ala residue was not positioned into this pocket, but gave the H-bond with the side-chain of ***Gln718*** (Figure 30). The repositioning of Ala residue could probably be attributed to the different positioning of its adjacent Arg (corresponding to *Arg2* in H3) in the co-crystals of conjugates, allowed by more 'open' conformation of kinase due to the flexible Ahx linker (see above). In the previously published structure (PDB 4OUC), *Arg2* was buried into the hydrophilic pocket of N-lobe

and gave a polar contact with ***Asn588*** positioned at the upper layer.[54] Differently, in co-crystals of Haspin with conjugates, the side-chain of the corresponding Arg residue pointed downward, whereas this position was stabilized *via* charge-assisted H-bonds with ***Asn654*** and ***Asp687***.

Next, the repositioning of Arg residue (corresponding to *Arg2* in H3) in the co-crystals of conjugates affected the binding of rest of the residues in peptidic fragment. Due to the charge-assisted H-bonds with ***Asn654*** and ***Asp687*** in the structure with **Compound 16**, the C-terminal carboxyl group of chiral spacer was moved towards Arg residue of conjugate (Figure 32). In the structure with **Compound 15**, the latter movement did not occur; instead, the C-terminal amide formed an intramolecular H-bond with the carbonyl of Lys residue (corresponding to *Lys4* in H3). As a result, Lys was able to give the charge-assisted H-bond with ***Asp707*** and ***Asp709***, which was also seen in structure of 4OUC. However, in case of **Compound 16**, the interaction of Lys with ***Asp709*** was missing, hence allowing two different conformation of Lys of conjugate when bound to Haspin. In one conformation, this Lys developed H-bond only with ***Asp707***. In another conformation, the side-chain of Lys participated in the formation of the aforementioned hydrophobic pocket (including ***Val494***, ***Phe495***, and ***Lys527***) and additionally gave H-bond with ***Ser524*** (Figure 32).

Furthermore, the C-terminal part of H3(1-7)-like peptide adopted different conformation in co-crystals of conjugates with Haspin compared to the native H3(1-7). In case of the native H3 peptide, amide of *Gln5* gave H-bond between ***Gly713*** and ***Asp714*** (activation loop of Haspin), whereas the rest of peptide was directed towards the N-lobe of Haspin (Figure 32). Differently, in complexes of Haspin with novel conjugates, the corresponding Gln residue together with the rest of C-terminal fragment was folded upwards and, at the same time, directed into solvent. However, in case of **Compound 15** (note: Lys in peptidic part in one conformation, see above), the peptidic fragment of conjugate located closer to the N-lobe of Haspin, while the H-bond was formed between the Thr (corresponding to *Thr6* in H3) and the side-chain of ***Asn588***. In case of **Compound 16** (note: Lys in peptidic part in two conformations, see above), the C-terminal fragment of peptidic part adopted different conformations, whereas the H-bond formed between the Thr (corresponding to *Thr6* in H3) and ***Asn522*** (Figure 32).

Overall, the co-crystal structures of novel conjugates with Haspin confirmed the bisubstrate nature of conjugates. Also, Haspin-bound conjugates maintained the main signature binding modes of both Adc moiety and H3 sequence. At the same time, it was demonstrated that small variation in the structure of compounds (*i.e.*, different C-termini of chiral spacer) may cause a considerable rearrangement of the spatial structure of the conjugate-PK complex.

4. Design and Biochemical Characterization of New Set of Haspin-Targeting Conjugates [Paper III: Kestav *et al.*, 2017]

Itc-Incorporating Novel Haspin-Targeting Conjugates

As the affinity of the previously discussed most potent novel conjugates lacking Arg_6 sequence (**Compound 15** and **16**) remained at the moderate range, the following development involved the improvement of affinity as well as selectivity of conjugates towards Haspin over other PKs. It was assumed that the replacement of Adc moiety (K_d value of 15 μM for Haspin) with 5-ITu (K_d value of 4 nM for Haspin) could result in improved affinity. The comparison of the co-crystal structures of Haspin with **Compound 15** (PDB 5HTB) and **16** (PDB 5HTC) *versus* Haspin with 5-ITu:H3(1-7) (PDB 4OUC) revealed that the incorporation of 5-ITu did not require the readjustment of linking unit between the nucleosidic fragment and peptide (Figure 33). However, the incorporation of 5-ITu into the structure of conjugates required chemical modification of the compound, *i.e.*, oxidation of the 5′-hydroxyl of ribose to a carboxylic acid, resulting in 5-iodotubercidin-4'-dehydroxymethyl-4'-carboxylic acid moiety (Itc).

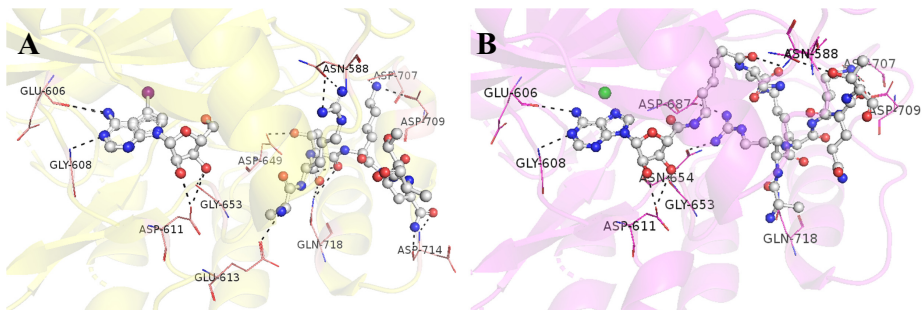

Figure 33. Comparison of binding patterns in ternary complex of Haspin with 5-ITu and H3(1-7) (PDB 4OUC; A), and binary complex of Haspin with **Compound 15** (PDB 5HTB; B). PK is shown as cartoon; 5-ITu, H3(1-7) and **Compound 15** are shown in ball-and-stick mode (C atoms grey, O atoms red, N atoms dark blue); H-bonds are shown as black dotted lines; residues of PK that form the interactions with the co-crystallized compounds are shown as lines. The water molecule discussed in the text is depicted as a green sphere.

Not surprisingly, the replacement of Adc with Itc (**Compound 26**) resulted in significant increase in affinity of the conjugate (*i.e.*, possessed subnanomolar range of affinity) compared to its Adc counterparts (**Compound 15** and **16**) or reference compound 5-ITu (Table 12). Furthermore, the selectivity of Itc-incorporating conjugate towards Haspin over PKA C was remarkably improved. Thus, **Compound 26** served as an outstanding example of a novel Haspin-targeting compound possessing picomolar affinity as well as improved selectivity compared to its nucleosidic fragment 5-ITu.

Table 12. Values of equlibrium dissociation constant and selectivity index of conjugates established in assays with Haspin and PKA C

Nr	*Schematic Structure*	K_d, *nM*** *Haspin*	K_d, *nM*** *PKA C*	*Selectivity Index****
15	Adc-Ahx-DAsp*[LAla-LArg-LLys*-LLys-LGln-LThr-LAla-NH_2]-NH_2	170 (40)	1600 (300)	9.4
16	Adc-Ahx-DAsp*[LAla-LArg-LLys*-LLys-LGln-LThr-LAla-NH_2]-OH	150 (19)	7700 (1400)	50
19	Adc-Ahx-DAsp*[LAla-LArg-LLys*-LLys-LGln-LThr-LAla-DArg_6-NH_2]-NH_2	0.88 (0.15)	27 (3)	30
26	Itc-Ahx-DAsp*[LAla-LArg-LLys*-LLys-LGln-LThr-LAla-NH_2]-OH	0.14 (0.05) [a] 0.019 [b]	94 (12)	4900
27	Itc-Ahx-DAsp*[LAla-LArg-LLys*-LArg-LGln-LThr-LAla-DLys[**TAMRA**]-NH_2]-OH	0.50 (0.06)	4.1 (0.3)	34
28	Adc-Ahx-DAsp*[LAla-LArg-LLys*-LArg-LGln-LThr-LAla-DLys[**TAMRA**]-NH_2]-OH	11 (3)	52 (1)	4.7
29	Adc-Ahx-DAsp*[LAla-LArg-LLys*-LArg-LGln-LThr-LAla-DLys[Myr]- DLys[**TAMRA**]-NH_2]-OH	8.4 (2.0)	9.6 (0.4)	1.1
30	Adc-Ahx-DAsp*[LAla-LArg-LLys*-LArg-LGln-LThr-LAla-DArg_6-DLys[**TAMRA**]-NH_2]-OH	0.6 (0.1)	10 (2)	17
ARC-902	Adc-Ahx-DArg_6-NH_2	2.6 (0.3)	2.7 (0.4)	1
-	5-iodotubercidin	3.9 (0.4)	over 15000	over 4000

* indicates attachment of the two fragments *via* the side-chain of the amino acid; ** standard error values are given in brackets (N ≥ 4); *** for each compound, selectivity index was calculated as the ratio of equilibrium dissociation constant values for PKA C and Haspin. The peptidic fragment corresponding to the modified histone H3(1-7) sequence is shown in square brackets. The fluorescent dye is marked in bold. [a] Apparent K_d value (the true equilibrium had not been achieved after 30 min of incubation). [b] Equilibrium dissociation constant K_d* value calculated from the kinetic measurements (see below).

Design of Fluorescent Probes (Compounds 27-30)

The novel conjugates incorporating Adc or Itc moiety and modified H3(1-7) sequence in peptidic part were converted into fluorescent probes by linking TAMRA dye *via* the side chain of C-terminal Lys residue of the compounds (Table 12). This modification also allowed the further investigation of kinetic characteristics of the novel probes. Furthermore, the fluorescent probe with Myr moiety was synthesized as in previous studies with PKA C, Myr moiety had shown to improve cell plasma membrane-penetrating properties of conjugates.[183] The equlibrium dissociation constants of probes were established by using binding assay with FA readout (Table 12). Again, PKA C was used as basophilic reference PK.

The labelling of Itc-incorporating **Compound 26** led to the formation of **Compound 27**. Importantly, the obtained probe maintained subnanomolar affinity (K_D value of 0.5 nM), but, on the other hand, the selectivity index towards Haspin over PKA C decreased significantly from 4900-fold to 34-fold (Table 12). Next, the labelling of **Compound 16** yielded **Compound 28**, which possessed increased affinity towards both Haspin and PKA C (selectivity index of 14- and 148-fold, respectively), but, again, the selectivity for Haspin decreased remarkably. The incorporation of Myr moiety (**Compound 29**) improved the affinity only for PKA C.

The decrease of selectivity of novel probes towards Haspin over PKA C can be attributed to the fact that the hydrophobic TAMRA dye as well as Myr moiety could interact with hydrophobic (P+1)-binding pocket in the substrate site of PKA C[184], hence improving the affinity of probes towards PKA C.

Compound 19 comprising Arg_6 fragment was used as a backbone to derive the fluorescent probe **Compound 30**, which showed slighly decreased selectivity towards Haspin *versus* PKA C (selectivity index of 20 in case of **Compound 30** *versus* selectivity index of 30 in case of **Compound 19**; Table 12). In this way, the maintenance of selectivity towards Haspin confirmed the importance of positioning of oligoarginine fragment (see above).

Overall, it was demonstrated that the incorporation of fluorescent dye into the structure of conjugates may lead to considerable changes in the biochemical characteristics of compounds. The effect may be insignificant in general biochemical assays, where purified targets are often used, but, in turn, should definitely be taken into account in more complex biological systems (*e.g.*, living cells, cell lysates, bodily fluids).

Determination of Kinetic Properties of Fluorescent Probes by Using Assays with FA Readout

Besides the high affinity as well as selectivity of a small molecular compound (inhibitor) to its biological target, the dissociation kinetics of the drug-target complex (or the residence time of inhibitor) has recently gained much attention. The long residence time leads to the durable (pharmacological) effect and reduced toxicity of the compound.[185,186] Furthermore, the kinetic properties of the compound can reflect the binding mode of the ligand to its biological target.[80] The common approach for describing the ligand-target interactions to

date is a double-induced-fit model, where the association (k_{on}) of the ligand with its target is accompanied with the conformational adaption of 3D-structures of both the ligand and target protein. Thereby, the association process may be relatively slow and include several steps.[186–188] With the aim to determine the correlation between the structural features, the kinetic profile as well as the binding mode of conjugates, the association and dissociation of new compounds and a previously reported reference compound (incorporating only Arg_6 fragment in peptidic part) were established in studies with Haspin.

First, the association constants of fluorescent probes **Compounds 27-30** and the reference compound **ARC-583** were determined from the increase of anisotropy during the association of probes with Haspin. Slow association kinetics for Itc-incorporating **Compound 27** (k_{on}=6.11 × 10^5 M^{-1} s^{-1}; Table 13; Figure 34, A) was found. Its Adc-containing counterpart, **Compound 28** possessed 4.3-fold faster association than **Compound 27**. The association constant of **Compound 29** comprising Myr moiety was in the same range as that of **Compound 28**.

Importantly, the association rate constants of all compounds (**Compound 27-29**) incorporating the N-terminal H3-like sequence were by over 10-fold smaller than that of the reference compound **ARC-583**, which contained only oligoarginine sequence in its peptidic part (Table 13). On the other hand, the incorporation of oligoarginine fragment to the C-terminus of H3 sequence (**Compound 30**) led to 4.4-fold increase of the association rate. Based on the established data, it was concluded that the sequence of H3 caused slow association kinetics, but, on the other hand, the incorporation of oligoarginine fragment resulted in increase of the association rate constant. The slow association kinetics was also observed in thermal shift assay (see below) in case of conjugate **Compound 26** comprising Itc moiety.

Thereafter, the dissociation rate constants of fluorescent probes were determined from the decrease of anisotropy values during the dissociation of a probe from the complex with Haspin in the presence of large excess of displacing compound (ATP-site inhibitor 5-ITu or bisubstrate inhibitor **ARC-902**). The compounds that comprised Adc moiety as the ATP-site targeting fragment did not show uncommonly slow dissociation (Table 13). On the other hand, **Compound 27** possessed extremely slow dissociation kinetics, and hence required a different experimental setup for determination of the dissociation constant. In particular, the data points were taken within 5 h, whereas the signal of free probe was used as a minimum value of anisotropy for fitting the data (Figure 34, B). According to the measurements, **Compound 27** showed remarkably long residence time of 4.5 h (Table 13). The comparison of the residence times of compounds revealed that the Adc moiety-incorporating counterpart **Compound 28** had 160-fold shorter residence time than **Compound 27**. Moreover, the incorporation of oligoarginine fragment to the C-terminus of H3(1-7) analogue sequence (**Compound 30**) resulted in increase of the residence time around 2-fold. On the other hand, the addition of Myr (**Compound 29**) led to 8-fold reduction of residence time compared to Adc-incorporating **Compound 28** (Table 13). Finally, the reference probe **ARC-583** (incorporating Adc moiety and oligoarginine fragment, but no H3(1-7)-like peptide in peptidic part) possessed the fastest dissociation kinetics.

Table 13. Kinetic parameters of association and dissociation of fluorescent probes with/from Haspin established in assays with FA readout

Compound	*Schematic structure*	k_{on}, M^{-1} s^{-1}	k_{off}, s^{-1}	τ, *s*	K_D', *nM*
27	Itc-Ahx-DAsp*[LAla-LArg-LLys*-LArg-LGln-LThr-LAla-DLys[**TAMRA**]-NH_2]-OH	6.11×10^5 [0.58×10^5]	6.13×10^{-5} [0.66×10^{-5}] [a]	16 300	0.100
28	Adc-Ahx-DAsp*[LAla-LArg-LLys*-LArg-LGln-LThr-LAla-DLys[**TAMRA**]-NH_2]-OH	2.65×10^6 [0.92×10^6]	9.83×10^{-3} [0.89×10^{-3}] [b]	102	2.84
29	Adc-Ahx-DAsp*[LAla-LArg-LLys*-LArg-LGln-LThr-LAla-DLys[Myr]-DLys[**TAMRA**]-NH_2]-OH	5.10×10^6 [0.47×10^6]	7.61×10^{-2} [0.64×10^{-2}] [b]	13.1	14.9
30	Adc-Ahx-DAsp*[LAla-LArg-LLys*-LArg-LGln-LThr-LAla-$DArg_6$-DLys[**TAMRA**]-NH_2]-OH	1.17×10^7 [0.86×10^7]	4.63×10^{-3} [0.66×10^{-3}] [c]	216	0.395
ARC-583		2.81×10^7 [0.73×10^7]	2.35×10^{-2} [0.19×10^{-2}] [b]	42.6	0.835

k_{on}, second-order association rate constant; k_{off}, first-order dissociation rate constant; τ, residence time calculated as the reciprocal of k_{off}. Standard deviation values are given in square brackets (N ≥ 3). The equilibrium dissociation constants of the probe were calculated from the ratio of k_{on} and k_{off} values ($K_D' = k_{off}/k_{on}$). [a] 20 μM 5-ITu was used as the competing compound. [b] 1 μM 5-ITu or 1 μM **ARC-902** were used as the competing compounds. [c] 1 μM **ARC-902** was used as the competing compound.

Table 14. Kinetic parameters of association and dissociation of novel compounds and 5-ITu with Haspin established by using the photo-luminescent probe **ARC-1063**

Compound	*Schematic structure*	k_{on}*, M^{-1} s^{-1}	k_{off}*, s^{-1}	τ, s	K_D*, *nM*
26	Itc-Ahx-DAsp*[LAla-LArg-LLys*-LArg-LGln-LThr-LAla-DLys-NH_2]-OH	1.97×10^6 [0.09×10^6]	3.84×10^{-5} [0.66×10^{-5}]	26 000	0.019
27	Itc-Ahx-DAsp*[LAla-LArg-LLys*-LArg-LGln-LThr-LAla-DLys[**TAMRA**]-NH_2]-OH	5.41×10^5 [0.56×10^5]	6.68×10^{-5} [0.89×10^{-3}]	15 000	0.12
	5-iodotubercidin	3.43×10^6 [0.95×10^6]	3.29×10^{-3} [0.64×10^{-2}]	304	0.96

τ, residence time calculated as the reciprocal of k_{off}*. Standard deviation values are given in square brackets (N ≥ 2). The equilibrium dissociation constant values of the probes were calculated from the ratio of the corresponding k_{on}* and k_{off}* values ($K_D^* = k_{off}^*/k_{on}^*$).

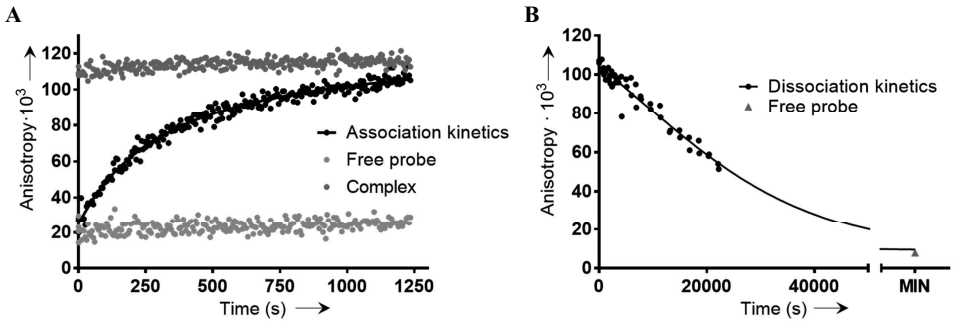

Figure 34. Association and dissociation kinetics measurements for the complex of **Compound 27** and Haspin. A) Association of **Compound 27** (1 nM) with Haspin (2 nM). The data are fitted to the second-order association kinetics equation. As controls, free probe and pre-mixed PK-bound probe were used. The data of one representative experiment are shown (N=6). B) Displacement of **Compound 27** (2 nM) from its complex with Haspin by 5-ITu (20 μM). The data are fitted to the first-order dissociation kinetics equation. The signal of free probe was used to define the minimum anisotropy value. The data of 2 representative experiments are shown (N=3).

Based on the obtained data, the equilibrium dissociation constants (K_D*'*) were calculated, whereas the results showed the good accordance of K_D*'* values with dissociation constants (K_D) obtained from the binding assay with FA readout (Table 4, Table 12, Table 13).

Determination of Kinetic Properties of Compounds Devoid of Long-Lifetime Photoluminescence by Using Photoluminescent Probe ARC-1063

In order to show whether the very slow dissociation kinetics of 5-ITu containing conjugates was caused by the nucleosidic moiety, H3(1-7) imitating peptide or the cooperative effect of both fragments, the binding kinetics for non-labelled compounds **Compound 26** and 5-ITu was additionally established. For this, the PK binding-responsive photoluminescent bisubstrate probe **ARC-1063** was used, which possesses strong long-lifetime (in microsecond scale) photoluminescence at 647 nm after pulse-exitation at 337 nm (measured in 80–480 μs time-window) in complex with PK. Furthermore, **ARC-1063** gives a negligible background signal as a free probe in solution (discussed in Methods under section *2.4. ARC-Lum(Fluo) Probes*).[133] Due to the slow decay of photoluminescence of complex of the PK and **ARC-1063**, the probe allows measurement of samples containing other fluorescent compounds not endowed with long-lifetime photoluminescence property. In binding assay with Haspin, **ARC-1063** showed K_D value of 15 nM and, at the same time, fast kinetic properties (both association and dissociation; residence time below 10 s); thus, this probe is a suitable tool for the determination of kinetic data of compounds devoid of long-lifetime photoluminescence (non-Lum).

The association constants of non-Lum compounds were assessed as follows. Haspin was pre-incubated with **ARC-1063** and, subsequently, an excess of non-Lum competitive compound was added to the solution (Figure 35). The addition of competing compound led to the decrease of photoluminescence signal of **ARC-1063**, whereby the slower the association of non-Lum compound, the slower was the decrease of photoluminescence.

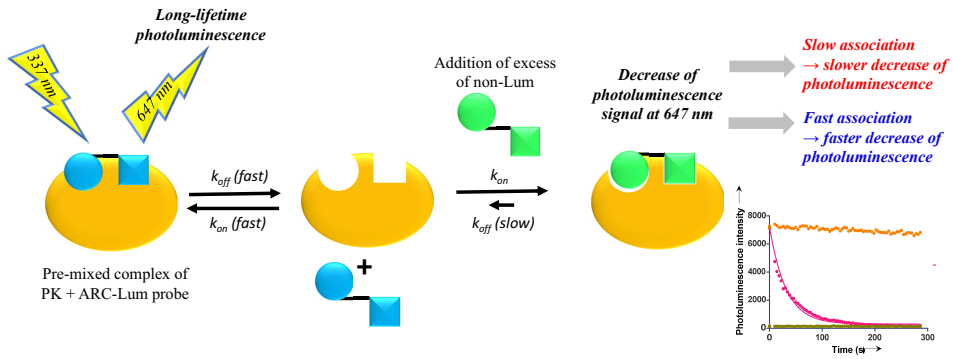

Figure 35. Schematic illustration of measurement of association kinetics by using photoluminescent probe **ARC-1063**. PK is depicted as orange shape; photoluminescent probe **ARC-1063** and non-Lum competing compound are shown in blue and green, respectively.

Indeed, the results confirmed the slowest on-rate of **Compound 27** (k_{on}*=1.97 × 10^6 M^{-1} s^{-1}), which was followed by **Compound 26** and 5-ITu (Table 14, Figure 37). The association of the reference compound **ARC-902** was so quick that its on-rate could not be determined with sufficient reliability with present assay. Importantly, the k_{on}* value of **Compound 27** determined with the current method was in good accordance with the k_{on} value established in the binding assay with FA readout (5.41 × 10^5 M^{-1} s^{-1} *versus* 6.11 × 10^5 M^{-1} s^{-1}).

To establish the dissociation constants of non-Lum compounds, Haspin was pre-incubated with a non-Lum compound; thereafter, **ARC-1063** was added in large excess (100- to 500-fold excess compared to non-Lum compound) and establishment of luminescence signal was monitored (Figure 36). The addition of **ARC-1063** caused increase of luminescence signal of **ARC-1063** due to the dissociation of non-Lum compound from PK and the subsequent binding of large excess of **ARC-1063** with Haspin. Hence, in case of non-Lum compound with slow dissociation kinetics, the increase in photoluminescence is likewise slow. The obtained data was fitted to the one-phase exponential association equation and off-rate constant k_{off}* values were calculated.

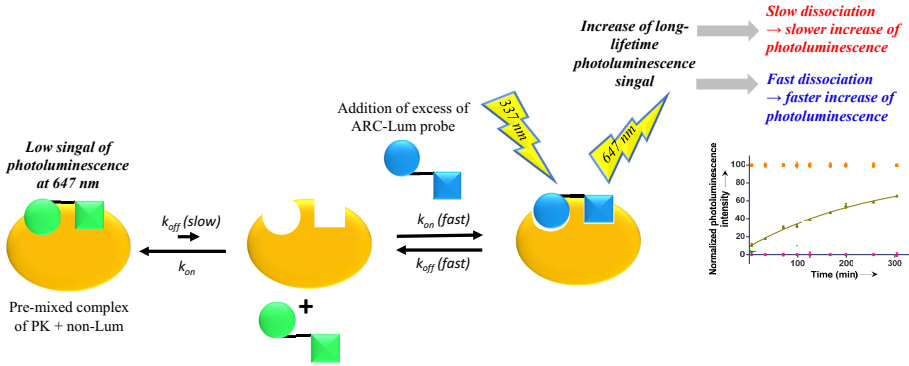

Figure 36. Experimental layout for measurement of dissociation kinetics by using photoluminescent probe **ARC-1063**. PK is depicted as orange shape; photoluminescent probe **ARC-1063** and non-Lum competing compound are shown in blue and green, respectively.

As expected, **Compound 26** possessed the slowest dissociation from Haspin and a remarkably long residence time of 7.2 h. This was followed by **Compound 27** and 5-ITu (Table 14, Figure 37). As in case of association assay, it was not possible to determine the dissociation rate constant for **ARC-902** with sufficient reliability due to its very fast dissociation from Haspin. Again, the k_{off}* value of **Compound 27** was in good agreement with the k_{off} value established in the assay with FA readout (k_{off}* values of 6.68×10^{-5} s^{-1} and 6.13×10^{-5} s^{-1}, respectively).

Again, based on the kinetic data obtained from the photoluminescence assay, the equlibrium dissociation constants (K_D*) were calculated as the ratio of corresponding rate constants (k_{off}*/ k_{on}*). The K_D* values of **Compound 27** and 5-ITu were in reasonably good accordance with dissociation constants (K_D) obtained from the binding/displacement assay with FA readout (Table 14). On the contrary, the K_D* value for **Compound 26** (K_D* value of 0.019 nM; Table 14) was significantly different from the apparent K_D value established in assay with FA readout (K_d value of 0.14 nM; Table 12), where the true equilibrium was not reached.

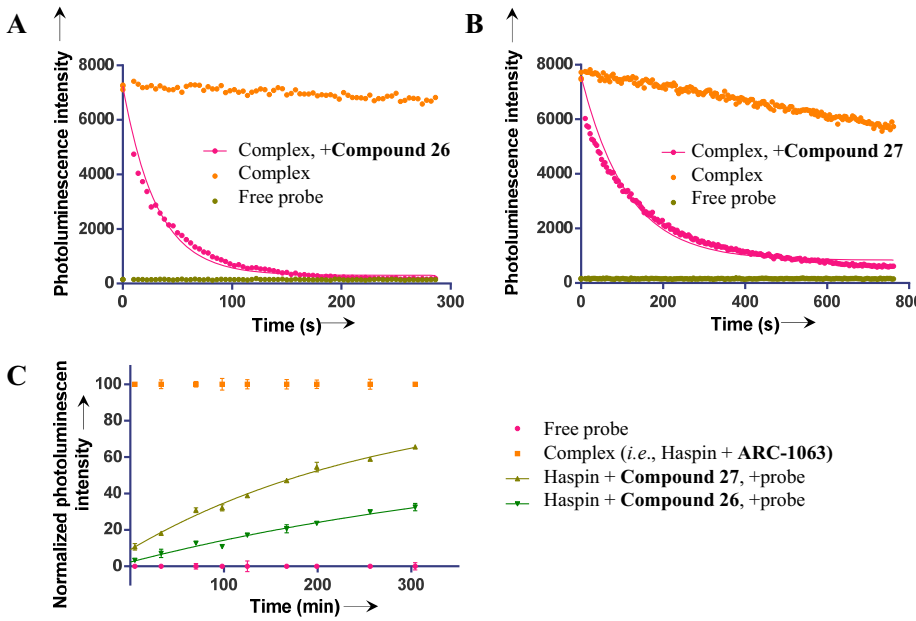

Figure 37. Examples of association and dissociation curves obtained by using the photoluminescent probe **ARC-1063**. A) Determination of association rate constant of **Compound 26**. B) Determination of association rate constant of **Compound 27**. The solid pink line represens the fit of data to the one-phase exponential decay equation. C) Determination of dissociation rate constants of **Compound 26** and **Compound 27**. The signal of mixture was normalized to the signal of free probe (0%) and the signal of complex of Haspin with **ARC-1063** (100%). The data were fitted to the one-phase exponential association equation.

Based on the obtained results, it can be concluded that the slow binding kinetics of Haspin with **Compounds 26** and **27** is caused by both moieties of conjugates, Itc as well as H3(1-7)-like sequence. According to the overlay of the co-crystal structures of Haspin with 5-ITu and **Compound 15**, it is evident that in the region where the iodine of 5-ITu was bound, one water molecule was expelled from the kinase site (Figure 38). Thus, it may be assumed that the slow association kinetics of 5-ITu moiety could be partially attributed to the dehydration of the ATP-site of Haspin which is required for binding of 5-ITu.[182] Besides, it had previously been reported that the slow association kinetics of 5-ITu is caused by the strong interactions between the electron cloud of iodine of 5-ITu with the π-electrons of aromatic system of ***Phe605***, whereas ***Phe605*** functions as the gatekeeper residue in Haspin (Figure 38).[182] H3(1-7)-like peptide adopts unusual U-turn shape when bound to Haspin, the conformational adaption of peptide may be relatively time consuming. In turn, disruption of this unusual conformation during the dissociation from Haspin could lead to the extremely slow dissociation of conjugates.

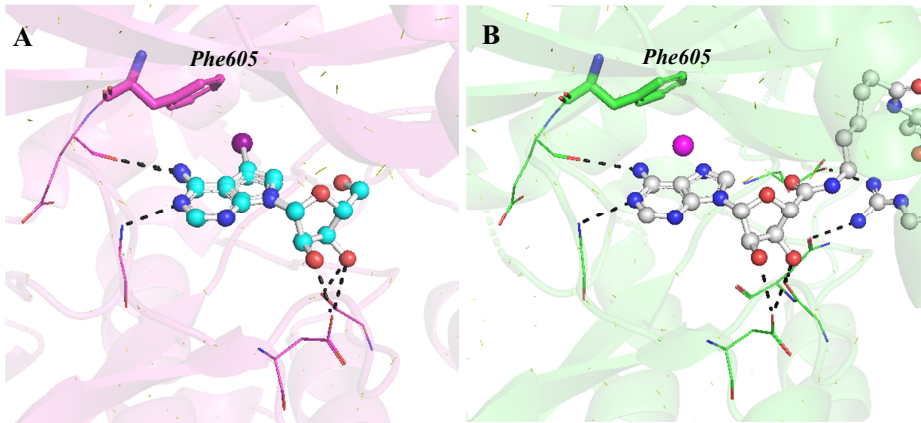

Figure 38. Co-crystal structures of Haspin kinase domain with **Compound 15** (PDB 5HTB) and 5-ITu (PDB 4OUC) for the comparison of binding patterns. A) The binding of 5-ITu to ATP-site of Haspin. PK is shown as a magenta cartoon and the inhibitor is presented in ball-and-stick mode (C atoms cyan, O atoms red, N atoms dark blue, I atoms violet). B) The binding of Adc moiety of **Compound 15** to ATP-site of Haspin. PK is shown as a green cartoon and the inhibitor is presented in ball-and-stick mode (C atoms grey, O atoms red, N atoms dark blue). The residues of PK that form the interactions with the co-crystallized inhibitor are shown as lines; hydrogen bonds are shown as black dotted lines. The gatekeeper residue Phe605 is labelled and highlighted as sticks. The water molecule discussed in the text is depicted as a magenta sphere.

On the other hand, the very fast binding of **ARC-583** and Haspin may be attributed to the non-oriented charge-charge interactions of positively charged guanidinium groups of oligoarginine fragment with the negatively charged substrate-binding site of Haspin. From the co-crystal structure of **ARC-902** (representing the non-fluorescent analogue of **ARC-583**) with Haspin, it was evident that the electron density of peptidic part of **ARC-902** was defined only for three arginine residues out of six, which indicated that the Arg_6 fragment was rather flexible and most likely possessed several conformations when bound to Haspin (Figure 24).

Finally, the temporal target selectivity of **Compound 27** with reference basophilic kinase PKA C was established (Table 15). The temporal target selectivity shows the difference how long is the compound bound to its desired target compared to the off-target(s): the longer the residence time of compound with its target and lower with other proteins, the lower is the off-target-derived toxicity.[189] The results revealed that the temporal target selectivity (*i.e.*, the ratio of residence times) was in favour to Haspin over PKA C by factor of 1600.

Table 15. Kinetic parameters of association and dissociation of **Compound 27** with/from Haspin and PKA C established in the assay with fluorescence anisotropy readout

Parameter	*Haspin*	*PKA C*
k_{on}, M^{-1} s^{-1}	6.11×10^5 [0.58×10^5]	1.89×10^7 [0.51×10^7]
k_{off}, s^{-1}	6.13×10^{-5} [0.66×10^{-5}]	9.87×10^{-2} [1.84×10^{-2}]
τ, s	16 300	10.1

Standard deviation values are given in square brackets (N ≥ 3). τ, residence time calculated as the reciprocal of k_{off}.

5. PK Selectivity of Itc-Incorporating Conjugate [Paper III: Kestav *et al.*, 2017]

Selectivity Profiling of Itc-Incorporating Novel Conjugate with Off-Targets of 5-ITu by Using Thermal Shift Assay

The previously reported PK off-targets of 5-ITu are the CMGC kinase family Clks (Cdc2-like kinases) and PKs of the DYRK (dual-specificity tyrosine (Y)-phosphorylation regulated kinases) family.[54,90] Moreover, adenosine kinase (ADK) that belongs to the phosphofructokinase B family of sugar kinases is also acknowledged target of 5-ITu.[92] ADK catalyses the γ-phosphoryl transfer from ATP to adenosine, resulting in the formation of ADP and AMP.[190,191] Hence, 5-ITu functions as both inhibitor of ADK (IC_{50} value of 26 nM) as well as substrate by competing with adenosine.[92,192] In order to determine whether the addition of H3(1-7)-like peptide to 5-ITu increased the selectivity of conjugate over 5-ITu, the thermal shift assay was performed with Clk1, Clk2 and ADK. **ARC-902** was used as the reference compound.

Initially, in case of thermal shift measurement with Haspin, 15 min was chosen for pre-incubation time at room temperature after the components of assay were mixed on ice. The obtained melting curves of **Compound 26** and 5-ITu showed unusual shape with two peaks (Figure 39, A), whereas the first maximum of the curve was located close to the melting temperature of the native kinase and the second maximum was near the melting temperature of ligand-bound PK. Thus, it was assumed that the pre-incubation time of 15 min was not sufficient for binding of **Compound 26** or 5-ITu to Haspin, since some amount of PK still remained native (first peak), but, at the same time, the other fraction was already ligand-bound (second peak). Therefore, the pre-incubation time of samples was extended up to 30 min and, as expected, the melting curves with normal-shape were obtained for both compounds (Figure 39, B). Again, this observation pointed indirectly to the slow association kinetics of Itc-incorporating conjugate as well as 5-ITu itself.

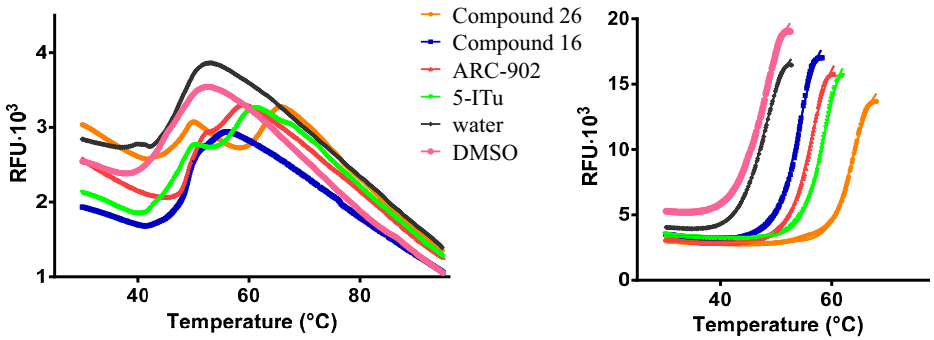

Figure 39. Examples of melting curves of Haspin in complex with the non-fluorescent conjugates and 5-ITu. A) Pre-incubation time 15 min at 30 °C. B) Pre-incubation time 30 min at 30 °C. For determination of thermal shift values, three values after maxima were taken into account and Boltzmann equation was used for fitting of curves. Final total concentrations: Haspin 2 μM, compounds 12.5 μM. The volumes of deionized water and DMSO added as references corresponded to the maximal added volumes of inhibitor stock solutions in DMSO. RFU, relative fluorescence unit.

The thermal shift assay results revealed that the established ΔT_m values were in good agreement with the previously reported values (Table 16).[90] Consistently with the data established in displacement assay (Table 9), the ΔT_m value of **Compound 26** in complex with Haspin was remarkably higher than that of its Adc-incorporating counterpart **Compound 16** or 5-ITu (16.4 ^{o}C, 6.6 ^{o}C, and 10.8 ^{o}C, respectively). On the contrary, ΔT_m values of **Compound 26** in complex with off-targets of 5-ITu showed significant decrease compared to the ΔT_m values of 5-ITu with the corresponding PKs. Furthermore, even more significant decrease in ΔT_m value of **Compound 26** *versus* 5-ITu in complex with ADK was observed (from 15.4 to 5.0 ^{o}C). Based on the established data, it may be concluded that the incorporation of H3(1-7)-like peptide to the structure of conjugate not only improved its affinity towards Haspin, but also led to the increase of selectivity properties of conjugate over 5-ITu.

Table 16. Values of thermal shift (ΔT_m) of novel conjugates with Haspin, Clk1, Clk2, and ADK

Compound	*Schematic Structure*	ΔT_m, °C** *Haspin*	ΔT_m, °C** *Clk1*	ΔT_m, °C** *Clk2*	ΔT_m, °C** *ADK*
16	Adc-Ahx-DAsp*[LAla-LArg-LLys*-LLys-LGln-LThr-LAla-NH_2]-OH	6.6 (0.2)	0.2 (0.2)	0.5 (0.2)	NE
26	Itc-Ahx-DAsp*[LAla-LArg-LLys*-LLys-LGln-LThr-LAla-NH_2]-OH	**16.4 (0.6)**	5.9 (0.3)	3.6 (0.4)	5.0 (0.2)
ARC-902	Adc-Ahx-LArg_6-NH_2	**8.7 (0.2)**	2.9 (0.4)	1.3 (0.2)	NE
	5-iodotubercidin	**10.8 (0.2)**	**9.8 (0.4)**	6.2 (0.3)	**15.4 (0.1)**

* points to the DLys residue whose side-chain amine group was used for the attachment of the fragment in brackets; **standard error values are given in brackets (N ≥ 2). ΔT_m values over 8 °C (corresponding to K_d values below 100 nM[163]) are shown in bold. NE, not established.

Selectivity Profiling of Itc-Conjugate Towards In-House Panel of PKs

With the aim to establish a wider selectivity profile of the Itc-comprising conjugate **Compound 26**, equilibrium binding/displacement assay was performed with an in-house panel of PKs. Additionally to Haspin and PKA C, the panel contained nine PKs, including basophilic kinases ROCK2 (Rho-associated protein kinase 2), MSK1 (mitogen- and stress-activated protein kinase-1), Akt3/ PKBγ (Rac-gamma serine/threonine-protein kinase; protein kinase B), Aurora A and B, acidophilic kinase CK2 and proline-directed kinases of the Pim family (proto-oncogene serine/threonine-protein kinase) Pim1, Pim2, and Pim3 (Table 17). 5-ITu was used as the reference compound in all experiments.

The results revealed that **Compound 26** possessed sub-micromolar affinity only for two PKs out of nine, *i.e.*, Pim3 (K_d of 370 nM) and ROCK2 (K_d of 700 nM). However, these K_d values were significantly higher compared to the subpicomolar K_d value of **Compound 26** towards Haspin (K_d* of 0.019 nM). Thus, the selectivity index of **Compound 26** in favour to Haspin remained remarkably high (19000-fold over Pim3, and more than 1 600 000-fold over CK2). Also, 5-ITu showed high selectivity for Haspin; relative to Haspin, its lowest selectivity indices within this panel were for Aurora A and Pim1 (670- and 750-fold, respectively).

Table 17. Values of equlibrium dissociation constant and selectivity index of **Compound 26** and 5-ITu established in assays with different PKs

Kinase	*Compound 26* K_d, *nM**	*Selectivity Index***	*5-ITu* K_d, *nM**	*Selectivity Index***
Haspin	0.14 (0.05) [a] 0.019 [b]		3.9 (0.4)	
PKA	94 (12)	4900	over 15 000	over 3800
ROCK2	700 (80)	1600	10 300 (1000)	2600
MSK1	4000 (1000)	9070	6700 (500)	1700
Akt3	2700 (600)	6110	74 000 (3000)	19 000
Pim1	3900 (200)	8880	2900 (200)	750
Pim2	over 30 000	over 68 000	27 000 (5000)	6900
Pim3	370 (120)	852	7300 (400)	1900
Aurora A	15 600 (2000)	35500	2600 (100)	670
Aurora B	2800 (600)	6340	6100 (2900)	1600
CK2	over 30 000	over 68 000	25 000 (3000)	6500

* Standard error values are given in brackets (N ≥ 3). ** The selectivity index was calculated as the ratio of the K_d values of an inhibitor in experiments with the corresponding PK and Haspin (in case of **Compound 26**, the K_d* value obtained from kinetic data was used). [a] Apparent K_d value (the true equilibrium had not been achieved after 30 min of incubation). [b] Equilibrium dissociation constant K_d* value calculated from the results of kinetic measurements.

To sum up, it can be concluded that the kinetic behaviour of conjugates is affected by the type of interactions between the ligand (conjugate) and PK. Hence, the slow association kinetics as well as the long residence time of conjugates comprising Itc moiety and H3(1-7)-like peptide result from the precise positioning of the 'hotspots' of specific interactions. On the other hand, the fast kinetic properties of oligoarginine-comprising conjugates can be attributed to the guanidinium groups of multiple arginine residues of the peptide moiety give relatively random and less localized interactions with the negatively charged substrate-site of Haspin. Besides the long residence time, the Itc-incorporating conjugate exhibited improved selectivity towards the selection of PKs (including off-tagets of 5-ITu) compared to that of 5-ITu. Finally, the novel conjugates incorporating Itc moiety and H3(1-7)-like peptide serve as excellent examples of Haspin-selective compounds with long residence time.

CONCLUSIONS AND PERSPECTIVES

Within this study, a new target represented by the mitotic basophilic protein kinase Haspin was taken under investigation. The chemical space of tested compounds targeting Haspin has been relatively small. On the other hand, this protein kinase has been declared to be a promising target for development of drugs that could be suitable for regulation of uncontrollable division of cells (*e.g.*, in case of cancer). Hence, taking advantage of the prior structural knowledge gained with X-ray analysis of complexes of inhibitors and Haspin as well as our initial results of structure-affinity studies with ARC-inhibitors, enabled the construction of novel bisubstrate inhibitors for Haspin. New conjugates incorporated an adenosine analogue Adc or a 5-iodotubercidin analogue Itc as the nucleosidic fragment and histone H3(1-7)-like peptide analogue sequence as the peptide moiety. The affinity of constructed inhbitors towards Haspin kinase as well as their selectivity towards several protein kinases was established in biochemical studies. The study also established the structural elements of the conjugates that affect the binding kinetics of the compounds.

The main outcomes of the present thesis were as follows:

- Biochemical screening of the initial set of ARC-scaffolds with variable structural features (including fluorescent probes as well as non-labelled conjugates) revealed the structure-affinity relationship for the structure-guided design of novel Haspin-targeting conjugates.
- Two most effective lead compounds (**ARC-1141** and **ARC-902**) of the initial set were chosen for the co-crystallization with kinase domain of Haspin. The obtained crystal structures of binary complexes were compared with the available co-crystal structure of substrate peptide of Haspin (histone H3), providing clues for the further improvement of Haspin-targeting conjugates.
- The novel Haspin-targeting conjugates comprised Adc, AMTH or Itc as the ATP-pocket fragment, and histone H3-like sequence as the peptidic part. These compounds showed improved selectivity towards Haspin over a basophilic reference kinase PKA C, and the importance of chiral spacer in the structure of linker fragment to obtain high affinity for Haspin (required for the correct positioning of the conjugates to Haspin as the chiral spacer directs the peptidic fragment of conjugate towards the substrate-site) was demonstrated.
- Next, inhibitory potency of Adc-comprising **Compounds 15** (incorporating only histone H3 sequence in peptidic part) and **18** (incorporating histone H3 sequence plus oligoarginine fragment in peptidic part) was determined towards 43 PKs (included important players in mitosis). **Compound 18** inhibited a variety of basophilic protein kinases, whereas **Compound 15** showed a narrow selectivity profile and hence demonstrated that the selectivity of substrate of Haspin translated into selectivity of H3-containing conjugates.
- Two most potent lead compounds of novel conjugates comprising Adc and histone H3-like peptide (**Compounds 15** and **16,** possessing K_d values of

170 and 150 nM, respectively) were co-crystallized with Haspin. The obtained 3D-structures of complexes featured high resolution and revealed that a small change in the structure of conjugates resulted in considerable difference in binding modes of interacting partners; at the same time, the signature of point interactions of histone H3 peptide was maintained for the histone peptide if it was incorporated into structure of the conjugates. Also, the bisubstrate nature of compounds was confirmed.

- The biochemical characterization of Itc- and histone H3(1-7)-like peptide-incorporating conjugates revealed subnanomolar affinity of **Compounds 26** and **27** (K_D* value of 0.019 nM and K_D' value of 0.100 nM, respectively). Moreover, **Compounds 26** and **27** (TAMRA-labelled analogue of **Compound 26**) possessed remarkably long residence times of 7.2 and 4.5 h, respectively.
- **Compound 26** showed improved selectivity towards a selection of PKs (including off-targets of 5-iodotubercidin) compared to that of 5-iodotubercidin, a nucleoside analogue that is actively used in biological research as a potent inhibitor of Haspin.

Perspectives

In future studies, the further development of Haspin-targeting inhibitors should first concentrate on improvement of the cell plasma membrane-penetrative properties as well as the proteolytic stability of conjugates. Briefly, in our initial studies, the effect of the developed inhibitors on the Haspin regulated histone H3 phosphorylation balance (established by monitoring decrease in the phosphorylation of *Thr3* of histone H3) was low.[127,128] The incorporation of either oligoarginine fragment or Myr moiety seemed to be insufficient for the successful internalization of Haspin-targeting conjugates into live cells. Moreover, the lack of significant effect of novel conjugates might be caused by degradation of conjugates by proteases in complex biological systems, as the histone H3 sequence in peptidic fragment of conjugates was built up of L-amino acids. One strategy to increase the proteolytic stability of compounds is the replacement of the 'classical' amino acid residues in peptidic fragment with peptidomimetics.[97–99,193] Also, the cyclization of histone H3-like peptide in the structure of novel conjugates may improve the succesful internalization of conjugates into the live cells as well as improve the stability for proteolytic degradation in cellular milieu.[194,195] Other strategies involve the linkage of transport peptide to the structure of conjugates (*e.g.*, folate, RPARPAR, or nonaarginine) *via* disulphide bridge to enhance the cellular uptake of Haspin-selective conjugates. The effect of transport peptides in the structure of ARC inhibitors had been demonstrated in our group when targeting acidophilic protein kinase CK2.[135] Our group is currently working on the development of synthetic strategies for generation of conjugates of the latter classes.

The perspective of the distant future could be to link the Haspin-targeting selective conjugates with the nano-based drug delivery carriers or nanocarriers.

An important benefit of nanocarriers is a site-specific delivery of compound to the tumor and hence the reduction of side effects and enhancement of efficiency of the drug.[196,197]

Another application of novel Haspin-targeting conjugates requires immobilization of the conjugates onto the surface. Thereafter, the surface-immobilized selective conjugates enable 'fishing out' of the kinase of interest from the various biological samples (*e.g.*, cell lysates, bodily fluids), and the following detection allows the quantification of amount of the kinase in the sample. Such studies would enable assessment of the value of Haspin as a biomarker in various diseases. The initial experiments have confirmed applicability of our novel Haspin-targeting conjugates for generation of affinity surfaces, and we expect to pursue this topic in the context of diagnostic applications in the nearest future.

SUMMARY IN ESTONIAN

Kristallstruktuuridest juhinduv bisubstraatsete inhibiitorite arendamine mitootilisele proteiinkinaasile Haspin

Bioteadustes (sh farmaatsiatööstus) pannakse suurt rõhku sellele, et töötada välja ühendeid, mis oleksid võimelised reguleerima rakkude kontrollimatu jagunemiseni viivaid signaaliradasid, st takistama (vähk)kasvajate arengut. Paralleelselt ravimiarendusega on üliloluline arendada lihtsa teostusega diagnostilisi meetodeid, mis võimaldaksid kindlaks teha haigusi juba varajases arenguetapis. Rakujagunemine (sh mitoos) on ülitäpselt reguleeritud teatud ensüümide perekonna – proteiinkinaaside – koostöö poolt. Proteiinkinaasid katalüüsivad fosforüülimist, mis toimib kui rakusisene märgis, käivitades või peatades signaaliradade toimimist ning seeläbi reguleerides raku eluks vajalikke protsesse. Proteiinkinaase kasutatakse ka biomarkeritena, kuna nende anomaalselt muutunud aktiivsust seostatakse erinevate haiguste tekke ja/või arenguga.

Käesoleva töö käigus võeti sihtmärgiks üsna väheuuritud, kuid mitoosi regulatsioonis üliloluline basofiilne proteiinkinaas Haspin. Haspinit on nimetatud ka „paljutõotavaks sihtmärgiks inhibiitorite kui potentsiaalsete vähivastaste ravimite arendamisel“.[3] Haspinile suunatud ühendite konstruktsioonil kasutati Tartu Ülikooli meditsiinilise keemia uurimisrühmas arendatud bisubstraatsete inhibiitorite adenosiini ja oligoarginiini konjugaatide (ARC-de) printsiipi: ATP-sidumistaskusse seostuv nukleosiidne osa ning substraadi-taskusse seostuv peptiidne fragment (nt proteiinkinaasi substraadi analoog) ühendatakse paindliku linkeriga. Uute ühendite disain põhines informatsioonil, mis oli saadud nii Haspini koos-kristallstruktuuridest kui ka varasemalt sünteesitud laia selektiivsusprofiiliga ARC-de struktuur-afiinsus sõltuvustel Haspini suhtes (tehti kindlaks ARC-de esialgse valimi biokeemilisel iseloomustamisel Haspiniga). Antud töö raames arendatud Haspinile suunatud konjugaadid koosnesid adenosiini analoogist (Adc) või Haspin-selektiivse inhibiitori 5-iodotubercidini fragmendist (Itc), mis ühendati linkeriga Haspini substraadi histoon H3 järjestust jäljendava peptiidse osaga. Seejärel teostati Haspinile suunatud konjugaatide afiinsuse, selektiivsuse ja kineetiliste omaduste uuringud.

Antud uurimistöö peamised tulemused on järgmised:

- Töö esimeses etapis teostati valim erineva struktuuriga olemasolevate ARC-de seast, sisaldades nii fluorestsentsonde kui ka märgistamata konjugaate. ARC-konjugaatide biokeemilisel analüüsil Haspiniga tehti kindlaks struktuur-afiinsus sõltuvused, mida kasutati Haspinile suunatud konjugaatide disainil.
- Kaks kõige efektiivsemat ühendit (**ARC-1141** ja **ARC-902**) algsest ARC-de valmist koos-kristalliti Haspiniga. Saadud binaarseid komplekse võrreldi eelnevalt publitseeritud Haspini substraadi histoon H3(1-7) peptiidi kristallstruktuuriga ning saadud infot kasutati lisainformatsioonina järgneval Haspin-selektiivsete ühendite konstrueerimisel.

- Uued Haspinile suunatud konjugaadid sisaldasid Adc, AMTH või Itc fragmenti ning histoon H3(1-7) järjestust imiteerivat peptiidset osa. Uutel konjugaatidel oli parem selektiivsus Haspinile kui algühenditel (st **ARC-1141** ja **ARC-902**, mis sisaldasid peptiidse osana oligoarginiini fragmenti), võrredes basofiilse referentskinaasiga PKA C. Lisaks näidati kiraalse elemendi olulisus linkeri struktuuris.
- Kahe Haspinile suunatud konjugaadi selektiivsusprofiil tehti kindlaks uuringutes 43 proteiinkinaasist koosneva valimiga, mis hõlmas endas olulisi mitoosi-regulaatoreid. Konjugaat, mis sisaldas nii histoon H3 järjestust kui ka oligoarginiini fragmenti peptiidses osas, inhibeeris enamikke basofiilseid proteiinkinaase. Samas konjugaat, mis sisaldas ainult histoon H3 järjestust peptiidses osas, omas väga kitsast selektiivsusprofiili. Seega tõestati, et substraadi selektiivsed omadused säilisid konjugaadi struktuuris.
- Kaks kõige efektiivsemat Haspin-selektiivset konjugaati, mis sisaldasid Adc ja histoon H3(1-7) sarnast peptiidi (K_d väärtus 150-170 nM), koos-kristalliti Haspiniga. Saadud kõrge resolutsiooniga kristallstruktuurid näitasid, et väikesed muutused konjugaadi struktuuris põhjustavad arvestatavaid erinevusi ühendite seostumismustris. Sealjuures olid säilinud histoon H3-le iseloomulikud interaktsioonid ning tõestati uute konjugaatide bisubstraatne olemus.
- Uued Itc and histoon H3(1-7) sarnast fragmenti sisaldavad konjugaadid omasid subnanomolaarset afiinsust Haspinile ning olid märkimisväärselt aeglase dissotsatsioonikineetikaga. Lisaks oli paranenud ühendite selektiivsus, võrreldes 5-iodotubercidini kui konjugaadi ühe algfragmendiga.

Haspinile suunatud konjugaatide edasise arenduse käigus peaks keskenduma ühendite rakumebraani läbimisvõime ja stabiilsuse parandamisele rakukeskonnas. Oma uurimistöö käigus oleme näidanud, et uute konjugaatide mõju Haspini signaaliradadele (jälgiti histoon H3 *Thr3* fosforüülimise vähenemist elusrakkudes) on ebapiisav.[127,128] See võib olla põhjustatud konjugaatide kehvast rakumembraani läbimisvõimest, kusjuures nii oligoarginiini fragmendi kui ka müristüülijäägi lisamine ei andnud märgatavat efektiivsuse kasvu. Lisaks koosneb konjugaatide peptiidne osa L-aminohapetest, mida on võimelised proteaasid rakukeskkonnas lagundama. Võimalikuks strateegiaks on asendada „klassikalised“ aminohapped peptidomimeetikutega[97–99,193] või tsükliseerida histoon H3 imiteeriv peptiidne fragment.[194,195] Teiseks võimaluseks on Haspin-selektiivsete konjugaatide struktuuri lisada transportpeptiidi järjestus (nt folaat, RPARPAR, nonaarginiini fragment), kasutades disulfiid-silda. Transportpeptiidide mõju ARC inhibiitorite struktuuris on meie uurimisrühmas eelnevalt uuritud seoses atsidofiilsele proteiinkinaasile CK2 suunatud konjugaatidega.[135]

Käesoleva töö käigus arendatud Haspin-selektiivsete ühendite pikaajalisemaks perspektiiviks on nende ühendamine nanokandjatega, mis võimaldaksid sihtmärkspetsiifilist transporti kasvajakoesse, suurendades seeläbi ühendite efektiivsust ning vähendades kõrvalmõjusid.[196,197] Teiseks võimalikuks rakenduseks on nende immobiliseerimine pinnale. Immobiliseeritud Haspin-selektiivsete konjugaatidega on erinevatest bioloogilistest proovidest (nt rakulüsaadid, bioloogilised vedelikud) võimalik pinnale püüda kinaasi ning määrata Haspini

kui biomarkeri hulka proovis. Teostatud pilootkatsed on näidanud Haspinile suunatud konjugaatide rakendatavust afiinsuspindadena ning antud teemat on lähitulevikus plaanis edasi uurida juba diagnostiliste rakenduste kontekstis.

REFERENCES

(1) Wu, P.; Nielsen, T. E.; Clausen, M. H. Small-Molecule Kinase Inhibitors: An Analysis of FDA-Approved Drugs. *Drug Discov. Today* **2016**, *21* (1), 5–10.

(2) Roskoski Jr, R. Properties of USFDA Approved Drugs that Inhibit Protein Kinases http://www.brimr.org/PKI/PKIs.htm (accessed Jan 23, 2018).

(3) Amoussou, N. G.; Bigot, A.; Roussakis, C.; Robert, M. H. Haspin: A Promising Target for the Design of Inhibitors as Potent Anticancer Drugs. *Drug Discov. Today* **2017**, *23* (2), 409–415.

(4) Roskoski, R. A Historical Overview of Protein Kinases and Their Targeted Small Molecule Inhibitors. *Pharmacol. Res.* **2015**, *100*, 1–23.

(5) Schwartz, P. A.; Murray, B. W. Protein Kinase Biochemistry and Drug Discovery. *Bioorg. Chem.* **2011**, *39* (5–6), 192–210.

(6) Scapin, G. Structural Biology in Drug Design: Selective Protein Kinase Inhibitors. *Drug Discov. Today* **2002**, *7* (11), 601–611.

(7) Knapp, S.; Sundström, M. Recently Targeted Kinases and Their Inhibitors - The Path to Clinical Trials. *Curr. Opin. Pharmacol.* **2014**, *17*, 58–63.

(8) Manning, G.; Whyte, D.; Martinez, R.; Hunter, T.; Sudarsanam, S. The Protein Kinase Complement of the Human Genome. *Science.* **2002**, *289*, 1912–1934.

(9) Ezkurdia, I.; Juan, D.; Rodriguez, J. M.; Frankish, A.; Diekhans, M.; Harrow, J.; Vazquez, J.; Valencia, A.; Tress, M. L. Multiple Evidence Strands Suggest That There May Be as Few as 19 000 Human Protein-Coding Genes. *Hum. Mol. Genet.* **2014**, *23* (22), 5866–5878.

(10) ter Haar, E.; Coll, J. T.; Austen, D. A.; Hsiao, H.-M.; Swenson, L.; Jain, J. Structure of GSK3β Reveals a Primed Phosphorylation Mechanism. *Nat. Struct. Biol.* **2001**, *8* (7), 593–596.

(11) Zhou, J.; Tien, A.; Alberta, J. A.; Ficarro, S. B.; Griveau, A.; Sun, Y.; Deshpande, J. S.; Card, J. D.; Morgan-smith, M.; Hashizume, R.; et al. A Sequentially Priming Phosphorylation Cascade Activates the Gliomagenic Transcription Factor Olig2. *Cell Rep.* **2017**, *18* (13), 3167–3177.

(12) Kung, J. E.; Jura, N. Structural Basis for the Non-Catalytic Functions of Protein Kinases. *Structure* **2016**, *24* (1), 7–24.

(13) Byrne, D. P.; Foulkes, D. M.; Eyers, P. A. Pseudokinases: Update on Their Functions and Evaluation as New Drug Targets. *Future Med. Chem.* **2017**, *9* (2), 245–265.

(14) Taylor, S. S.; Zhang, P.; Steichen, J. M.; Keshwani, M. M.; Kornev, A. P. PKA: Lessons Learned After Twenty Years. *Biochim. Biophys. Acta* **2013**, *1834* (7), 1271–1278.

(15) Walsh, D.; Perkins, J. P.; Krebs, E. G. An Adenosine 3′,5′-Monophosphate-Dependent Protein Kinase from Rabbit Skeletal Muscle. *J. Biol. Chem.* **1968**, *243* (13), 3763–3766.

(16) Smith, C. M.; Radzio-Andzelm, E.; Madhusudan; Akamine, P.; Taylor, S. S. The Catalytic Subunit of cAMP-Dependent Protein Kinase: Prototype for an Extended Network of Communication. *Prog. Biophys. Mol. Biol.* **1999**, *71* (3–4), 313–341.

(17) Taylor, S. S.; Yang, J.; Wu, J.; Haste, N. M.; Radzio-Andzelm, E.; Anand, G. PKA: A Portrait of Protein Kinase Dynamics. *Biochim. Biophys. Acta* **2004**, *1697* (1–2), 259–269.

(18) Skålhegg, B. S.; Funderud, A.; Henanger, H. H.; Hafte, T. T.; Larsen, C.; Kvissel, A.; Eikvar, S.; Ørstavik, S. Protein Kinase A (PKA) - A Potential Target for

Therapeutic Intervention of Dysfunctional Immune Cells. *Curr. Drug Targets* **2005**, *6*, 655–664.
(19) Kostenko, S.; Johannessen, M.; Moens, U. PKA-Induced F-Actin Rearrangement Requires Phosphorylation of Hsp27 by the MAPKAP Kinase MK5. *Cell. Signal.* **2009**, *21* (5), 712–718.
(20) Shabb, J. B. Physiological Substrates of cAMP-Dependent Protein Kinase. *Chem. Rev.* **2001**, *101*, 2381–2411.
(21) Knighton, D. R.; Zheng, J.; Ten Eyck, L. F.; Xuong, N.-H.; Taylor, S. S.; Sowadski, J. M. Structure of a Peptide Inhibitor Bound to the Catalytic Subunit of Cyclic Adenosine Monophosphate-Dependent Protein Kinase. *Science.* **1991**, *253* (5018), 414–420.
(22) Eigenthaler, M.; Nolte, C.; Halbrügge, M.; Walter, U. Concentration and Regulation of Cyclic Nucleotides, Cyclic-Nucleotide-Dependent Protein Kinases and One of Their Major Substrates in Human Platelets. Estimating the Rate of cAMP-Regulated and cGMP-Regulated Protein Phosphorylation in Intact Cells. *Eur. J. Biochem.* **1992**, *205*, 471–481.
(23) Pflug, A.; Oliveira, M. D. E.; Bossemeyer, D.; Engh, R. A. Mutants of Protein Kinase A That Mimic the ATP-Binding Site of Aurora Kinase. *Biochem. J.* **2011**, *440* (1), 85–93.
(24) Taylor, S. S.; Ilouz, R.; Zhang, P.; Kornev, A. P. Assembly of Allosteric Macromolecular Switches: Lessons from PKA. *Nat. Rev. Mol. Cell Biol.* **2012**, *13* (10), 646–658.
(25) Taylor, S. S.; Kim, C.; Cheng, C. Y.; Brown, S. H. J.; Wu, J.; Kannan, N. Signaling Through cAMP and cAMP-Dependent Protein Kinase: Diverse Strategies for Drug Design. *Biochim. Biophys. Acta* **2008**, *1784*, 16–26.
(26) Pidoux, G.; Taskén, K. Specificity and Spatial Dynamics of PKA Signaling Organized by A Kinase Anchoring Proteins. *J. Mol. Endocrinol.* **2010**, *44*, 271–284.
(27) Torres-Quesada, O.; Mayrhofer, J. E.; Stefan, E. The Many Faces of Compartmentalized PKA Signalosomes. *Cell. Signal.* **2017**, *37*, 1–11.
(28) Kinnings, S. L.; Jackson, R. M. Binding Site Similarity Analysis for the Functional Classification of the Protein Kinase Family. *J. Chem. Inf. Model.* **2009**, *49*, 318–329.
(29) Arencibia, J. M.; Pastor-Flores, D.; Bauer, A. F.; Schulze, J. O.; Biondi, R. M. AGC Protein Kinases: From Structural Mechanism of Regulation to Allosteric Drug Development for the Treatment of Human Diseases. *Biochim. Biophys. Acta* **2013**, *1834* (7), 1302–1321.
(30) Pearce, L. R.; Komander, D.; Alessi, D. R. The Nuts and Bolts of AGC Protein Kinases. *Nat. Rev. Mol. Cell Biol.* **2010**, *11* (1), 9–22.
(31) Taylor, S. S.; Kornev, A. P. Protein Kinases: Evolution of Dynamic Regulatory Proteins. *Trends Biochem. Sci.* **2011**, *36* (2), 65–77.
(32) Hu, J.; Ahuja, L. G.; Meharena, H. S.; Kannan, N.; Kornev, A. P.; Taylor, S. S.; Shaw, A. S. Kinase Regulation by Hydrophobic Spine Assembly in Cancer. *Mol. Cell. Biol.* **2015**, *35* (1), 264–276.
(33) Liou, Y.; Huang, H.; Ho, S. A Hydrophobic Spine Stabilizes a Surface-Exposed α-Helix According to Analysis of the Solvent-Accessible Surface Area. *BMC Bioinformatics* **2016**, *17* (19), 171–182.
(34) Holland, J.; Frei, E. *Cancer Medicine*, Fifth Edit.; BC Decker Inc: Hamilton, 2000.

(35) Dominguez-Brauer, C.; Thu, K. L.; Mason, J. M.; Blaser, H.; Bray, M. R.; Mak, T. W. Targeting Mitosis in Cancer: Emerging Strategies. *Mol. Cell* **2015**, *60* (4), 524–536.
(36) Bayliss, R.; Fry, A.; Haq, T.; Yeoh, S. On the Molecular Mechanisms of Mitotic Kinase Activation. *Open Biol.* **2012**, *2*, 120–136.
(37) Malumbres, M.; Barbacid, M. Cell Cycle, CDKs and Cancer: A Changing Paradigm. *Nat. Rev. Cancer* **2009**, *9*, 153–166.
(38) Dodson, C. A.; Haq, T.; Yeoh, S.; Fry, A. M.; Bayliss, R. The Structural Mechanisms That Underpin Mitotic Kinase Activation. *Biochem. Soc. Trans.* **2013**, *41*, 1037–1041.
(39) Fu, J.; Jiang, Q.; Zhang, C. Collaboration of Mitotic Kinases in Cell Cycle Control. *Nat. Educ.* **2010**, *3* (9), 82.
(40) Ma, H. T.; Poon, R. Y. C. How Protein Kinases Co-Ordinate Mitosis in Animal Cells. *Biochem. J.* **2011**, *435*, 17–31.
(41) Tanaka, H.; Iguchi, N.; Nakamura, Y.; Kohroki, J.; Carvalho, C. E. De; Nishimune, Y. Cloning and Characterization of Human Haspin Gene Encoding Haploid Germ Cell-Specific Nuclear Protein Kinase. *Mol. Hum. Reprod.* **2001**, *7* (3), 211–218.
(42) Higgins, J. M. Haspin-Like Proteins: A New Family of Evolutionarily Conserved Putative Eukaryotic Protein Kinases. *Protein Sci.* **2001**, *10* (8), 1677–1684.
(43) Tanaka, H.; Yoshimura, Y.; Nishina, Y.; Nozaki, M.; Nojima, H.; Nishimune, Y. Isolation and Characterization of cDNA Clones Specifically Expressed in Testicular Germ Cells. *FEBS Lett.* **1994**, *355* (1), 4–10.
(44) Tanaka, H.; Yoshimura, Y.; Nozaki, M.; Yomogida, K.; Tsuchida, J.; Tosaka, Y.; Habu, T.; Nakanishi, T.; Okada, M.; Nojima, H.; et al. Identification and Characterization of a Haploid Germ Cell-Specific Nuclear Protein Kinase (Haspin) in Spermatid Nuclei and Its Effects on Somatic Cells. *J. Biol. Chem.* **1999**, *274* (24), 17049–17057.
(45) Higgins, J. M. G. The Haspin Gene: Location in an Intron of the Integrin αE Gene, Associated Transcription of an Integrin αE-Derived RNA and Expression in Diploid as Well as Haploid Cells. *An Int. J. Genes Genomes* **2001**, *267*, 55–69.
(46) Yoshimura, Y.; Tanaka, H.; Nozaki, M.; Yomogida, K. Nested Genomic Structure of Haploid Germ Cell Specific Haspin Gene. **2001**, *267*, 49–54.
(47) Higgins, J. M. G. Structure, Function and Evolution of Haspin and Haspin-Related Proteins, a Distinctive Group of Eukaryotic Protein Kinases. *Cell. Mol. Life Sci.* **2003**, *60*, 446–462.
(48) Higgins, J. M. G. Haspin: A Newly Discovered Regulator of Mitotic Chromosome Behavior. *Chromosoma* **2010**, *119* (2), 137–147.
(49) Dai, J.; Sultan, S.; Taylor, S. S.; Higgins, J. M. G. The Kinase Haspin Is Required for Mitotic Histone H3 Thr 3 Phosphorylation and Normal Metaphase Chromosome Alignment. *Genes Dev.* **2005**, *19* (4), 472–488.
(50) Eswaran, J.; Patnaik, D.; Filippakopoulos, P.; Wang, F.; Stein, R. L.; Murray, J. W.; Higgins, J. M. G.; Knapp, S. Structure and Functional Characterization of the Atypical Human Kinase Haspin. *PNAS* **2009**, *106* (48), 20198–20203.
(51) Han, A.; Lee, K. H.; Hyun, S.; Lee, N. J.; Lee, S. J.; Hwang, H.; Yu, J. Methylation-Mediated Control of Aurora Kinase B and Haspin with Epigenetically Modified Histone H3 N-Terminal Peptides. *Bioorg. Med. Chem.* **2011**, *19* (7), 2373–2377.
(52) Villa, F.; Capasso, P.; Tortorici, M.; Forneris, F.; Marco, A. De; Mattevi, A.; Musacchio, A. Crystal Structure of the Catalytic Domain of Haspin, an Atypical

Kinase Implicated in Chromatin Organization. *PNAS* **2009**, *106* (48), 20204–20209.
(53) Johnson, D. A.; Akamine, P.; Radzio-Andzelm, E.; Madhusudan; Taylor, S. S. Dynamics of cAMP-Dependent Protein Kinase. *Chem. Rev.* **2001**, *101*, 2243–2270.
(54) Maiolica, A.; Medina-redondo, M. De; Schoof, E. M.; Chaikuad, A.; Villa, F.; Gatti, M.; Jeganathan, S.; Lou, H. J.; Novy, K.; Hauri, S.; et al. Modulation of the Chromatin Phosphoproteome by the Haspin Protein Kinase. *Mol. Cell. Proteomics* **2014**, *13* (7), 1724–1740.
(55) Balzano, D.; Santaguida, S.; Musacchio, A.; Villa, F. A General Framework for Inhibitor Resistance in Protein Kinases. *Chem. Biol.* **2011**, *18* (8), 966–975.
(56) Patnaik, D.; Xian, J.; Glicksman, M. A.; Cuny, G. D.; Stein, R. L.; Higgins, J. M. G. Identification of Small Molecule Inhibitors of the Mitotic Kinase Haspin by High-Throughput Screening Using a Homogeneous Time-Resolved Fluorescence Resonance Energy Transfer Assay. *J. Biomol. Screen.* **2008**, *13* (10), 1025–1034.
(57) Zimmermann, B.; Chiorini, J. A.; Ma, Y.; Kotin, R. M.; Herberg, F. W. PrKX Is a Novel Catalytic Subunit of the cAMP-Dependent Protein Kinase Regulated by the Regulatory Subunit Type I. *J. Biol. Chem.* **1999**, *274* (9), 5370–5378.
(58) Bogoyevitch, M. A.; Barr, R. K.; Ketterman, A. J. Peptide Inhibitors of Protein Kinases - Discovery, Characterisation and Use. *Biochim. Biophys. Acta* **2005**, *1754* (1–2), 79–99.
(59) Hada, M.; Kim, J.; Inoue, E.; Fukuda, Y.; Tanaka, H.; Watanabe, Y.; Okada, Y. TH2A Is Phosphorylated at Meiotic Centromere by Haspin. *Chromosoma* **2017**, *126*, 769–780.
(60) Dai, J.; Kateneva, A. V; Higgins, J. M. G. Studies of Haspin Depleted Cells Reveal That Spindle Pole Integrity in Mitosis Requires Chromosome Cohesion. *J. Cell Sci.* **2009**, *122* (22), 4168–4176.
(61) Wang, F.; Dai, J.; Daum, J. R.; Niedzialkowska, E.; Banerjee, B.; Stukenberg, P. T.; Gorbsky, G. J.; Higgins, J. M. G. Histone H3 Thr-3 Phosphorylation by Haspin Positions Aurora B at Centromeres in Mitosis. *Science.* **2010**, *330* (6001), 231–235.
(62) Wang, F.; Ulyanova, N. P.; van der Waal, M. S.; Patnaik, D.; Lens, S. M. A.; Higgins, J. M. G. A Positive Feedback Loop Involving Haspin and Aurora B Promotes CPC Accumulation at Centromeres in Mitosis. *Curr. Biol.* **2011**, *21* (12), 1061–1069.
(63) Dai, J.; Sullivan, B. A.; Higgins, J. M. G. Regulation of Mitotic Chromosome Cohesion by Haspin and Aurora B. *Dev. Cell* **2006**, *11*, 741–750.
(64) Markaki, Y.; Christogianni, A.; Politou, A. S.; Georgatos, S. D. Phosphorylation of Histone H3 at Thr3 Is Part of a Combinatorial Pattern That Marks and Configures Mitotic Chromatin. *J. Cell Biol.* **2009**, *122* (16), 2809–2819.
(65) Shimada, M.; Goshima, T.; Matsuo, H.; Johmura, Y.; Haruta, M.; Murata, K.; Tanaka, H.; Ikawa, M.; Nakanishi, K.; Nakanishi, M. Essential Role of Autoactivation Circuitry on Aurora B-Mediated H2AX-pS121 in Mitosis. *Nat. Commun.* **2016**, *7*, 1–11.
(66) Yamagishi, Y.; Honda, T.; Tanno, Y.; Watanabe, Y. Two Histone Marks Establish the Inner Centromere and Chromosome Bi-Orientation. *Science.* **2010**, *330*, 239–243.
(67) Ruiz-Torres, M.; Rodriguez-Corsino, M.; Barthelemy, I.; Losada, A. Pds5B Is Required for Cohesion Establishment and Aurora B Accumulation at Centromeres. *EMBO J.* **2013**, *32* (22), 2938–2949.

(68) Ghenoiu, C.; Wheelock, M. S.; Funabiki, H. Article Autoinhibition and Polo-Dependent Multisite Phosphorylation Restrict Activity of the Histone H3 Kinase Haspin to Mitosis. *Mol. Cell* **2013**, *52* (5), 734–745.
(69) Carmena, M.; Wheelock, M.; Funabiki, H.; Earnshaw, W. C. The Chromosomal Passenger Complex (CPC): From Easy Rider to the Godfather of Mitosis. *Nat. Rev. Mol. Cell Biol.* **2012**, *13* (12), 789–803.
(70) van de Werken, C.; Santos, M. A.; Laven, J. S. E.; Eleveld, C.; Fauser, B. C. J. M.; Lens, S. M. A.; Baart, E. B. Chromosome Segregation Regulation in Human Zygotes: Altered Mitotic Histone Phosphorylation Dynamics Underlying Centromeric Targeting of the Chromosomal Passenger Complex. *Hum. Reprod.* **2015**, *30* (10), 2275–2291.
(71) Polioudaki, H.; Markaki, Y.; Kourmouli, N.; Dialynas, G.; Theodoropoulos, P. A.; Singh, P. B.; Georgatos, S. D. Mitotic Phosphorylation of Histone H3 at Threonine 3. *FEBS Lett.* **2004**, *560*, 39–44.
(72) Hirota, T.; Lipp, J. J.; Toh, B.-H.; Peters, J.-M. Histone H3 Serine 10 Phosphorylation by Aurora B Causes HP1 Dissociation from Heterochromatin. *Nature* **2005**, *438*, 1176–1180.
(73) Kelly, A. E.; Ghenoiu, C.; Xue, J. Z.; Zierhut, C.; Kimura, H.; Funabiki1, H. Survivin Reads Phosphorylated Histone H3 Threonine 3 to Activate the Mitotic Kinase Aurora B. *Science.* **2010**, *330* (6001), 235–239.
(74) van der Horst, A.; Lens, S. M. A. Cell Division: Control of the Chromosomal Passenger Complex in Time and Space. *Chromosoma* **2014**, *123*, 25–42.
(75) Qian, J.; Lesage, B.; Beullens, M.; Eynde, A. Van; Bollen, M. PP1/Repo-Man Dephosphorylates Mitotic Histone H3 at T3 and Regulates Chromosomal Aurora B Targeting. *Curr. Biol.* **2011**, *21* (9), 766–773.
(76) Qian, J.; Beullens, M.; Lesage, B.; Bollen, M. Aurora B Defines Its Own Chromosomal Targeting by Opposing the Recruitment of the Phosphatase Scaffold Repo-Man. *Curr. Biol.* **2013**, *23* (12), 1136–1143.
(77) Nelson, D. L.; Cox, M. M. *Lehninger Principles of Biochemistry*, Sixth Edit.; Freeman: New York, 2013.
(78) Knight, Z. A.; Shokat, K. M. Features of Selective Kinase Inhibitors. *Chem. Biol. Biol.* **2005**, *12* (6), 621–637.
(79) Parang, K.; Sun, G. Design Strategies for Protein Kinase Inhibitors. *Curr. Opin. Drug Discov. Devel.* **2004**, *7* (5), 617–629.
(80) Müller, S.; Chaikuad, A.; Gray, N. S.; Knapp, S. The Ins and Outs of Selective Kinase Inhibitor Development. *Nat. Chem. Biol.* **2015**, *11* (11), 818–821.
(81) Dar, A. C.; Shokat, K. M. The Evolution of Protein Kinase Inhibitors from Antagonists to Agonists of Cellular Signaling. *Annu. Rev. Biochem.* **2011**, *80*, 769–795.
(82) Roskoski Jr, R. Classification of Small Molecule Protein Kinase Inhibitors Based Upon the Structures of Their Drug-Enzyme Complexes. *Pharmacol. Res.* **2016**, *103*, 26–48.
(83) Lochner, A.; Moolman, J. A. The Many Faces of H89: A Review. *Cardiovasc. Drug Rev.* **2006**, *24* (3–4), 261–274.
(84) Capdeville, R.; Buchdunger, E.; Zimmermann, J.; Matter, A. Glivec (STI571, Imatinib), a Rationally Developed, Targeted Anticancer Drug. *Nat. Rev. Drug Discov.* **2002**, *1* (7), 493–502.
(85) Gillis, N. K.; McLeod, H. L. The Pharmacogenomics of Drug Resistance to Protein Kinase Inhibitors. *Drug Resist. Updat.* **2016**, *28*, 28–42.

(86) Daub, H.; Specht, K.; Ullrich, A. Strategies to Overcome Resistance to Targeted Protein Kinase Inhibitors. *Nat. Rev. Drug Discov.* **2004**, *3*, 1001–1010.
(87) Kooistra, A. J.; Kanev, G. K.; Linden, O. P. J. Van; Leurs, R.; Esch, I. J. P. De; Graaf, C. De. KLIFS: A Structural Kinase-Ligand Interaction Database. *Nucleic Acids Res.* **2016**, *44*, 365–371.
(88) Kooistra, A. J.; Volkamer, A. Chapter Six - Kinase-Centric Computational Drug Development. *Annu. Rep. Med. Chem.* **2017**, *50*, 197–236.
(89) Zhao, Z.; Wu, H.; Wang, L.; Liu, Y.; Knapp, S.; Liu, Q.; Gray, N. S. Exploration of Type II Binding Mode: A Privileged Approach for Kinase Inhibitor Focused Drug Discovery? *ACS Chem. Biol.* **2014**, *9*, 1230–1241.
(90) De Antoni, A.; Maffini, S.; Knapp, S.; Musacchio, A.; Santaguida, S. A Small-Molecule Inhibitor of Haspin Alters the Kinetochore Functions of Aurora B. *J. Cell Biol.* **2012**, *199* (2), 269–284.
(91) Massillon, D.; Stalmans, W.; van de WErve, G.; Bollen, M. Identification of the Glycogenic Compound 5-Iodotubercidin as a General Protein Kinase Inhibitor. *Biochem. J.* **1994**, *299* (1), 123–128.
(92) Ugarkar, B. G.; DaRe, J. M.; Kopcho, J. J.; Browne, C. E.; Schanzer, J. M.; Wiesner, J. B.; Erion, M. D. Adenosine Kinase Inhibitors. 1. Synthesis, Enzyme Inhibition, and Antiseizure Activity of 5-Iodotubercidin Analogues. *J. Med. Chem.* **2000**, *43* (15), 2883–2893.
(93) Kestav, K.; Uri, A.; Lavogina, D. Structure, Roles and Inhibitors of a Mitotic Protein Kinase Haspin. *Curr. Med. Chem.* **2017**, *24* (21), 2276–2293.
(94) Peyressatre, M.; Prével, C.; Pellerano, M.; Morris, M. C. Targeting Cyclin-Dependent Kinases in Human Cancers: From Small Molecules to Peptide Inhibitors. *Cancers.* **2015**, *7* (1), 179–237.
(95) Eldar-Finkelman, H.; Eisenstein, M. Peptide Inhibitors Targeting Protein Kinases. *Curr. Pharm. Des.* **2009**, *15* (21), 2463–2470.
(96) Scott, D. E.; Bayly, A. R.; Abell, C.; Skidmore, J. Small Molecules, Big Targets: Drug Discovery Faces the Protein–Protein Interaction Challenge. *Nat. Rev. Drug Discov.* **2016**, *15* (8), 533–550.
(97) Grauer, A.; König, B. Peptidomimetics–A Versatile Route to Biologically Active Compounds. *European J. Org. Chem.* **2009**, No. 30, 5099–5111.
(98) Guichard, G.; Benkirane, N.; Zeder-Lutz, G.; van Regenmortel, M. H.; Briand, J. P.; Muller, S. Antigenic Mimicry of Natural L-Peptides with Retro-Inverso-Peptidomimetics. *Proc. Natl. Acad. Sci. U. S. A.* **1994**, *91* (21), 9765–9769.
(99) Su, L.; Xu, W. Peptidomimetics and Metalloprotease Inhibitors as Anticancer Drugs. *Sci. China, Ser. B Chem.* **2009**, *52* (5), 535–548.
(100) Walsh, D. A.; Ashby, C. D.; Gonzalez, C.; Calkins, D.; Fischer, E. H.; Krebs, E. G. Purification and Characterization of a Protein Inhibitor of Adenosine 3′,5′-Monophosphate-Dependent Protein Kinase. *J. Biol. Chem.* **1971**, *246* (7), 1977–1985.
(101) Dalton, G. D.; Dewey, W. L. Protein Kinase Inhibitor Peptide (PKI): A Family of Endogenous Neuropeptides That Modulate Neuronal cAMP-Dependent Protein Kinase Function. *Neuropeptides* **2006**, *40*, 23–34.
(102) Wen, W.; Taylor, S. S. High Affinity Binding of the Heat-Stable Protein Kinase Inhibitor to the Catalytic Subunit of CAMP-Dependent Protein Kinase Is Selectively Abolished. *J. Biol. Chem.* **1994**, *269* (11), 8423–8430.
(103) Lavogina, D.; Enkvist, E.; Uri, A. Bisubstrate Inhibitors of Protein Kinases: From Principle to Practical Applications. *ChemMedChem* **2010**, *5* (1), 23–34.

(104) Jencks, W. P. On the Attribution and Additivity of Binding Energies. *Proc. Natl. Acad. Sci. U. S. A.* **1981**, *78* (7), 4046–4050.
(105) Saxty, G.; Woodhead, S. J.; Berdini, V.; Davies, T. G.; Verdonk, M. L.; Wyatt, P. G.; Boyle, R. G.; Barford, D.; Downham, R.; Garrett, M. D.; et al. Identification of Inhibitors of Protein Kinase B Using Fragment-Based Lead Discovery. *J. Med. Chem.* **2007**, *50* (10), 2293–2296.
(106) Kane, R. S. Thermodynamics of Multivalent Interactions: Influence of the Linker. *Langmuir* **2010**, *26* (11), 8636–8640.
(107) Lavogina, D.; Lust, M.; Viil, I.; König, N.; Raidaru, G.; Rogozina, J.; Enkvist, E.; Uri, A.; Bossemeyer, D. Structural Analysis of ARC-Type Inhibitor (ARC-1034) Binding to Protein Kinase A Catalytic Subunit and Rational Design of Bisubstrate Analogue Inhibitors of Basophilic Protein Kinases. *J. Med. Chem.* **2009**, *52* (2), 308–321.
(108) Enkvist, E.; Viht, K.; Bischoff, N.; Vahter, J.; Saaver, S.; Raidaru, G.; Issinger, O.-G.; Niefind, K.; Uri, A. A Subnanomolar Fluorescent Probe for Protein Kinase CK2 Interaction Studies. *Org. Biomol. Chem.* **2012**, *10*, 8645–8653.
(109) Lavogina, D.; Kestav, K.; Chaikuad, A.; Heroven, C.; Knapp, S.; Uri, A. Co-Crystal Structures of the Protein Kinase Haspin with Bisubstrate Inhibitors. *Acta Crystallogr. Sect. F Struct. Biol. Commun.* **2016**, *F72*, 339–345.
(110) Kuzmič, P. Program DYNAFIT for the Analysis of Enzyme Kinetic Data: Application to HIV Proteinase. *Anal. Biochem.* **1996**, *237* (2), 260–273.
(111) Vaasa, A.; Viil, I.; Enkvist, E.; Viht, K.; Raidaru, G.; Lavogina, D.; Uri, A. High-Affinity Bisubstrate Probe for Fluorescence Anisotropy Binding/Displacement Assays with Protein Kinases PKA and ROCK. *Anal. Biochem.* **2009**, *385* (1), 85–93.
(112) Viht, K.; Schweinsberg, S.; Lust, M.; Vaasa, A.; Raidaru, G.; Lavogina, D.; Uri, A.; Herberg, F. W. Surface-Plasmon-Resonance-Based Biosensor with Immobilized Bisubstrate Analog Inhibitor for the Determination of Affinities of ATP- and Protein-Competitive Ligands of cAMP-Dependent Protein Kinase. *Anal. Biochem.* **2007**, *362* (2), 268–277.
(113) Wolfenden, R. Analog Approaches to the Structure of the Transition State in Enzyme Reactions. *Acc. Chem. Res.* **1972**, *5* (1), 10–18.
(114) Lienhard, G.; Secemski, I. P1,P5-Di(adenosine-5')pentaphosphate, a Potent Multisubstrate Inhibitor of Adenylate Kinase. *J. Biol. Chem.* **1973**, *248*, 1121–1123.
(115) Schramm, V. L. Enzymatic Transition States, Transition-State Analogs, Dynamics, Thermodynamics, and Lifetimes. *Annu. Rev. Biochem.* **2011**, *80* (1), 703–732.
(116) Ricouart, A.; Gesquiere, J. C.; Tartar, A.; Sergheraert, C. Design of Potent Protein Kinases Inhibitors Using the Bisubstrate Approach. *J. Med. Chem.* **1991**, *34* (1), 73–78.
(117) Loog, M.; Uri, A.; Raidaru, G.; Järv, J.; Ek, P. Adenosine-5′-Carboxylic Acid Peptidyl Derivatives as Inhibitors of Protein Kinases. *Bioorg. Med. Chem. Lett.* **1999**, *9*, 1447–1452.
(118) Nakase, I.; Takeuchi, T.; Tanaka, G.; Futaki, S. Methodological and Cellular Aspects That Govern the Internalization Mechanisms of Arginine-Rich Cell-Penetrating Peptides. *Adv. Drug Deliv. Rev.* **2008**, *60* (4–5), 598–607.
(119) Viht, K.; Padari, K.; Raidaru, G.; Subbi, J.; Tammiste, I.; Pooga, M.; Uri, A. Liquid-Phase Synthesis of a Pegylated Adenosine-Oligoarginine Conjugate,

Cell-Permeable Inhibitor of cAMP-Dependent Protein Kinase. *Bioorg. Med. Chem. Lett.* **2003**, *13* (18), 3035–3039.
(120) Uri, A.; Raidaru, G.; Subbi, J.; Padari, K.; Pooga, M. Identification of the Ability of Highly Charged Nanomolar Inhibitors of Protein Kinases to Cross Plasma Membranes and Carry a Protein into Cells. *Bioorganic Med. Chem. Lett.* **2002**, *12* (16), 2117–2120.
(121) Enkvist, E.; Lavogina, D.; Raidaru, G.; Vaasa, A.; Viil, I.; Lust, M.; Viht, K.; Uri, A. Conjugation of Adenosine and Hexa-(D-Arginine) Leads to a Nanomolar Bisubstrate-Analog Inhibitor of Basophilic Protein Kinases. *J. Med. Chem.* **2006**, *49* (24), 7150–7159.
(122) Räägel, H.; Lust, M.; Uri, A.; Pooga, M. Adenosine-Oligoarginine Conjugate, a Novel Bisubstrate Inhibitor, Effectively Dissociates the Actin Cytoskeleton. *FEBS J.* **2008**, *275* (14), 3608–3624.
(123) Uri, A.; Lust, M.; Vaasa, A.; Lavogina, D.; Viht, K.; Enkvist, E. Bisubstrate Fluorescent Probes and Biosensors in Binding Assays for HTS of Protein Kinase Inhibitors. *Biochim. Biophys. Acta* **2010**, *1804* (3), 541–546.
(124) Vaasa, A.; Ligi, K.; Mohandessi, S.; Enkvist, E.; Uri, A.; Miller, L. W. Time-Gated Luminescent Microscopy with Responsive Nonmetal Probes for Mapping Activity of Protein Kinases in Living Cells. *Chem. Commun.* **2012**, *48* (68), 8595–8597.
(125) Kasari, M.; Ligi, K.; Williams, J. A. G.; Vaasa, A.; Enkvist, E.; Viht, K.; Pålsson, L. O.; Uri, A. Responsive Microsecond-Lifetime Photoluminescent Probes for Analysis of Protein Kinases and Their Inhibitors. *Biochim. Biophys. Acta - Proteins Proteomics* **2013**, *1834* (7), 1330–1335.
(126) Lavogina, D.; Lust, M.; Viil, I.; König, N.; Raidaru, G.; Rogozina, J.; Enkvist, E.; Uri, A.; Bossemeyer, D. Structural Analysis of ARC-Type Inhibitor (ARC-1034) Binding to Protein Kinase A Catalytic Subunit and Rational Design of Bisubstrate Analogue Inhibitors of Basophilic Protein Kinases. *J. Med. Chem.* **2009**, *52* (2), 308–321.
(127) Kestav, K.; Lavogina, D.; Raidaru, G.; Chaikuad, A.; Knapp, S.; Uri, A. Bisubstrate Inhibitor Approach for Targeting Mitotic Kinase Haspin. *Bioconjug. Chem.* **2015**, *26* (2), 225–234.
(128) Kestav, K.; Viht, K.; Konovalov, A.; Enkvist, E.; Uri, A.; Lavogina, D. Slowly On, Slowly off: Bisubstrate-Analogue Conjugates of 5-Iodotubercidin and Histone H3 Peptide Targeting Protein Kinase Haspin. *ChemBioChem* **2017**, *18* (8), 790–798.
(129) Lavogina, D.; Kalind, K.; Bredihhina, J.; Hurt, M.; Vaasa, A.; Kasari, M.; Enkvist, E.; Raidaru, G.; Uri, A. Conjugates of 5-Isoquinolinesulfonylamides and Oligo-D-Arginine Possess High Affinity and Selectivity Towards Rho Kinase (ROCK). *Bioorganic Med. Chem. Lett.* **2012**, *22* (10), 3425–3430.
(130) Viht, K.; Saaver, S.; Vahter, J.; Enkvist, E.; Lavogina, D.; Sinijärv, H.; Raidaru, G.; Guerra, B.; Issinger, O. G.; Uri, A. Acetoxymethyl Ester of Tetrabromo-benzimidazole-Peptoid Conjugate for Inhibition of Protein Kinase CK2 in Living Cells. *Bioconjug. Chem.* **2015**, *26* (12), 2324–2335.
(131) Ekambaram, R.; Enkvist, E.; Vaasa, A.; Kasari, M.; Raidaru, G.; Knapp, S.; Uri, A. Selective Bisubstrate Inhibitors with Sub-Nanomolar Affinity for Protein Kinase Pim-1. *ChemMedChem* **2013**, *8* (6), 909–913.

(132) Vahter, J.; Viht, K.; Uri, A.; Enkvist, E. Oligo-Aspartic Acid Conjugates With Benzo[c][2,6]naphthyridine-8-Carboxylic Acid Scaffold as Picomolar Inhibitors of CK2. *Bioorg. Med. Chem.* **2017**, *25* (7), 2277–2284.
(133) Enkvist, E.; Vaasa, A.; Kasari, M.; Kriisa, M.; Ivan, T.; Ligi, K.; Raidaru, G.; Uri, A. Protein-Induced Long Lifetime Luminescence of Nonmetal Probes. *ACS Chem. Biol.* **2011**, *6* (10), 1052–1062.
(134) Manoharan, G. B.; Enkvist, E.; Uri, A. Combining Chemical and Genetic Approaches for Development of Responsive FRET-Based Sensor Systems for Protein Kinases. *Biophys. Chem.* **2016**, *211*, 39–48.
(135) Rahnel, H.; Viht, K.; Lavogina, D.; Mazina, O.; Haljasorg, T.; Enkvist, E.; Uri, A. A Selective Biligand Inhibitor of CK2 Increases Caspase-3 Activity in Cancer Cells and Inhibits Platelet Aggregation. *ChemMedChem* **2017**, *12* (20), 1723–1736.
(136) Vaasa, A.; Lust, M.; Terrin, A.; Uri, A.; Zaccolo, M. Small-Molecule FRET Probes for Protein Kinase Activity Monitoring in Living Cells. *Biochem. Biophys. Res. Commun.* **2010**, *397* (4), 750–755.
(137) Loog, M.; Uri, A.; Järv, J.; Ek, P. Bi-Substrate Analogue Ligands for Affinity Chromatography of Protein Kinases. *FEBS Lett.* **2000**, *480* (2–3), 244–248.
(138) Ivan, T.; Enkvist, E.; Viira, B.; Manoharan, G. B.; Raidaru, G.; Pflug, A.; Alam, K. A.; Zaccolo, M.; Engh, R. A.; Uri, A. Bifunctional Ligands for Inhibition of Tight-Binding Protein-Protein Interactions. *Bioconjug. Chem.* **2016**, *27* (8), 1900–1910.
(139) Merrifield, R. B. Solid Phase Peptide Synthesis. I. The Synthesis of Tetrapeptide. *J. Am. Chem. Soc.* **1963**, *85* (14), 2149.
(140) Culf, A. S.; Ouellette, R. J. Solid-Phase Synthesis of N-Substituted Glycine Oligomers (α-Peptoids) and Derivatives. *Molecules* **2010**, *15* (8), 5282–5335.
(141) Caruthers, M. H. The Chemical Synthesis of DNA/RNA: Our Gift to Science. *J. Biol. Chem.* **2013**, *288* (2), 1420–1427.
(142) Dirin, M.; Urban, E.; Noe, C. R.; Winkler, J. Fragment-Based Solid-Phase Assembly of Oligonucleotide Conjugates with Peptide and Polyethylene Glycol Ligands. *Eur. J. Med. Chem.* **2016**, *121*, 132–142.
(143) Benoiton, N. L. *Chemistry of Peptide Synthesis*; CRC Press Taylor and Francis Group: Boka Raton, 2006.
(144) Lloyd-Williams, P.; Albericio, F.; Giralt, E. *Chemical Approaches to the Synthesis of Peptides and Proteins*; CRC Press LLC: Boka Raton, 1997.
(145) Shin, D.-S.; Kim, D.-H.; Chung, W.-J.; Lee, Y.-S. Combinatorial Solid Phase Peptide Synthesis and Bioassays. *J. Biochem. Mol. Biol.* **2005**, *38* (5), 517–525.
(146) Kim, M.; Shin, D.-S.; Kim, J.; Lee, Y.-S. Substrate Screening of Protein Kinases: Detection Methods and Combinatorial Peptide Libraries. *Biopolymers* **2010**, *94* (6), 753–762.
(147) Mařík, J.; Song, A.; Lam, K. S. Detection of Primary Aromatic Amines on Solid Phase. *Tetrahedron Lett.* **2003**, *44*, 4319–4320.
(148) Attardi, M. E.; Falchi, A.; Taddei, M. A Sensitive Visual Test for Detection of OH Groups on Resin. *Tetrahedron Lett.* **2001**, *42* (15), 7395–7399.
(149) Kaiser, E.; Colescott, R. L.; Bossinger, C. D.; Cook, P. I. Color Test for Detection of Free Terminal Amino Groups in the Solid-Phase Synthesis of Peptides. *Anal. Biochem.* **1970**, *34* (2), 595–598.
(150) Lakowicz, J. R. *Principles of Fluorescence Spectroscopy*, Third Edit.; Springer Science+Business Media, LLC: New York, 2006.

(151) McNaught, A.; Wilkinson, A.; Nic, M.; Jirat, J.; Kosata, B.; Jenkins, A. IUPAC. Compendium of Chemical Terminology, 2nd ed. (The "Gold Book", version 2.3.3.) http://goldbook.iupac.org/index.html (accessed Jan 4, 2018).
(152) Ligi, K.; Enkvist, E.; Uri, A. Deoxygenation Increases Photoluminescence Lifetime of Protein-Responsive Organic Probes with Triplet-Singlet Resonant Energy Transfer. *J. Phys. Chem. B* **2016**, *120* (22), 4945–4954.
(153) Roehrl, M. H. A.; Wang, J. Y.; Wagner, G. A General Framework for Development and Data Analysis of Competitive High-Throughput Screens for Small-Molecule Inhibitors of Protein – Protein Interactions by Fluorescence Polarization. *Biochemistry* **2004**, *43*, 16056–16066.
(154) Rinken, A.; Lavogina, D.; Kopanchuk, S. Assays with Detection of Fluorescence Anisotropy: Challenges and Possibilities for Characterizing Ligand Binding to GPCRs. *Trends Pharmacol. Sci.* **2017**, *39* (2), 187–199.
(155) Atkins, P. W. *Physical Chemistry*; Oxford University Press: Oxford, 2010.
(156) Pan, A. C.; Borhani, D. W.; Dror, R. O.; Shaw, D. E. Molecular Determinants of Drug-Receptor Binding Kinetics. *Drug Discov. Today* **2013**, *18* (13–14), 667–673.
(157) Ivan, T.; Enkvist, E.; Sinijarv, H.; Uri, A. Competitive Ligands Facilitate Dissociation of the Complex of Bifunctional Inhibitor and Protein Kinase. *Biophys. Chem.* **2017**, *228*, 17–24.
(158) Niesen, F. H.; Berglund, H.; Vedadi, M. The Use of Differential Scanning Fluorimetry to Detect Ligand Interactions That Promote Protein Stability. *Nat. Protoc.* **2007**, *2* (9), 2212–2221.
(159) Vedadi, M.; Niesen, F. H.; Allali-hassani;, A.; Fedorov, O. Y.; Finerty, P. J. J.; Wasney, G. A.; Yeung, R.; Arrowsmith, C.; Ball, L. J.; Berglund, H.; et al. Chemical Screening Methods to Identify Ligands That Promote Protein Stability, Protein Crystallization, and Structure Determination. *Proc. Natl. Acad. Sci. U. S. A.* **2006**, *103* (43), 15835–15840.
(160) Sorrell, F. J.; Greenwood, G. K.; Birchall, K.; Chen, B. Development of a Differential Scanning Fluorimetry Based High Throughput Screening Assay for the Discovery of Affinity Binders Against an Anthrax Protein. *J. Pharm. Biomed. Anal.* **2010**, *52*, 802–808.
(161) Fedorov, O.; Huber, K.; Eisenreich, A.; Filippakopoulos, P.; King, O.; Bullock, A. N.; Szklarczyk, D.; Jensen, L. J.; Fabbro, D.; Trappe, J.; et al. Specific CLK Inhibitors from a Novel Chemotype for Regulation of Alternative Splicing. *Chem. Biol.* **2011**, *18* (1), 67–76.
(162) Filippakopoulos, P.; Qi, J.; Picaud, S.; Shen, Y.; Smith, W. B.; Morse, E. M.; Keates, T.; Hickman, T. T.; Felletar, I.; Munro, S.; et al. Selective Inhibition of BET Bromodomains. *Nature* **2010**, *468* (7327), 1067–1073.
(163) Fedorov, O.; Marsden, B.; Pogacic, V.; Rellos, P.; Müller, S.; Bullock, A. N.; Schwaller, J.; Sundström, M.; Knapp, S. A Systematic Interaction Map of Validated Kinase Inhibitors with Ser/Thr Kinases. *Proc. Natl. Acad. Sci. U. S. A.* **2007**, *104* (51), 20523–20528.
(164) Hellman, L. M.; Yin, L.; Wang, Y.; Blevins, S. J.; Riley, T. P.; Belden, O. S.; Spear, T. T.; Nishimura, M. I.; Stern, L. J.; Baker, B. M. Differential Scanning Fluorimetry Based Assessments of the Thermal and Kinetic Stability of Peptide – MHC Complexes. *J. Immunol. Methods* **2016**, *432*, 95–101.
(165) Cimmperman, P.; Baranauskiene, L.; Jachimoviciūte, S.; Jachno, J.; Torresan, J.; Michailoviene, V.; Matuliene, J.; Sereikaite, J.; Bumelis, V.; Matulis, D. A

Quantitative Model of Thermal Stabilization and Destabilization of Proteins by Ligands. *Biophys. J.* **2008**, *95* (7), 3222–3231.
(166) Rupp, B. *Biomolecular Crystallography: Principles, Practice, and Application to Structural Biology*; Taylor & Francis Group, LCC: New York, 2010.
(167) Jubb, H.; Higueruelo, A. P.; Winter, A.; Blundell, T. L. Structural Biology and Drug Discovery for Protein-Protein Interactions. *Trends Pharmacol. Sci.* **2012**, *33* (5), 241–248.
(168) Higueruelo, A. P.; Jubb, H.; Blundell, T. L. Protein-Protein Interactions as Druggable Targets: Recent Technological Advances. *Curr. Opin. Pharmacol.* **2013**, *13* (5), 791–796.
(169) Jubb, H.; Blundell, T. L.; Ascher, D. B. Flexibility and Small Pockets at Protein-Protein Interfaces: New Insights into Druggability. *Prog. Biophys. Mol. Biol.* **2015**, *119* (1), 2–9.
(170) Drenth, J. *Principles of Protein X-Ray Crystallography*, Third Edit.; Springer Science+Business Media, LLC: New York, 2007.
(171) Messerschmidt, A. *X-Ray Crystallography of Biomacromolecules: A Practical Guide*; WILEY-VCH Verlag GmbH & Co. KGaA: Weinheim, 2007.
(172) Wlodawer, A.; Minor, W.; Dauter, Z.; Jaskolski, M. Protein Crystallography for Non-Crystallographers, or How to Get the Best (But Not More) From Published Macromolecular Structures. *FEBS J.* **2008**, *275*, 1–21.
(173) Lavogina, D.; Nickl, C. K.; Enkvist, E.; Raidaru, G.; Lust, M.; Vaasa, A.; Uri, A.; Dostmann, W. R. Adenosine Analogue–Oligo-Arginine Conjugates (ARCs) Serve as High-Affinity Inhibitors and Fluorescence Probes of Type I cGMP-Dependent Protein Kinase (PKGIα). *Biochim. Biophys. Acta* **2010**, *1804* (9), 1857–1868.
(174) Lavogina, D.; Budu, A.; Enkvist, E.; Hopp, C. S.; Baker, D. A.; Langsley, G.; Garcia, C. R. S.; Uri, A. Targeting Plasmodium Falciparum Protein Kinases with Adenosine Analogue–Oligoarginine Conjugates. *Exp. Parasitol.* **2014**, *138*, 55–62.
(175) Bullock, A. N.; Das, S.; Debreczeni, J. E.; Rellos, P.; Fedorov, O.; Niesen, F. H.; Guo, K.; Papagrigoriou, E.; Amos, A. L.; Cho, S.; et al. Kinase Domain Insertions Define Distinct Roles of CLK Kinases in SR Protein Phosphorylation. *Structure* **2009**, *17* (3), 352–362.
(176) Soundararajan, M.; Roos, A. K.; Savitsky, P.; Filippakopoulos, P.; Kettenbach, A. N.; Olsen, J. V; Gerber, S. A.; Eswaran, J.; Knapp, S.; Elkins, J. M. Structures of Down Syndrome Kinases, DYRKs, Reveal Mechanisms of Kinase Activation and Substrate Recognition. *Structure* **2013**, *21* (6), 986–996.
(177) Pflug, A.; Rogozina, J.; Lavogina, D.; Enkvist, E.; Uri, A.; Engh, R. A.; Bossemeyer, D. Diversity of Bisubstrate Binding Modes of Adenosine Analogue – Oligoarginine Conjugates in Protein Kinase A and Implications for Protein Substrate Interactions. *J. Mol. Biol.* **2010**, *403* (1), 66–77.
(178) Futaki, S.; Hirose, H.; Nakase, I. Arginine-Rich Peptides: Methods of Translocation Through Biological Membranes. *Curr. Pharm. Des.* **2013**, *19* (16), 2863–2868.
(179) Kettenbach, A. N.; Wang, T.; Faherty, B. K.; Madden, D. R.; Knapp, S.; Bailey-kellogg, C.; Gerber, S. A. Rapid Determination of Multiple Linear Kinase Substrate Motifs by Mass Spectrometry. *Chem. Biol.* **2012**, *19* (5), 608–618.

(180) Yang, J.; Garrod, S. M.; Deal, M. S.; Anand, G. S.; Jr, V. L. W.; Taylor, S. Allosteric Network of cAMP-Dependent Protein Kinase Revealed by Mutation of Tyr204 in the P+1 Loop. *J. Mol. Biol.* **2005**, *346*, 191–201.
(181) Eswaran, J.; Patnaik, D.; Filippakopoulos, P.; Wang, F.; Stein, R. L.; Murray, J. W.; Higgins, J. M. G.; Knapp, S. Structure and Functional Characterization of the Atypical Human Kinase Haspin. *Proc. Natl. Acad. Sci. U. S. A.* **2009**, *106* (48), 20198–20203.
(182) Chaikuad, A.; Tacconi, E.; Zimmer, J.; Liang, Y.; Gray, N. S.; Tarsounas, M.; Knapp, S. A Unique Inhibitor Binding Site in ERK1/2 Is Associated with Slow Binding Kinetics. *Nat. Chem. Biol.* **2014**, *10* (10), 853–860.
(183) Kriisa, M.; Sinijärv, H.; Vaasa, A.; Enkvist, E.; Kostenko, S.; Moens, U.; Uri, A. Inhibition of CREB Phosphorylation by Conjugates of Adenosine Analogues and Arginine-Rich Peptides , Inhibitors of PKA Catalytic Subunit. *ChemBioChem* **2015**, *16*, 312–319.
(184) Goldsmith, E. J.; Akella, R.; Min, X.; Zhou, T.; Humphreys, J. M. Substrate and Docking Interactions in Serine/Threonine Protein Kinases. *Chem. Rev.* **2007**, *107*, 5065–5081.
(185) Copeland, R. A.; Pompliano, D. L.; Meek, T. D. Drug-Target Residence Time and Its Implications for Lead Optimization. *Nat. Rev. Drug Discov.* **2006**, *5* (9), 730–739.
(186) Copeland, R. A. Conformational Adaptation in Drug-Target Interactions and Residence Time. *Future Med. Chem.* **2011**, *3* (12), 1491–1501.
(187) Copeland, R. A. The Dynamics of Drug-Target Interactions: Drug-Target Residence Time and Its Impact on Efficacy and Safety. *Expert Opin. Drug Discov.* **2010**, *5* (4), 305–310.
(188) Copeland, R. A. The Drug–Target Residence Time Model: A 10-Year Retrospective. *Nat. Rev. Drug Discov.* **2016**, *15* (2), 87–95.
(189) Copeland, R. A. Conformational Adaptation in Drug-Target Interactions and Residence Time. *Future Med. Chem.* **2011**, *3* (12), 1491–1501.
(190) Sinclair, C. J. D.; Powell, A. E.; Xiong, W.; LaRiviere, C. G.; Baldwin, S. A.; Cass, C. E.; Young, J. D.; Parkinson, F. E. Nucleoside Transporter Subtype Expression: Effects on Potency of Adenosine Kinase Inhibitors. *Br. J. Pharmacol.* **2001**, *134*, 1037–1044.
(191) Hurley, M. C.; Lin, B.; Fox, H. Regulation of Deoxyadenosine and Nucleoside Analog Phosphorylation by Human Placental Adenosine Kinase. *J. Biol. Chem.* **1985**, *260* (29), 15675–15681.
(192) Zhang, X.; Jia, D.; Liu, H.; Zhu, N.; Zhang, W.; Feng, J.; Yin, J.; Hao, B.; Cui, D.; Deng, Y.; et al. Identification of 5-Iodotubercidin as a Genotoxic Drug with Anti-Cancer Potential. *PLoS One* **2013**, *8* (5), e62527.
(193) Livnah, N.; Yechezkel, T.; Salitra, Y.; Perlmutter, B.; Ohne, O.; Cohen, I.; Litman, P.; Senderowitz, H. Protein Kinase Inhibitors Comprising ATP Mimetics Conjugated to Peptides or Peptidomimetics. EP1416934, 2004.
(194) Zorzi, A.; Deyle, K.; Heinis, C. Cyclic Peptide Therapeutics: Past, Present and Future. *Curr. Opin. Chem. Biol.* **2017**, *38*, 24–29.
(195) Qian, Z.; Dougherty, P. G.; Pei, D. Targeting Intracellular Protein – Protein Interactions with Cell-Permeable Cyclic Peptides. *Curr. Opin. Chem. Biol.* **2017**, *38*, 80–86.

(196) Zhao, M.; Zhu, B. The Research and Applications of Quantum Dots as Nano-Carriers for Targeted Drug Delivery and Cancer Therapy. *Nanoscale Res. Lett.* **2016**, *11* (207), 1–9.
(197) Sanna, V.; Pala, N.; Sechi, M. Targeted Therapy Using Nanotechnology: Focus on Cancer. *Int. J. Nanomedicine* **2014**, *9*, 467–483.

ACKNOWLEDGEMENTS

First of all, I would like to express my sincere gratitude and appreciation to Dr Darja Lavõgina for continuous guidance, inexhaustible patience and support for all those years when she was my supervisor. Her energy, positivism, ideas and curiosity about the knowledge and science are admirable.

Secondly, my special thankfulness goes to Dr Asko Uri for the opportunity to work in his research group. I appreciate your dedicated commitment. I would also like to express special thanks for Kaido for the interesting conversations and advice, which made the working atmosphere even more enjoyable. Overall, the current and former members of the medicinal chemistry research group are the brilliant examples of the persons who work hard.

Also, I would like to thank Prof Stefan Knapp for the successful collaboration and opportunity to work in the lab of Structural Genomic Consortium in Oxford, during which a lot of new knowledge together with the practical skills in protein crystallography were acquired. Sincere thanks for SA Archimedes for this experience.

The last but not least, my sincere gratitude goes to my family, especially to my little son Leo.

PUBLICATIONS

CURRICULUM VITAE

Name:	Katrin Kestav (until 26.07.2014 Katrin Kalind)
Date of birth:	December 30, 1991
Citizenship:	Estonian
Address:	University of Tartu, Institute of Chemistry 14A Ravila St., 50411, Tartu, Estonia
Phone:	+372 5340 3571
E-mail:	katrin.kestav@ut.ee

Education

2014 to present	University of Tartu, Institute of Chemistry, PhD studies in chemistry
2013–2014	University of Tartu, Institute of Chemistry, MSc in chemistry (*Cum Laude*)
2010–2013	University of Tartu, Institute of Chemistry, BSc in chemistry (*Cum Laude*)

Professional employment

2015 to present	Estonian University of Life Science, Institute of Veterinary Medicine and Animal Sciences; lecturer (0.5)
2014–2015	Estonian University of Life Science, Institute of Veterinary Medicine and Animal Sciences; lecturer (0.5)
2014–2014	Estonian University of Life Science, Institute of Veterinary Medicine and Animal Sciences; lecturer
2013–2013	University of Tartu, Faculty of Science and Technology, Institute of Chemistry, Chair of Bioorganic Chemistry; laboratory technician (0.5)

Professional self-improvement

2016 Conference *Kinase 2016: Next Generation Inhibitors*, Nottingham, UK, 16-17 May 2016

2015 EMBO workshop on "Cell Division: Molecular Machineries and Cancer Targeted Therapies" with co-sponsorship from UNIA, Baeza, Spain (19^{th} – 21^{th} October 2015)

2013 Structural Genomics Consortium, University of Oxford, United Kingdom (3 months)

Professional acknowledgement

2016 RSC Books Prize poster runner up at conference Kinase 2016: Next Generation Inhibitors, Nottingham UK, 16-17 May 2016

2015 Estonian Biochemical Society competition of student research projects, prize, competition work „Bisubstrate Inhibitor Approach for Targeting Mitotic Kinase Haspin"

2012 National competition of student research projects, I prize within Bachelor degree student´s group

2012 Estonian Biochemical Society competition of student research projects, prize, competition work „Conjugates of 5-isoquinolinesulfonylamides and oligo-D-arginine possess high affinity and selectivity towards Rho kinase (ROCK)"

Scientific publications

1. **Kestav, K**.; Uri, A.; Lavogina, D. Structure, Roles and Inhibitors of a Mitotic Protein Kinase Haspin. *Curr. Med. Chem.* **2017**, *24*(21), 2276–2293.
2. **Kestav, K**.; Viht, K.; Konovalov, A.; Enkvist, E.; Uri, A.; Lavogina, D. Slowly on, Slowly off: Bisubstrate-Analogue Conjugates of 5-Iodotubercidin and Histone H3 Peptide Targeting Protein Kinase Haspin. *ChemBioChem.* **2017**, *18*(8), 790–798.
3. Lavogina, D.; **Kestav, K**.; Chaikuad, A.; Heroven, C.; Knapp, S.; Uri, A. Co-crystal Structures of the Protein Kinase Haspin with Bisubstrate Inhibitors. *Acta Crystallogr. F-Struct. Biol. Cryst. Commun.* **2016**, *72*(5), 339–345.
4. **Kestav, K**.; Lavogina, D.; Raidaru, G.; Chaikuad, A.; Knapp, S.; Uri, A. Bisubstrate Inhibitor Approach for Targeting Mitotic Kinase Haspin. *Bioconjugate Chem*. 2015, *26*(2), 225–234.
5. Lavogina, D.; **Kalind, K**.; Bredihhina, J.; Hurt, M.; Vaasa, A.; Kasari, M.; Enkvist, E. Conjugates of 5-isoquinolinesulfonylamides and oligo-D-arginine possess high affinity and selectivity towards Rho kinase (ROCK). *Bioorg. Med. Chem. Lett*. **2012**, *22*(10), 3425–3430.

ELULOOKIRJELDUS

Nimi: Katrin Kestav (kuni 26.07.2014 Katrin Kalind)
Sünniaeg: 30. detsember, 1991
Kodakondsus: Eesti
Aadress: Tartu Ülikool, Keemia Instituut,
Ravila 14A, 50411, Tartu, Estonia
Telefon: +372 5340 3571
E-mail: katrin.kestav@ut.ee

Haridus

2014 praeguseni	Tartu Ülikool, Keemia Instituut, keemia eriala, doktoriõpe
2013–2014	Tartu Ülikool, Keemia Instituut, keemia eriala, magistriõpe (*Cum Laude*)
2010–2013	Tartu Ülikool, Keemia Instituut, keemia eriala, bakalaureuseõpe (*Cum Laude*)

Teenistuskäik

2015 praeguseni	Eesti Maaülikool, Veterinaarmeditsiini ja loomakasvatuse instituut, Toiduteaduse ja toiduainete tehnoloogia osakond; bioorgaanilise keemia lektor (0.50)
2014–2015	Eesti Maaülikool, Veterinaarmeditsiini ja loomakasvatuse instituut, Toiduteaduse ja toiduainete tehnoloogia osakond; bioorgaanilise keemia nimetatud lektor (0.50)
2014–2014	Eesti Maaülikool, Veterinaarmeditsiini ja loomakasvatuse instituut, Toiduteaduse ja toiduainete tehnoloogia osakond; õppeülesannete täitja
2013–2013	Tartu Ülikool, Loodus- ja tehnoloogiateaduskond, Keemia Instituut, Bioorgaanilise keemia õppetool; laborant (0.50)

Erialane enesetäiendus

2016 Konverents *Kinase 2016: Next Generation Inhibitors*, Nottingham, Suurbritannia, 16.–17. mai 2016 (poster)

2015 Stažeerimiskursus *EMBO Workshop on "Cell Division: Molecular Machineries and Cancer Targeted Therapies" with Co-Sponsorship from UNIA*, Baeza, Hispaania, 18.–21. oktoober 2015 (poster ja suuline ettekanne)

2013 Structural Genomics Consortium, Oxfordi Ülikool, Oxford, Suurbritannia (3 kuud)

Erialane tunnustus

2016 RSC Books Prize postri teine auhind konverentsil *Kinase 2016: Next Generation Inhibitors*, Nottingham, Suurbritannia, 16.–17. mai 2016

2015 Eesti Biokeemia Seltsi üliõpilaste teadustööde konkursi auhind, konkursitöö „Bisubstrate Inhibitor Approach for Targeting Mitotic Kinase Haspin“

2012 Üliõpilaste teadustööde riiklik konkurss, I preemia bakalaureuseõppe üliõpilaste astmes, konkursitöö “Isokinoliinil põhinevad bisubstraatsed inhibiitorid proteiinkinaasidele”

2012 Eesti Biokeemia Seltsi üliõpilaste teadustööde konkursi auhind, konkursitöö „Isokinoliini fragmenti sisaldavad oligoarginiini konjugaadid on kõrge afiinsusega Rho-kinaasi inhibiitorid“

Teaduspublikatsioonid

1. **Kestav, K**.; Uri, A.; Lavogina, D. Structure, Roles and Inhibitors of a Mitotic Protein Kinase Haspin. *Curr. Med. Chem.* **2017**, *24*(21), 2276–2293.
2. **Kestav, K**.; Viht, K.; Konovalov, A.; Enkvist, E.; Uri, A.; Lavogina, D. Slowly on, Slowly off: Bisubstrate-Analogue Conjugates of 5-Iodotubercidin and Histone H3 Peptide Targeting Protein Kinase Haspin. *ChemBioChem.* **2017**, *18*(8), 790–798.
3. Lavogina, D.; **Kestav, K**.; Chaikuad, A.; Heroven, C.; Knapp, S.; Uri, A. Co-crystal Structures of the Protein Kinase Haspin with Bisubstrate Inhibitors. *Acta Crystallogr. F-Struct. Biol. Cryst. Commun.* **2016**, *72* (5), 339–345.
4. **Kestav, K**.; Lavogina, D.; Raidaru, G.; Chaikuad, A.; Knapp, S.; Uri, A. Bisubstrate Inhibitor Approach for Targeting Mitotic Kinase Haspin. *Bioconjugate Chem*. 2015, *26* (2), 225–234.
5. Lavogina, D.; **Kalind, K**.; Bredihhina, J.; Hurt, M.; Vaasa, A.; Kasari, M.; Enkvist, E. Conjugates of 5-isoquinolinesulfonylamides and oligo-D-arginine possess high affinity and selectivity towards Rho kinase (ROCK). *Bioorg. Med. Chem. Lett*. **2012**, *22* (10), 3425–3430.

DISSERTATIONES CHIMICAE UNIVERSITATIS TARTUENSIS

1. **Toomas Tamm.** Quantum-chemical simulation of solvent effects. Tartu, 1993, 110 p.
2. **Peeter Burk.** Theoretical study of gas-phase acid-base equilibria. Tartu, 1994, 96 p.
3. **Victor Lobanov.** Quantitative structure-property relationships in large descriptor spaces. Tartu, 1995, 135 p.
4. **Vahur Mäemets.** The ^{17}O and ^{1}H nuclear magnetic resonance study of H_2O in individual solvents and its charged clusters in aqueous solutions of electrolytes. Tartu, 1997, 140 p.
5. **Andrus Metsala.** Microcanonical rate constant in nonequilibrium distribution of vibrational energy and in restricted intramolecular vibrational energy redistribution on the basis of slater's theory of unimolecular reactions. Tartu, 1997, 150 p.
6. **Uko Maran.** Quantum-mechanical study of potential energy surfaces in different environments. Tartu, 1997, 137 p.
7. **Alar Jänes.** Adsorption of organic compounds on antimony, bismuth and cadmium electrodes. Tartu, 1998, 219 p.
8. **Kaido Tammeveski.** Oxygen electroreduction on thin platinum films and the electrochemical detection of superoxide anion. Tartu, 1998, 139 p.
9. **Ivo Leito.** Studies of Brønsted acid-base equilibria in water and non-aqueous media. Tartu, 1998, 101 p.
10. **Jaan Leis.** Conformational dynamics and equilibria in amides. Tartu, 1998, 131 p.
11. **Toonika Rinken.** The modelling of amperometric biosensors based on oxidoreductases. Tartu, 2000, 108 p.
12. **Dmitri Panov.** Partially solvated Grignard reagents. Tartu, 2000, 64 p.
13. **Kaja Orupõld.** Treatment and analysis of phenolic wastewater with microorganisms. Tartu, 2000, 123 p.
14. **Jüri Ivask.** Ion Chromatographic determination of major anions and cations in polar ice core. Tartu, 2000, 85 p.
15. **Lauri Vares.** Stereoselective Synthesis of Tetrahydrofuran and Tetrahydropyran Derivatives by Use of Asymmetric Horner-Wadsworth-Emmons and Ring Closure Reactions. Tartu, 2000, 184 p.
16. **Martin Lepiku.** Kinetic aspects of dopamine D_2 receptor interactions with specific ligands. Tartu, 2000, 81 p.
17. **Katrin Sak.** Some aspects of ligand specificity of P2Y receptors. Tartu, 2000, 106 p.
18. **Vello Pällin.** The role of solvation in the formation of iotsitch complexes. Tartu, 2001, 95 p.
19. **Katrin Kollist.** Interactions between polycyclic aromatic compounds and humic substances. Tartu, 2001, 93 p.

20. **Ivar Koppel.** Quantum chemical study of acidity of strong and superstrong Brønsted acids. Tartu, 2001, 104 p.
21. **Viljar Pihl.** The study of the substituent and solvent effects on the acidity of OH and CH acids. Tartu, 2001, 132 p.
22. **Natalia Palm.** Specification of the minimum, sufficient and significant set of descriptors for general description of solvent effects. Tartu, 2001, 134 p.
23. **Sulev Sild.** QSPR/QSAR approaches for complex molecular systems. Tartu, 2001, 134 p.
24. **Ruslan Petrukhin.** Industrial applications of the quantitative structure-property relationships. Tartu, 2001, 162 p.
25. **Boris V. Rogovoy.** Synthesis of (benzotriazolyl)carboximidamides and their application in relations with *N*- and *S*-nucleophyles. Tartu, 2002, 84 p.
26. **Koit Herodes.** Solvent effects on UV-vis absorption spectra of some solvatochromic substances in binary solvent mixtures: the preferential solvation model. Tartu, 2002, 102 p.
27. **Anti Perkson.** Synthesis and characterisation of nanostructured carbon. Tartu, 2002, 152 p.
28. **Ivari Kaljurand.** Self-consistent acidity scales of neutral and cationic Brønsted acids in acetonitrile and tetrahydrofuran. Tartu, 2003, 108 p.
29. **Karmen Lust.** Adsorption of anions on bismuth single crystal electrodes. Tartu, 2003, 128 p.
30. **Mare Piirsalu.** Substituent, temperature and solvent effects on the alkaline hydrolysis of substituted phenyl and alkyl esters of benzoic acid. Tartu, 2003, 156 p.
31. **Meeri Sassian.** Reactions of partially solvated Grignard reagents. Tartu, 2003, 78 p.
32. **Tarmo Tamm.** Quantum chemical modelling of polypyrrole. Tartu, 2003. 100 p.
33. **Erik Teinemaa.** The environmental fate of the particulate matter and organic pollutants from an oil shale power plant. Tartu, 2003. 102 p.
34. **Jaana Tammiku-Taul.** Quantum chemical study of the properties of Grignard reagents. Tartu, 2003. 120 p.
35. **Andre Lomaka.** Biomedical applications of predictive computational chemistry. Tartu, 2003. 132 p.
36. **Kostyantyn Kirichenko.** Benzotriazole – Mediated Carbon–Carbon Bond Formation. Tartu, 2003. 132 p.
37. **Gunnar Nurk.** Adsorption kinetics of some organic compounds on bismuth single crystal electrodes. Tartu, 2003, 170 p.
38. **Mati Arulepp.** Electrochemical characteristics of porous carbon materials and electrical double layer capacitors. Tartu, 2003, 196 p.
39. **Dan Cornel Fara.** QSPR modeling of complexation and distribution of organic compounds. Tartu, 2004, 126 p.
40. **Riina Mahlapuu.** Signalling of galanin and amyloid precursor protein through adenylate cyclase. Tartu, 2004, 124 p.

41. **Mihkel Kerikmäe.** Some luminescent materials for dosimetric applications and physical research. Tartu, 2004, 143 p.
42. **Jaanus Kruusma.** Determination of some important trace metal ions in human blood. Tartu, 2004, 115 p.
43. **Urmas Johanson.** Investigations of the electrochemical properties of polypyrrole modified electrodes. Tartu, 2004, 91 p.
44. **Kaido Sillar.** Computational study of the acid sites in zeolite ZSM-5. Tartu, 2004, 80 p.
45. **Aldo Oras.** Kinetic aspects of dATPαS interaction with $P2Y_1$ receptor. Tartu, 2004, 75 p.
46. **Erik Mölder.** Measurement of the oxygen mass transfer through the air-water interface. Tartu, 2005, 73 p.
47. **Thomas Thomberg.** The kinetics of electroreduction of peroxodisulfate anion on cadmium (0001) single crystal electrode. Tartu, 2005, 95 p.
48. **Olavi Loog.** Aspects of condensations of carbonyl compounds and their imine analogues. Tartu, 2005, 83 p.
49. **Siim Salmar.** Effect of ultrasound on ester hydrolysis in aqueous ethanol. Tartu, 2006, 73 p.
50. **Ain Uustare.** Modulation of signal transduction of heptahelical receptors by other receptors and G proteins. Tartu, 2006, 121 p.
51. **Sergei Yurchenko.** Determination of some carcinogenic contaminants in food. Tartu, 2006, 143 p.
52. **Kaido Tämm.** QSPR modeling of some properties of organic compounds. Tartu, 2006, 67 p.
53. **Olga Tšubrik.** New methods in the synthesis of multisubstituted hydrazines. Tartu. 2006, 183 p.
54. **Lilli Sooväli.** Spectrophotometric measurements and their uncertainty in chemical analysis and dissociation constant measurements. Tartu, 2006, 125 p.
55. **Eve Koort.** Uncertainty estimation of potentiometrically measured ph and pK_a values. Tartu, 2006, 139 p.
56. **Sergei Kopanchuk.** Regulation of ligand binding to melanocortin receptor subtypes. Tartu, 2006, 119 p.
57. **Silvar Kallip.** Surface structure of some bismuth and antimony single crystal electrodes. Tartu, 2006, 107 p.
58. **Kristjan Saal.** Surface silanization and its application in biomolecule coupling. Tartu, 2006, 77 p.
59. **Tanel Tätte.** High viscosity $Sn(OBu)_4$ oligomeric concentrates and their applications in technology. Tartu, 2006, 91 p.
60. **Dimitar Atanasov Dobchev**. Robust QSAR methods for the prediction of properties from molecular structure. Tartu, 2006, 118 p.
61. **Hannes Hagu**. Impact of ultrasound on hydrophobic interactions in solutions. Tartu, 2007, 81 p.
62. **Rutha Jäger.** Electroreduction of peroxodisulfate anion on bismuth electrodes. Tartu, 2007, 142 p.

63. **Kaido Viht.** Immobilizable bisubstrate-analogue inhibitors of basophilic protein kinases: development and application in biosensors. Tartu, 2007, 88 p.
64. **Eva-Ingrid Rõõm.** Acid-base equilibria in nonpolar media. Tartu, 2007, 156 p.
65. **Sven Tamp.** DFT study of the cesium cation containing complexes relevant to the cesium cation binding by the humic acids. Tartu, 2007, 102 p.
66. **Jaak Nerut.** Electroreduction of hexacyanoferrate(III) anion on Cadmium (0001) single crystal electrode. Tartu, 2007, 180 p.
67. **Lauri Jalukse.** Measurement uncertainty estimation in amperometric dissolved oxygen concentration measurement. Tartu, 2007, 112 p.
68. **Aime Lust.** Charge state of dopants and ordered clusters formation in CaF_2:Mn and CaF_2:Eu luminophors. Tartu, 2007, 100 p.
69. **Iiris Kahn**. Quantitative Structure-Activity Relationships of environmentally relevant properties. Tartu, 2007, 98 p.
70. **Mari Reinik.** Nitrates, nitrites, N-nitrosamines and polycyclic aromatic hydrocarbons in food: analytical methods, occurrence and dietary intake. Tartu, 2007, 172 p.
71. **Heili Kasuk.** Thermodynamic parameters and adsorption kinetics of organic compounds forming the compact adsorption layer at Bi single crystal electrodes. Tartu, 2007, 212 p.
72. **Erki Enkvist.** Synthesis of adenosine-peptide conjugates for biological applications. Tartu, 2007, 114 p.
73. **Svetoslav Hristov Slavov**. Biomedical applications of the QSAR approach. Tartu, 2007, 146 p.
74. **Eneli Härk.** Electroreduction of complex cations on electrochemically polished Bi(*hkl*) single crystal electrodes. Tartu, 2008, 158 p.
75. **Priit Möller.** Electrochemical characteristics of some cathodes for medium temperature solid oxide fuel cells, synthesized by solid state reaction technique. Tartu, 2008, 90 p.
76. **Signe Viggor.** Impact of biochemical parameters of genetically different pseudomonads at the degradation of phenolic compounds. Tartu, 2008, 122 p.
77. **Ave Sarapuu.** Electrochemical reduction of oxygen on quinone-modified carbon electrodes and on thin films of platinum and gold. Tartu, 2008, 134 p.
78. **Agnes Kütt.** Studies of acid-base equilibria in non-aqueous media. Tartu, 2008, 198 p.
79. **Rouvim Kadis.** Evaluation of measurement uncertainty in analytical chemistry: related concepts and some points of misinterpretation. Tartu, 2008, 118 p.
80. **Valter Reedo.** Elaboration of IVB group metal oxide structures and their possible applications. Tartu, 2008, 98 p.
81. **Aleksei Kuznetsov.** Allosteric effects in reactions catalyzed by the cAMP-dependent protein kinase catalytic subunit. Tartu, 2009, 133 p.

82. **Aleksei Bredihhin.** Use of mono- and polyanions in the synthesis of multisubstituted hydrazine derivatives. Tartu, 2009, 105 p.
83. **Anu Ploom.** Quantitative structure-reactivity analysis in organosilicon chemistry. Tartu, 2009, 99 p.
84. **Argo Vonk.** Determination of adenosine A_{2A}- and dopamine D_1 receptor-specific modulation of adenylate cyclase activity in rat striatum. Tartu, 2009, 129 p.
85. **Indrek Kivi.** Synthesis and electrochemical characterization of porous cathode materials for intermediate temperature solid oxide fuel cells. Tartu, 2009, 177 p.
86. **Jaanus Eskusson.** Synthesis and characterisation of diamond-like carbon thin films prepared by pulsed laser deposition method. Tartu, 2009, 117 p.
87. **Marko Lätt.** Carbide derived microporous carbon and electrical double layer capacitors. Tartu, 2009, 107 p.
88. **Vladimir Stepanov.** Slow conformational changes in dopamine transporter interaction with its ligands. Tartu, 2009, 103 p.
89. **Aleksander Trummal.** Computational Study of Structural and Solvent Effects on Acidities of Some Brønsted Acids. Tartu, 2009, 103 p.
90. **Eerold Vellemäe.** Applications of mischmetal in organic synthesis. Tartu, 2009, 93 p.
91. **Sven Parkel.** Ligand binding to 5-HT_{1A} receptors and its regulation by Mg^{2+} and Mn^{2+}. Tartu, 2010, 99 p.
92. **Signe Vahur.** Expanding the possibilities of ATR-FT-IR spectroscopy in determination of inorganic pigments. Tartu, 2010, 184 p.
93. **Tavo Romann**. Preparation and surface modification of bismuth thin film, porous, and microelectrodes. Tartu, 2010, 155 p.
94. **Nadežda Aleksejeva.** Electrocatalytic reduction of oxygen on carbon nanotube-based nanocomposite materials. Tartu, 2010, 147 p.
95. **Marko Kullapere.** Electrochemical properties of glassy carbon, nickel and gold electrodes modified with aryl groups. Tartu, 2010, 233 p.
96. **Liis Siinor.** Adsorption kinetics of ions at Bi single crystal planes from aqueous electrolyte solutions and room-temperature ionic liquids. Tartu, 2010, 101 p.
97. **Angela Vaasa.** Development of fluorescence-based kinetic and binding assays for characterization of protein kinases and their inhibitors. Tartu 2010, 101 p.
98. **Indrek Tulp.** Multivariate analysis of chemical and biological properties. Tartu 2010, 105 p.
99. **Aare Selberg.** Evaluation of environmental quality in Northern Estonia by the analysis of leachate. Tartu 2010, 117 p.
100. **Darja Lavõgina.** Development of protein kinase inhibitors based on adenosine analogue-oligoarginine conjugates. Tartu 2010, 248 p.
101. **Laura Herm.** Biochemistry of dopamine D_2 receptors and its association with motivated behaviour. Tartu 2010, 156 p.

102. **Terje Raudsepp.** Influence of dopant anions on the electrochemical properties of polypyrrole films. Tartu 2010, 112 p.
103. **Margus Marandi.** Electroformation of Polypyrrole Films: *In-situ* AFM and STM Study. Tartu 2011, 116 p.
104. **Kairi Kivirand.** Diamine oxidase-based biosensors: construction and working principles. Tartu, 2011, 140 p.
105. **Anneli Kruve.** Matrix effects in liquid-chromatography electrospray mass-spectrometry. Tartu, 2011, 156 p.
106. **Gary Urb.** Assessment of environmental impact of oil shale fly ash from PF and CFB combustion. Tartu, 2011, 108 p.
107. **Nikita Oskolkov.** A novel strategy for peptide-mediated cellular delivery and induction of endosomal escape. Tartu, 2011, 106 p.
108. **Dana Martin.** The QSPR/QSAR approach for the prediction of properties of fullerene derivatives. Tartu, 2011, 98 p.
109. **Säde Viirlaid.** Novel glutathione analogues and their antioxidant activity. Tartu, 2011, 106 p.
110. **Ülis Sõukand.** Simultaneous adsorption of Cd^{2+}, Ni^{2+}, and Pb^{2+} on peat. Tartu, 2011, 124 p.
111. **Lauri Lipping.** The acidity of strong and superstrong Brønsted acids, an outreach for the "limits of growth": a quantum chemical study. Tartu, 2011, 124 p.
112. **Heisi Kurig.** Electrical double-layer capacitors based on ionic liquids as electrolytes. Tartu, 2011, 146 p.
113. **Marje Kasari.** Bisubstrate luminescent probes, optical sensors and affinity adsorbents for measurement of active protein kinases in biological samples. Tartu, 2012, 126 p.
114. **Kalev Takkis.** Virtual screening of chemical databases for bioactive molecules. Tartu, 2012, 122 p.
115. **Ksenija Kisseljova**. Synthesis of aza-β^3-amino acid containing peptides and kinetic study of their phosphorylation by protein kinase A. Tartu, 2012, 104 p.
116. **Riin Rebane.** Advanced method development strategy for derivatization LC/ESI/MS. Tartu, 2012, 184 p.
117. **Vladislav Ivaništšev.** Double layer structure and adsorption kinetics of ions at metal electrodes in room temperature ionic liquids. Tartu, 2012, 128 p.
118. **Irja Helm.** High accuracy gravimetric Winkler method for determination of dissolved oxygen. Tartu, 2012, 139 p.
119. **Karin Kipper.** Fluoroalcohols as Components of LC-ESI-MS Eluents: Usage and Applications. Tartu, 2012, 164 p.
120. **Arno Ratas.** Energy storage and transfer in dosimetric luminescent materials. Tartu, 2012, 163 p.
121. **Reet Reinart-Okugbeni**. Assay systems for characterisation of subtype-selective binding and functional activity of ligands on dopamine receptors. Tartu, 2012, 159 p.

122. **Lauri Sikk.** Computational study of the Sonogashira cross-coupling reaction. Tartu, 2012, 81 p.
123. **Karita Raudkivi.** Neurochemical studies on inter-individual differences in affect-related behaviour of the laboratory rat. Tartu, 2012, 161 p.
124. **Indrek Saar.** Design of GalR2 subtype specific ligands: their role in depression-like behavior and feeding regulation. Tartu, 2013, 126 p.
125. **Ann Laheäär.** Electrochemical characterization of alkali metal salt based non-aqueous electrolytes for supercapacitors. Tartu, 2013, 127 p.
126. **Kerli Tõnurist.** Influence of electrospun separator materials properties on electrochemical performance of electrical double-layer capacitors. Tartu, 2013, 147 p.
127. **Kaija Põhako-Esko.** Novel organic and inorganic ionogels: preparation and characterization. Tartu, 2013, 124 p.
128. **Ivar Kruusenberg.** Electroreduction of oxygen on carbon nanomaterial-based catalysts. Tartu, 2013, 191 p.
129. **Sander Piiskop.** Kinetic effects of ultrasound in aqueous acetonitrile solutions. Tartu, 2013, 95 p.
130. **Ilona Faustova**. Regulatory role of L-type pyruvate kinase N-terminal domain. Tartu, 2013, 109 p.
131. **Kadi Tamm.** Synthesis and characterization of the micro-mesoporous anode materials and testing of the medium temperature solid oxide fuel cell single cells. Tartu, 2013, 138 p.
132. **Iva Bozhidarova Stoyanova-Slavova.** Validation of QSAR/QSPR for regulatory purposes. Tartu, 2013, 109 p.
133. **Vitali Grozovski**. Adsorption of organic molecules at single crystal electrodes studied by *in situ* STM method. Tartu, 2014, 146 p.
134. **Santa Veikšina**. Development of assay systems for characterisation of ligand binding properties to melanocortin 4 receptors. Tartu, 2014, 151 p.
135. **Jüri Liiv.** PVDF (polyvinylidene difluoride) as material for active element of twisting-ball displays. Tartu, 2014, 111 p.
136. **Kersti Vaarmets.** Electrochemical and physical characterization of pristine and activated molybdenum carbide-derived carbon electrodes for the oxygen electroreduction reaction. Tartu, 2014, 131 p.
137. **Lauri Tõntson**. Regulation of G-protein subtypes by receptors, guanine nucleotides and Mn^{2+}. Tartu, 2014, 105 p.
138. **Aiko Adamson.** Properties of amine-boranes and phosphorus analogues in the gas phase. Tartu, 2014, 78 p.
139. **Elo Kibena**. Electrochemical grafting of glassy carbon, gold, highly oriented pyrolytic graphite and chemical vapour deposition-grown graphene electrodes by diazonium reduction method. Tartu, 2014, 184 p.
140. **Teemu Näykki.** Novel Tools for Water Quality Monitoring – From Field to Laboratory. Tartu, 2014, 202 p.
141. **Karl Kaupmees.** Acidity and basicity in non-aqueous media: importance of solvent properties and purity. Tartu, 2014, 128 p.

142. **Oleg Lebedev**. Hydrazine polyanions: different strategies in the synthesis of heterocycles. Tartu, 2015, 118 p.
143. **Geven Piir.** Environmental risk assessment of chemicals using QSAR methods. Tartu, 2015, 123 p.
144. **Olga Mazina.** Development and application of the biosensor assay for measurements of cyclic adenosine monophosphate in studies of G protein-coupled receptor signalinga. Tartu, 2015, 116 p.
145. **Sandip Ashokrao Kadam.** Anion receptors: synthesis and accurate binding measurements. Tartu, 2015, 116 p.
146. **Indrek Tallo.** Synthesis and characterization of new micro-mesoporous carbide derived carbon materials for high energy and power density electrical double layer capacitors. Tartu, 2015, 148 p.
147. **Heiki Erikson.** Electrochemical reduction of oxygen on nanostructured palladium and gold catalysts. Tartu, 2015, 204 p.
148. **Erik Anderson.** *In situ* Scanning Tunnelling Microscopy studies of the interfacial structure between Bi(111) electrode and a room temperature ionic liquid. Tartu, 2015, 118 p.
149. **Girinath G. Pillai.** Computational Modelling of Diverse Chemical, Biochemical and Biomedical Properties. Tartu, 2015, 140 p.
150. **Piret Pikma.** Interfacial structure and adsorption of organic compounds at Cd(0001) and Sb(111) electrodes from ionic liquid and aqueous electrolytes: an *in situ* STM study. Tartu, 2015, 126 p.
151. **Ganesh babu Manoharan.** Combining chemical and genetic approaches for photoluminescence assays of protein kinases. Tartu, 2016, 126 p.
152. **Carolin Siimenson**. Electrochemical characterization of halide ion adsorption from liquid mixtures at Bi(111) and pyrolytic graphite electrode surface. Tartu, 2016, 110 p.
153. **Asko Laaniste.** Comparison and optimisation of novel mass spectrometry ionisation sources. Tartu, 2016, 156 p.
154. **Hanno Evard.** Estimating limit of detection for mass spectrometric analysis methods. Tartu, 2016, 224 p.
155. **Kadri Ligi.** Characterization and application of protein kinase-responsive organic probes with triplet-singlet energy transfer. Tartu, 2016, 122 p.
156. **Margarita Kagan.** Biosensing penicillins' residues in milk flows. Tartu, 2016, 130 p.
157. **Marie Kriisa.** Development of protein kinase-responsive photoluminescent probes and cellular regulators of protein phosphorylation. Tartu, 2016, 106 p.
158. **Mihkel Vestli.** Ultrasonic spray pyrolysis deposited electrolyte layers for intermediate temperature solid oxide fuel cells. Tartu, 2016, 156 p.
159. **Silver Sepp**. Influence of porosity of the carbide-derived carbon on the properties of the composite electrocatalysts and characteristics of polymer electrolyte fuel cells. Tartu, 2016, 137p.
160. **Kristjan Haav**. Quantitative relative equilibrium constant measurements in supramolecular chemistry. Tartu, 2017, 158 p.

161. **Anu Teearu**. Development of MALDI-FT-ICR-MS methodology for the analysis of resinous materials. Tartu, 2017, 205 p.
162. **Taavi Ivan**. Bifunctional inhibitors and photoluminescent probes for studies on protein complexes. Tartu, 2017, 140 p.
163. **Maarja-Liisa Oldekop**. Characterization of amino acid derivatization reagents for LC-MS analysis. Tartu, 2017, 147 p.
164. **Kristel Jukk**. Electrochemical reduction of oxygen on platinum- and palladium-based nanocatalysts. Tartu, 2017, 250 p.
165. **Siim Kukk**. Kinetic aspects of interaction between dopamine transporter and *N*-substituted nortropane derivatives. Tartu, 2017, 107 p.
166. **Birgit Viira**. Design and modelling in early drug development in targeting HIV-1 reverse transcriptase and Malaria. Tartu, 2017, 172 p.
167. **Rait Kivi**. Allostery in cAMP dependent protein kinase catalytic subunit. Tartu, 2017, 115 p.
168. **Agnes Heering**. Experimental realization and applications of the unified acidity scale. Tartu, 2017, 123 p.
169. **Delia Juronen**. Biosensing system for the rapid multiplex detection of mastitis-causing pathogens in milk. Tartu, 2018, 85 p.
170. **Hedi Rahnel.** ARC-inhibitors: from reliable biochemical assays to regulators of physiology of cells. Tartu, 2018, 176 p.
171. **Anton Ruzanov.** Computational investigation of the electrical double layer at metal–aqueous solution and metal–ionic liquid interfaces. Tartu, 2018, 129 p.